TECHNISCHE UNIVERSITÄT MÜNCHEN

Wissenschaftszentrum Weihenstephan für Ernährung, Landnutzung und Umwelt

Lehrstuhl für Molekulare Ernährungsmedizin

Prevention of diet-induced obesity conferred by dietary bile acid supplementation in mice is strain specific and not dependent on uncoupling protein 1

Kristina Hüttinger

Vollständiger Abdruck der von der Fakultät Wissenschaftszentrum Weihenstephan für Ernährung, Landnutzung und Umwelt der Technischen Universität München zur Erlangung des akademischen Grades eines

Doktors der Naturwissenschaften

genehmigten Dissertation.

Vorsitzender:	Prof. Dr. Michael Schemann
Prüfer der Dissertation:	1. Prof. Dr. Martin Klingenspor
	2. Prof. Dr. Hannelore Daniel

Die Dissertation wurde am 28.11.2019 bei der Technischen Universität München eingereicht und durch die Fakultät Wissenschaftszentrum Weihenstephan für Ernährung, Landnutzung und Umwelt am 12.05.2020 angenommen.

TABLE OF CONTENT

ABBREVIATIONS

129S6	129S6/SvEvTac
ActB	beta-actin
ADP	adenosine diphosphate
ALAT	alanine aminotransferase
ANOVA	analysis of variation
ASAT	aspartate aminotransferase
ASBT	apical sodium-dependent bile acid transporter
ATP	adenosine triphosphate
AQP	aquaporins
B6	C57BL/6J
BA	bile acid
BAT	brown adipose tissue
BL6J	C57BL/6J
BM	body mass
BMI	body mass index
BMR	basal metabolic rate
bp	base pair
BSA	bovine serum albumin
BSEP	bile-salt export pump
C	control (diet)
CA	cholic acid
cAMP	cyclic adenosine monophosphate
CC	control diet supplemented with cholic acid
CDCA	chenodeoxycholic acid
cDNA	complementary deoxyribonucleic acid
CE	caloric equivalent
CIDEA	cell death-inducing DFFA-like effector a

COX	cytochrome-c-oxidase
CREB	cAMP response element-binding protein
CV	coefficient of variation
CYP7A1	cholesterol 7 alpha-hydroxylase
D2	type 2 iodothyronine deiodinase
Da	dalton
DAB	3,3'-diaminobenzidine
DAPI	4',6-diamidino-2-phenylindole
DCA	deoxycholic acid
DEE	daily energy expenditure
DIO	diet-induced obesity
DNA	deoxyribonucleic acid
EDTA	ethylenediaminetetraacetic acid
EI	energy intake
EO	enterohepatic organs
eWAT	epididymal white adipose tissue
FDG	fluorodesoxyglucose
FGF	fibroblast growth factor
FXR	farnesoid X receptor
G[-bile acid]	glycine conjugated bile acid
GCA	glycocholic acid
GCDCA	glycochenodeoxycholic acid
GDCA	glycodeoxycholic acid
GFP	green fluorescence protein
GLP-1	glucagon-like peptide-1
GPBAR-1	G-protein-coupled bile acid receptor 1 (TGR5)
GPCR	G-protein-coupled receptor
GUDCA	glycoursodeoxycholic acid

H	high-fat (diet)
HC	high-fat diet supplemented with cholic acid
H&E	hematoxylin & eosin
HRP	horseradish peroxidase
Hsp90	heat shock protein 90
iBAT	interscapular brown adipose tissue
IBABP	intestinal BA-binding protein
IC	indirect calorimetry
IHC	immunohistochemistry
iWAT	inguinal white adipose tissue
ko	knockout
LCA	lithocholic acid
LXR	liver X receptor
MAPK	mitogen-activated protein kinase
MCA	muricholic acid
MIM	mitochondrial inner membrane
MOPS	3-morpholinopropane-1-sulfonic acid
mRNA	messenger ribonucleic acid
MRP	multidrug resistance-related protein
Myf5	myogenic factor 5
NADH	nicotinamide adenine dinucleotide
NMR	nuclear magnetic resonance
NST	non-shivering thermogenesis
NTCP	sodium taurocholate co-transporting polypeptide
OATP	organic-anion-transporting polypeptide
PCR	polymerase chain reaction
PET/CT	positron emission tomography-computed tomography
PFA	paraformaldehyde

PKA	protein kinase A
qRT-PCR	quantitative real-time PCR
RCR	respiratory control ratio
RER	respiratory exchange ratio
RIPA	radioimmunoprecipitation assay
RMR	resting metabolic rate
RNA	ribonucleic acid
RT	room temperature
rWAT	retroperitoneal white adipose tissue
SD	standard deviation
SDS	sodium dodecyl sulfate
SHP	short heterodimer partner
T[-bile acid]	taurine conjugated bile acid
TCA	taurocholic acid
TCDCA	taurochenodeoxychlic acid
TDCA	taurodeoxycholic acid
TG	triglycerides
TGR5	G-protein-coupled BA receptor (GPBAR-1)
TLCA	taurolithocholic acid
TN	thermoneutral
TωMCA	tauro-omega-muricholic acid
TRIS	2-amino-2-hydroxymethyl-propane-1,3-diol
Ttest	student's t-test
TUDCA	tauroursodeoxycholic acid
UCP1	uncoupling protein 1
UDCA	ursodeoxycholic acid
WAT	white adipose tissue

ABSTRACT

In the last years, a new role for circulating bile acids has emerged, as they do not only aid in the absorption of dietary lipids but also may function as signaling molecules. Bile acids were identified to protect against diet-induced obesity (DIO) in C57BL/6J mice. It was hypothesized that this phenomenon is based on a bile acid-derived increase in thermogenic processes in brown adipose tissue, the adaptive heater organ in mammals. Yet, it has not been proven that the brown adipose tissue-specific Uncoupling Protein 1 (UCP1) which uncouples the respiratory chain and thereby dissipates energy as heat, is necessary within this context.

We were able to verify the DIO-protective effect of bile acids in mice of the inbred mouse strain C57BL/6J. The mice were fully protected from fat mass accumulation, if their high-fat diet was supplemented with the primary bile acid cholic acid. Moreover, bile acid-supplementation provoked browning and an increase in brown adipocyte markers in inguinal white adipose tissue. However, indirect calorimetry measurements revealed, that the adiposity-preventive effects could not be attributed to an increase in energy expenditure.

To elucidate the contribution of a browning effect of bile acids, we used 129S6/SvEvTac mice, which naturally have a high propensity to recruit brite adipocytes. In contrast to expectations, 129S6/SvEvTac mice were not at all influenced by cholic acid supplementation. All previously observed impacts on body mass, body composition, or brown adipocyte marker expression were absent in this strain, and no browning effect was detected. Differing bile acid concentrations in the organs of enterohepatic circulation reflected the strain specific response to bile acid supplementation. Eventually, variants of intestinal bile acid transporters may account for the observed variations and need to be further elucidated.

To clarify the role of UCP1 in this regard, we compared the effect of cholic acid supplementation in C57BL/6J wildtype and Ucp1 knockout mice. No differences between both genotypes were detected in body mass development or body composition. Yet, we observed pathological increases in liver enzyme levels that hint at an impairment of liver functionality in both genotypes.

Taking together, bile acid-derived prevention of diet-induced obesity in mice is strain specific and not dependent on Ucp1.

ZUSAMMENFASSUNG

Gallensäuren erfüllen neben ihrer klassischen Rolle als Endprodukt des Cholesterinstoffwechsels und in der Fettverdauung auch eine Funktion als Signalmoleküle und schützen beispielsweise C57BL/6J Mäuse vor einer ernährungsbedingten Adipositas. Dafür verantwortlich gemacht wurde eine durch Gallensäuren verstärkte Thermogenese und damit ein erhöhter Energieverbrauch des Braunen Fettgewebes. Die Notwendigkeit des Braunfett-Proteins *Uncoupling Protein 1* (UCP1), welches die Atmungskette entkoppelt und dadurch Energie als Wärme freisetzt, wurde bisher jedoch nicht zweifelsfrei bewiesen.

In unserer Studie konnte die protektive Wirkung der primären Gallensäure Cholsäure in Mäusen des Inzuchtstammes C57BL/6J nachgewiesen werden. Die Entstehung einer Adipositas durch eine fettreiche Diät konnte in den Tieren, welche zusätzlich mit Cholat supplementiert wurden, verhindert werden. Darüber hinaus bewirkte die Cholatsupplementation eine erhöhte Expression verschiedener Braunfett-Marker-Gene sowie das *Browning* des inguinalen weißen Fettgewebes. Mithilfe der indirekten Kalorimetrie konnte jedoch nachgewiesen werden, dass die gallensäurebedingte Adipositasprävention nicht auf eine Erhöhung des Energieverbrauchs zurückzuführen ist.

Um den *Browning*-Effekt der Gallensäuren zu verstärken, sollten die Ergebnisse in Mäusen des Inzuchtstamms 129S6/SvEvTac verifiziert werden, da Tiere dieses Stamms eine natürlich hohe Neigung besitzen, *Brite*-Adipozyten zu rekrutieren. Entgegen der Erwartungen zeigte die Cholatsupplementation keinerlei Einfluss auf diese Tiere. Weder der Adipositas-präventive Effekt des Cholats, noch dessen *Browning*-Kapazität konnte in 129S6/SvEvTac Mäusen nachgewiesen werden. Hinweise auf mögliche Stammunterschiede lieferte dabei die Gallensäure-Analytik, welche unterschiedliche Gallensäurekonzentrationen in den Organen des enterohepatischen Kreislaufs zu Tage brachte. Verschiedene Gallensäuretransporter-Varianten im Darm könnten hierbei die beobachteten Veränderungen erklären.

Um die Rolle von UCP1 in diesem Zusammenhang zweifelsfrei klären zu können, wurde die Wirkung der Cholatsupplementation in C57BL/6J-Wildtyp- und Ucp1-*Knockout*-Mäusen verglichen. Es wurden dabei keine Unterschiede zwischen den Genotypen identifiziert. Wir beobachteten jedoch einen pathologischen Anstieg der Leberenzymspiegel, der auf eine Beeinträchtigung der Leberfunktion in beiden Genotypen hindeutet.

Zusammenfassend wurde damit erstmals gezeigt, dass die Gallensäure-bedingte Prävention Diät-induzierter Adipositas in Mäusen stammspezifisch sowie Ucp1-unabhängig ist.

1 INTRODUCTION

1.1 Bile acid synthesis, chemistry and function

Bile acids (BAs) are a group of water-soluble steroids that are synthesized in hepatocytes during cholesterol catabolism. They are endogenous detergents (Berry and Reichen, 1983) and thereby help in digestion and absorption of fats. They emulsify dietary lipids and the products of digestion including cholesterol, phospholipids and fatty acids (Jenkins and Hardie, 2008).

Bile is formed by the net movement of water and solutes into the bile canaliculi (Reuben, 1984). Bile secretion is sensitive to metabolic inhibitors (Hofmann, 1990) and temperature changes, as bile flow increases with increasing temperature (Brauer et al., 1954), but it is independent of hepatic perfusion within physiological ranges (Tavoloni et al., 1978). Healthy human subjects normally possess an endogenous bile acid pool of 1.25 to 4 g and daily synthesize approximately 250 to 500 mg under steady-state conditions to compensate for the fecal loss. The whole BA pool daily cycles five to 15 times through the enterohepatic circulation (Berry and Reichen, 1983).

The human liver synthesizes the primary BAs cholic acid (CA) and chenodeoxycholic acid (CDCA) from cholesterol via different intermediates, with cholesterol 7 alpha-hydroxylase (CYP7A1) being the rate limiting enzyme. Prior to excretion, BAs are conjugated at the carboxyl group with glycine and taurine, normally in a ratio of 3 to 1. Glycine-conjugated BAs are the most abundant conjugated BAs, representing more than 70 % of bile, taurine-conjugated BAs represent more tha 20 % of bile (Jenkins and Hardie, 2008). Sulfation and glucuronidation can occur at the hydroxyl groups (Berry and Reichen, 1983). These detoxifying mechanisms can be intensified under pathologic conditions as e.g. intrahepatic cholestasis, where hepatic BA levels reach toxic concentrations (Makino et al., 1975; Stiehl et al., 1980). Bile salts form mixed micelles with phospholipids and cholesterol and are stored in the gallbladder (Chiang, 2013). After secretion into the intestine, secondary bile acids are formed by bacterial dehydroxylation, with deoxycholic acid (DCA) and lithocholic acid (LCA) being the main secondary bile acids. Tertiary bile acids are formed in the liver by epimerization of secondary BAs, which were recycled via enterohepatic circulation (term definition: see 1.2). In humans,

ursodeoxycholic acid (UDCA) is the main tertiary bile acid and is e.g. found in relatively large amounts in sera of hyperlipidemic patients (Pennington et al., 1978), as it possesses a lower toxicity compared to e.g. CDCA and DCA (Leuschner et al., 1989), and is nowadays used as a drug for the treatment of various liver diseases (Eggert et al., 2014). Different BAs possess different absorption efficiencies, therefore the daily synthesis and fractional turnover rates vary for individual BAs (Angelin et al., 1982).

In mice, the primary BAs cholic acid, alpha-muricholic acid (αMCA) and beta-muricholic acid (βMCA), as well as small amounts of chenodeoxycholic (CDCA) and allocholic acid are present, as studies in germ-free mice revealed. In conventional mice, the secondary BAS lithocholic (LCA), deoxycholic ACID (DCA) and omega-muricholic acid (ωMCA) were identified (Eyssen et al., 1976).

1.2 Physiologic bile acid regulation

Bile secretion has a pivotal role in the excretion of both endogenous and exogenous compounds. Many waste products, including bilirubin, are removed from the body by secretion into bile and elimination with feces (Hofmann, 1988). Due to their amphipathic properties, BAs can emulsify lipid compounds, e.g. for fat absorption. Their ability to solubilize fats into emulsions is also potentially toxic for cells depending on lipid membranes maintaining their integrity. Consequently, the process from BA synthesis through the enterohepatic circulation to excretion must be tightly regulated using complex arrangements of chemical pumps (Jenkins and Hardie, 2008). In plasma, BAs circulate mainly bound to albumin, minimizing free concentrations of BAs (Kramer et al., 1979). Protein-bound BAs in plasma are removed with high efficiency by the hepatocytes, with over 80 % extraction of BAs in one pass (Paumgartner and Reichen, 1976). Retuning in portal blood, they are taken up by the hepatocyte via the sodium taurocholate co-transporting polypeptide (NTCP) and organic-anion-transporting polypeptide (OATP) (Hagenbuch and Meier, 1996) (Fig. 1). The transport of BAs from hepatocyte into bile via the canaliculi is rate-limited by the activity of the bile-salt export pump (BSEP), playing a crucial role both in control of intra-cellular concentrations of BAs in the hepatocyte and in secretion of bile. Dietary supplementation of CA to mice leads to an up-regulation of BSEP gene expression by the nuclear BA receptor farnesoid X receptor (FXR), which also demonstrates the role of this receptor as a sensor for the intra-cellular BA

concentration (Sinal et al., 2000). Other transporters that export BAs from the hepatocyte e.g. are the multidrug resistance-related proteins MRP2 and MRP3, two ABC-transporters, that have a merely wide range of substrates and export BAs from hepatocytes into canaliculus (MRP2) or blood (MRP3), respectively, on a limited scale (Gerk and Vore, 2002; Teng and Piquette-Miller, 2007) (Fig. 2).

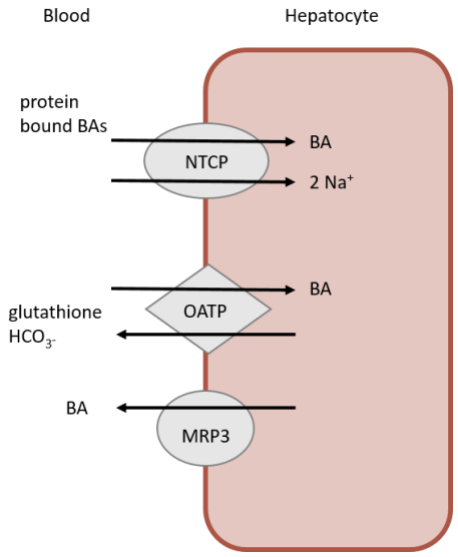

Fig. 1: Hepatocyte basolateral BA transporters. Protein-bound BAs returning in portal blood are taken up by the hepatocyte via the sodium taurocholate co-transporting poly-peptide (NTCP) and organic-anion-transporting polypeptide (OATP). In cholestasis BAs may be returned to blood by the multi-drug-resistance-associated protein 3 (MRP3). BAs cross the hepatocyte bound to 3a-hydroxysteroid dehydrogenase (adapted from Jenkins et al., 2008).

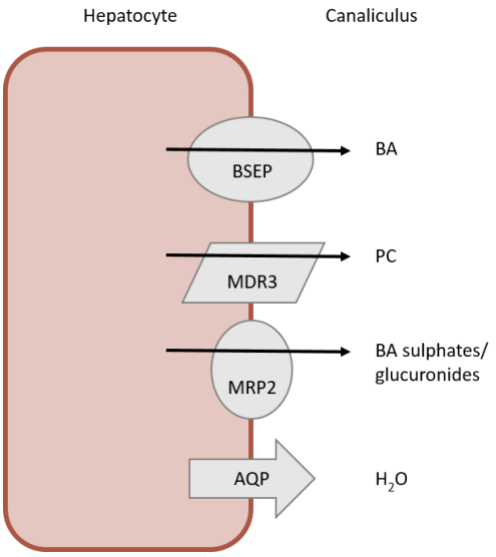

Fig. 2: Secretion of BAs and biliary components. BAs are exported into the canaliculus by the bile-salt export protein (BSEP). Phosphatidylcholine (PC) from the inner leaflet of the apical membrane is flipped to the outer layer and interacts with BAs secreted by BSEP. BAs, PC, together with cholesterol from the membrane form mixed micelles that are not toxic to epithelial membranes of the biliary tree. Aquaporins (AQP) secrete water into bile (adapted from Jenkins et al., 2008).

BA secretion into bile canaliculi stimulates secretion of phospholipids and probably cholesterol, protecting canalicular membrane against the toxic effects of BAs (Coleman et al., 1979). Cholangiocytes, which are the epithelial cells lining the bile ducts, possess amongst others the apical sodium-dependent BA transporter (ASBT). With ASBT, BAs can be absorbed from the bile-duct lumen to cycle back to hepatocytes. This uptake mechanism activates a process called “cholehepatic shunting”, which increases biliary lipid and fluid secretion by the

hepatocyte, thus eliminating toxic bile with high efficiency, especially during increased BA levels (Alpini et al., 2005; Lamri et al., 1992), e.g. occurring during cholestasis (Woolbright et al., 2015) or after dietary BA administration (Watanabe et al., 2006) (Fig. 3).

After its synthesis in hepatocytes and excretion to the ducts, bile can be stored in the gallbladder, a storage and concentrating system for bile during inter-digestive phases (Fahey et al., 1995). Subsequent to food intake, the gallbladder contracts and ejects a bolus of bile into the small bowel where they facilitate fat digestion. Water-soluble pancreatic lipase acts at the surface of intestinal lipid droplets to hydrolyze dietary triglycerides. BAs aid this process by their detergent properties that cause the formation of smaller lipid droplets and thereby increase surface area available for the lipase. The detergent molecules form micelles, which solubilize monoglycerides and fatty acid. Partially, intestinal BA absorption occurs passively, e.g. for unconjugated BAs that have pK values of around 6 and therefore are un-ionized in the intestinal lumen. However, the majority of BAs are conjugated and ionized and therefore require transporters to cross the enterocyte. The majority of BAs is transported Na^+-dependently by ASBT from the small bowel lumen into enterocytes. ASBT mainly transports conjugates, but can also transport unconjugated BAs (Jenkins and Hardie, 2008). In comparison to ileal absorption, the mechanisms responsible for transport of BAs in the proximal intestine and their quantitative significance are not as well defined (Dawson et al., 2009). As BAs enter the enterocyte, they are mostly bound to intestinal BA-binding protein (IBABP) to be transported intracellular across the enterocyte (Vodenlich et al., 1991). BA export from enterocytes into portal blood is majorly driven by the heteromeric organic-solute transporter (OST). OSTα and OSTβ actively transport BAs and some steroids (Seward et al., 2003).

Comparably high levels of OSTα/OSTβ are found at the basolateral membrane of ileal enterocytes and function via a facilitated diffusion mechanism (Ballatori et al., 2013). Other transporters that also are present at the basolateral side may have a role in BA efflux from the enterocyte, too, but this remains to be further defined (Jenkins and Hardie, 2008) (Fig. 4).

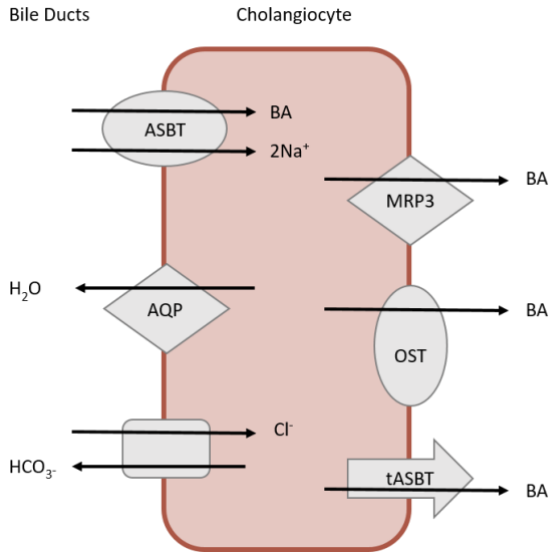

Fig. 3: BA absorption by the cholangiocyte in the cholehepatic shunt. BAs are absorbed at the apical membrane of the cholangiocyte by the apical sodium-dependent BA transporter (ASBT) that causes cholehepatic shunting of BAs back to the hepatocyte. Absorbed BAs are exported across the basolateral membrane by multi-drug-resistance-associated protein 3 (MRP3), a truncated form of ASBT or by OSTα/OSTβ. BAs cause choleresis that is rich in bicarbonate ions secreted by the chloride/bicarbonate ion exchanger (adapted from Jenkins et al., 2008).

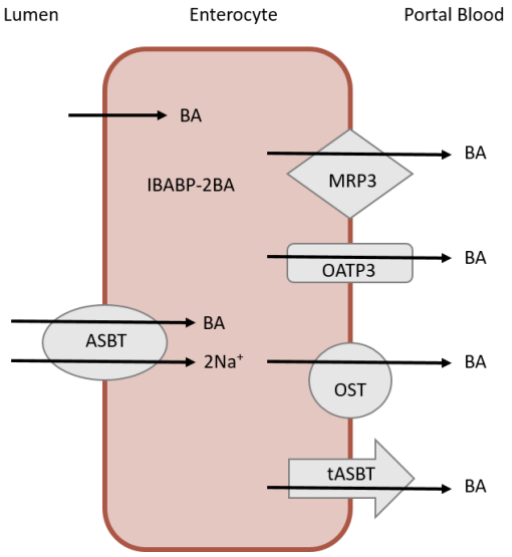

Fig. 4: BA absorption from the small bowel lumen. BAs are efficiently transported from the lumen of the terminal ileum by the apical sodium-dependent BA transporter (ASBT). Unconjugated BAs will be un-ionised at the pH of the lumen and may be passively absorbed. Within the enterocyte BAs are bound by the intestinal BA-binding protein (IBABP). Efflux from the enterocyte may involve the truncated ASBT (tASBT) and/or multi-drug-resistance-associated protein 3 (MRP3) but this remains to be defined. OSTα/OSTβ gene products together but not separately transport BAs out of the enterocyte. OATP3 mRNA has been identified but it is not yet clear whether the protein is functional (adapted from Jenkins et al., 2008).

Beyond enterohepatic circulation, BAs can also escape hepatic extraction and spillover into systemic circulation. As BAs are bound to plasma proteins, glomerular filtration and urinary excretion is reduced. Yet, a small fraction of BAs is also excreted in the urine. Due to a highly efficient tubular reabsorption (Weiner et al., 1964; Wilson et al., 1981), only 1-2 µmol of BAs are found in the urine of healthy patients despite an originally filtered amount of approx. 100 µmol per day (Stiehl, 1974). However, this process contributes to the rise in serum BA concentrations in patients with cholestatic liver disease (Dawson et al., 2009). Even in case of

elevated plasma BA concentrations, e.g. in patients with cholestatic liver disease, the 24-h urinary excretion of nonsulfated BAs is significantly less than the quantity that undergoes glomerular filtration (Raedsch et al., 1981; Rudman and Kendall, 1957; Stiehl et al., 1975).

1.3 Bile acids and metabolic regulation

In the last years, a new role for BAs as signaling molecules has emerged. BAs do not only aid in the absorption of dietary lipids, but also function as metabolic regulators. For example, BAs activate mitogen-activated protein kinase (MAPK) signaling pathways (Gupta et al., 2001; Qiao et al., 2003) and are natural ligands for the nuclear hormone receptor farnesoid X receptor (FXR) (Makishima et al., 1999; Parks et al., 1999; Wang et al., 1999) as well as G-protein-coupled receptors (GPCRs) such as TGR5 (Kawamata et al., 2003; Maruyama et al., 2002).

FXR is a transcription factor that controls both the biosynthesis and enterohepatic recycling of BAs and regulates the expression of the short heterodimer partner (SHP). SHP inhibits the activity of other nuclear receptors like the liver X receptors LXRα and LXRβ, both necessary for the transcriptional induction of CYP7A1, the rate-limiting enzyme of BA biosynthesis. Thereby, the FXR-mediated SHP-induction contributes to the negative feedback regulation of BA biosynthesis (Brendel et al., 2002; Goodwin et al., 2000; Lu et al., 2000). Moreover, FXR induces the fibroblast growth factor FGF19 (FGF15 in mice) in intestinal epithelial cells, which passes to the liver and acts on the FGFR4 (Inagaki et al., 2005; Stroeve et al., 2010) (Fig. 5). Thereby, the hepatic FXR-mediated SHP induction after BA administration inhibits fatty acid and triglyceride biosynthesis and VLDL production (Watanabe et al., 2004). In this way, BAs control their own levels as well as those of their precursor, cholesterol.

TGR5, as a member of GPCRs, was discovered in 2002 (Maruyama et al., 2002). High levels of TGR5 mRNA can be detected in several organs such as small intestine, stomach, liver, lung, placenta and spleen (Keitel et al., 2007; Tiwari and Maiti, 2009). Bile acids are the endogenous natural agonists of TGR5 (Guo et al., 2016). They activate TGR5 and thereby induce cAMP production (Maruyama et al., 2002). TGR5 activation also causes increased intracellular cAMP levels in brown adipose tissue (BAT) and skeletal muscle. This leads to an activation of type 2 iodothyronine deiodinase (D2), which converts inactive thyroxine (T4) to active 3,5,3'-triiodothyronine (T3) (Bianco et al., 2002). The following saturation of thyroid hormone

receptor as well as the activation of PGC-1α leads to an induction of energy expenditure in BAT and skeletal muscle (Watanabe et al., 2006). Moreover, TGR5 signaling induces intestinal glucagon-like peptide-1 (GLP-1) release in entero-endocrine L-cells and thereby increases insulin secretion (Thomas et al., 2009) (Fig. 5). Taken together, BAs not only help in lipid digestion, but were also shown to be potent metabolic regulators. The underlying mechanisms have to be further elucidated, yet.

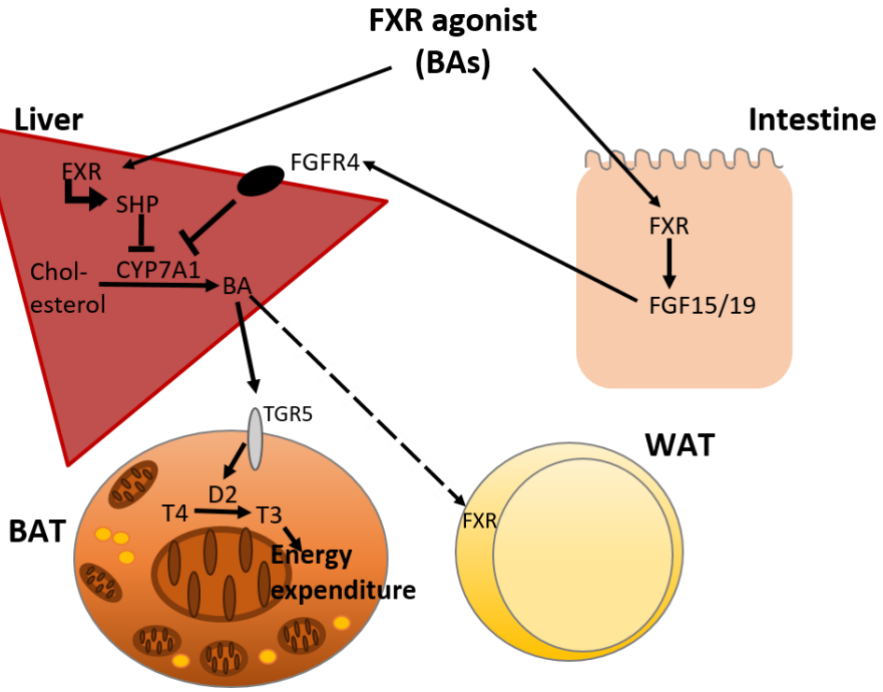

Fig. 5: Impact on energy metabolism after FXR activation, e.g. by BAs or GW4064. Administration of the synthetic FXR agonist GW4064 to high-fat diet fed mice leads to a reduction in BA synthesis and reduced BA pool size. This translates into reduced energy expenditure in BAT, TG accumulation in WAT, BAT, and liver, as well as insulin resistance. As BAs are natural ligands for FXR and activate equal signal transduction routes, similar effects can be observed (adapted from Watanabe et al., 2011).

1.4 Brown, white and brite- the different types of adipose tissue

To date we are aware of three different adipose tissue types: brown, white and brite adipose tissue.

White adipose tissue (WAT) principally is an energy storage that stores dietary energy in times of excess energy intake and releases fatty acids when fuel is required. In the last decades, however, WAT was also discovered to inherit a complex metabolic role. It is an endocrine organ that produces a myriad of endocrine factors called adipokines (Villarroya et al., 2013).

The tissue is e.g. needed for normal glucose homeostasis and plays a role in inflammatory processes through preadipocytes acting as macrophage-like cells (Cousin et al., 1999). A radical change in perspective followed the discovery of leptin, as this critical hormone in energy balance is produced principally by white fat, giving the tissue an endocrine function. Indeed, there is a growing list of protein signals and factors that are released from white adipocytes (Ailhaud, 2000; Mohamed-Ali et al., 1998). These proteins released by WAT are e.g. inflammatory cytokines, play a role in lipid metabolism, and are involved in vascular haemostasis or the complement system. In essence, WAT is a major secretory and endocrine organ, that plays a wide-ranging role in metabolic regulation and physiological homeostasis, far beyond the simple paradigm of fat storage (Trayhurn and Beattie, 2001).

In contrast to WAT, the brown adipose tissue (BAT) is not primarily responsible for lipid storage, but rather is the main site of non-shivering thermogenesis in mammals. BAT is found in almost all mammals and is mainly located at the interscapular region. The active brown fat cell has a round centrally placed nucleus and a granular cytoplasm containing multiple fat vacuoles. It is thus often referred to as multilocular, in contrast to white fat, which is unilocular (Heaton, 1972). The thermogenic processes in BAT are driven by its large number of mitochondria, which also confer the brownish appearance to BAT. They possess a unique biochemical property, wherein the brown adipocyte-specific protein, the mitochondrial carrier protein uncoupling protein 1 (UCP1), uncouples the respiratory chain and thereby dissipates chemical energy as heat. These effects are physiologically activated e.g. in response to cold (Klingenspor et al., 2008). Furthermore, BAT is also known to be a possible site of diet-induced thermogenesis. In response to cold as well as to overfeeding, an activation of the sympathetic nervous system is triggered. Thereby, the thermogenic activity of BAT is induced via distinct cellular processes, including the rapid activation of the existing UCP1 as well as transcriptional induction of the genes encoding UCP1. Moreover, enzymes responsible for oxidizing metabolic substrates, and components of the cellular machinery responsible for the active uptake of lipids and glucose from the circulation, are induced to sustain oxidation and thermogenesis (Cannon and Nedergaard, 2004; Giralt and Villarroya, 2013). In man, brown fat was once considered only necessary in newborns. However, recent morphological and imaging studies have provided evidence that, contrary to prior belief, this tissue is present and active in adult humans (Nedergaard et al., 2007; Townsend and Tseng, 2012). It is speculated,

that the functional BAT has a distinct influence on the prevention of obesity. Ablation of BAT has been shown to sensitize organisms to obesity in several experimental settings (Hamann et al., 1998; Lowell et al., 1993). In contrast, the genetic knockout of the UCP1-encoding gene provided partly conflicting data on the development of obesity under different experimental settings. On the one hand, Ucp1 ko mice were described to be DIO-resistant at room temperature (20° C), as they have to maintain normal body temperature without non-shivering thermogenesis, but by using less efficient, more energy consumptive pathways of metabolism (Liu et al., 2003). Some investigations failed to demonstrate an obese phenotype in Ucp1-ablated mice and did not observe differences in resting oxygen consumption between Ucp1-ko and wildtype mice at 28°C (Enerback et al., 1997). In contrast, another study showed that an Ucp1-ablation in itself is sufficient to induce obesity under thermoneutral conditions (Feldmann et al., 2009). For this reason, scientific examinations that investigate anti-obesogenic properties on Ucp1-ablated mice need to be performed with an adequate control group that investigates whether the ko-mice can develop obesity under the specific present conditions.

Besides its capacity of metabolite oxidation for thermogenesis, accumulating evidence indicates that BAT also exhibits an endocrine role, as genetically mediated ablation of BAT (Hamann et al., 1996; Lowell et al., 1993) had a much more profound impact on metabolism than specific blockage of BAT thermogenic activity via Ucp1 invalidation (Enerback et al., 1997). It is assumed, that the endocrine factors possibly released by BAT, and termed “batokines” (for “BAT adipokines”) (Stanford et al., 2013; Townsend and Tseng, 2012), may have different or probably opposite effects than those of the WAT adipokines, act on other tissues, and will be actively released if BAT is activated. The endocrine function of BAT is not doubtlessly proved, so far. However, BAT is deemed to release autocrine or paracrine factors, amongst others T3, angiotensinogen, or also FGF21, which is induced upon cold and adrenergic stimulation (Townsend and Tseng, 2012; Villarroya et al., 2013).

In humans, there were also found BAT-like depots, e.g. in the supraclavicular, but also in the interscapular regions of the body. Initially, it was believed to be the equivalent of the interscapular thermogenic organ of small mammals. However, this view was disputed, as it was demonstrated, that this depot consists of a newly identified type of brown adipocytes that is distinct from the classical brown adipocytes (Lidell et al., 2013):

In addition the “classical” two adipose tissues WAT and BAT, cells exhibiting a brown adipocyte thermogenic phenotype, but appear in WAT depots after thermogenic activation have been identified and characterized. These so-called “brite” (from “brown in white”) or also “beige” adipocytes are multilocular and express Ucp1. Classical brown adipocytes present in BAT depots are closely related to skeletal muscle precursors (Seale et al., 2008; Timmons et al., 2007) and in fact, both brown adipocytes and myocytes share a common precursor that expresses the myogenic lineage marker Myf5. In contrast, brite adipocytes were found to come from Myf5-negative cells that more closely resemble white adipocyte precursors (Seale et al., 2008). Different processes that give rise to brite adipocytes are discussed: On the one hand, the browning process seems to arise partly or in whole via the transdifferentiation of white adipocytes into brite adipocytes (Barbatelli et al., 2010). Besides, genetic labelling of adipose cells supports the existence of bidirectional interconversion processes between brite and white adipocytes (Rosenwald et al., 2013). Indeed, brite adipocytes apparently represent intermediate forms of adipocytes, as they do not only express Ucp1 and reside in WAT depots, but also are mitochondria-rich, multilocular and show a lipid droplet distribution intermediate between that of brown and white adipocytes. According to some, these “paucilocular” adipocytes may constitute transition states from white to brite adipocytes (Barbatelli et al., 1993; Himms-Hagen et al., 2000). On the other hand, some reports indicated that β_3-adrenergic activation induces browning through two different processes: white to brown transdifferentiation in inguinal WAT, but proliferation and further differentiation of precursors in epididymial WAT (Giralt and Villarroya, 2013; Lee et al., 2012). Moreover, the hitherto distinct separation into adipocytes with Myf5-positive or Myf5-negative precursor cells has been challenged to some extent by the finding that Myf5-positive precursors may also differentiate to white adipocytes (Sanchez-Gurmaches et al., 2012; Schulz et al., 2013).

Despite the unclear origination of brite cells, there is genetic evidence that the capacity to induce these cells is highly relevant for protection against obesity in rodents (Guerra et al., 1998). Inversely, mouse strains that have an increased tendency to become obese rather show decreased capacities for browning of WAT depots compared with those of obesity-resistant strains, despite similar BAT size, activity and capacity to recruit classical BAT in response to thermogenic activation (Guerra et al., 1998; Xue et al., 2007). These results suggest that the

browning process has a special, independent relevance in protection against obesity (Giralt and Villarroya, 2013).

1.5 Effect of bile acids on obesity

Obesity is a global epidemic that causes significant morbidity and mortality (Jenkins and Hardie, 2008). Manifold approaches from public education, to legislative procedures, to medical treatments are studied and applied to encounter this complex of problems. Thereby always new paths are struck. In the last years, a new role for bile acids as signaling molecules and metabolic regulators has emerged. Traditionally, BAs have been linked to the development of obesity through their role in the intestinal absorption of fatty acids. However, recent studies indicate that BAs have a much wider role in the regulation of energy balance in the body (Jenkins and Hardie, 2008).

In 1997, a study by Ikemoto and colleagues was the first to suggest a link for BAs in the regulation of obesity. They demonstrated that the addition of the common bile salt sodium cholate (0.5 %) to a high-fat diet prevented increases in total body weight and WAT in C57BL/6J mice compared to littermates fed a non-supplemented high-fat diet. These effects occurred despite similar energy intakes across control (high-carbohydrate), high-fat and cholate-supplemented high-fat diet groups, indicating that the cholate-associated effect was not simply a reflection of reduced calorie intake in the supplemented animals. Cholate supplementation also prevented the development of hyperglycemia and reduced blood insulin levels compared with high-fat-diet-fed animals. Similar effects were reported with supplementation of the other primary BA, CDCA (Ikemoto et al., 1997).

Watanabe and colleagues confirmed and extended these findings, as they directly linked BAs to the regulation of thermogenesis. It was demonstrated that CA-supplementation does not only reduce high-fat-diet-induced weight gain but also reverses the established weight gain in obese mice, resulting in reduced WAT mass and improved glucose tolerance. These effects were described to result from increased energy expenditure in CA-supplemented animals, rather than reduced caloric intake, as these animals showed a higher O_2 consumption and CO_2 production compared to control animals during short-term indirect calorimetry measurements (Watanabe et al., 2006) (Fig. 6).

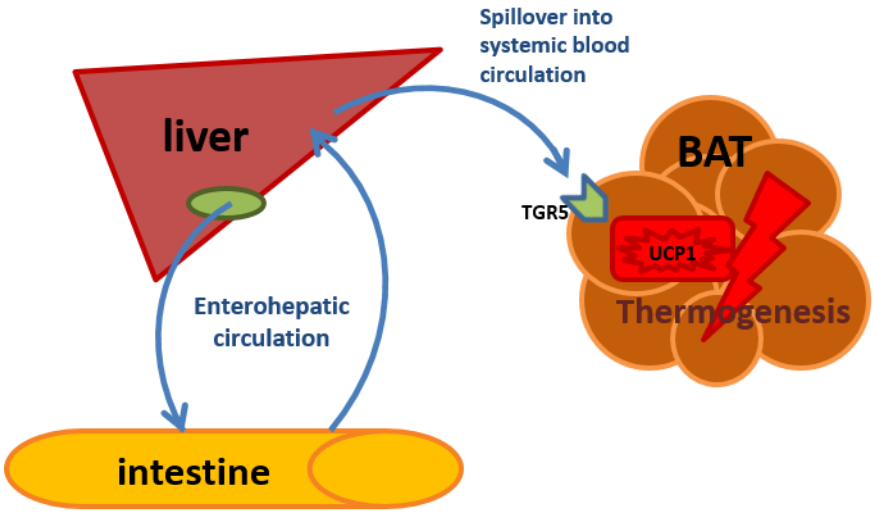

Fig. 6: Schematic illustration of bile acid-derived induction of thermogenesis. During digestion, bile acids are secreted with bile from the gallbladder and released into the intestine to emulsify dietary lipids, etc. They can be transferred back to the hepatocytes by intestinal reabsorption. Besides this recycling mechanism, which is called "enterohepatic circulation", BAs also spillover from liver into systemic blood circulation. Thereby they reach peripheral sites of action, amongst others brown adipose tissue, where they are supposed to bind to the G-protein-coupled BA receptor TGR5, thereby increase Ucp1 expression and induce thermogenesis.

Moreover, electron microscopy revealed that CA-supplementation resulted in an increased number of BAT mitochondrial lamellar cristae. Microarray analysis showed a strong up-regulation of type-2 iodothyronine deiodinase (D2) mRNA in BAT of CA supplemented animals (Watanabe et al., 2006). The enzyme D2 converts thyroxine (T4) to active 3,5,3-tri-iodothyronine (T3) and is required for adaptive thermogenesis in BAT (Bianco et al., 2002).

The authors suggested that this effect was mediated via the G-protein-coupled BA receptor (GPBAR-1 or TGR5) resulting in a BA-derived cAMP-PKA activation in BAT cells (Fig. 7). TGR5 is ubiquitously expressed in humans and animals (Duboc et al., 2014) and its signal transduction is stimulated in varying intense, dependent on the respective BA. For example in HEK293-hBG37 cells, the rank order of potency was LCA > DCA > CDCA > CA (Maruyama et al., 2002).

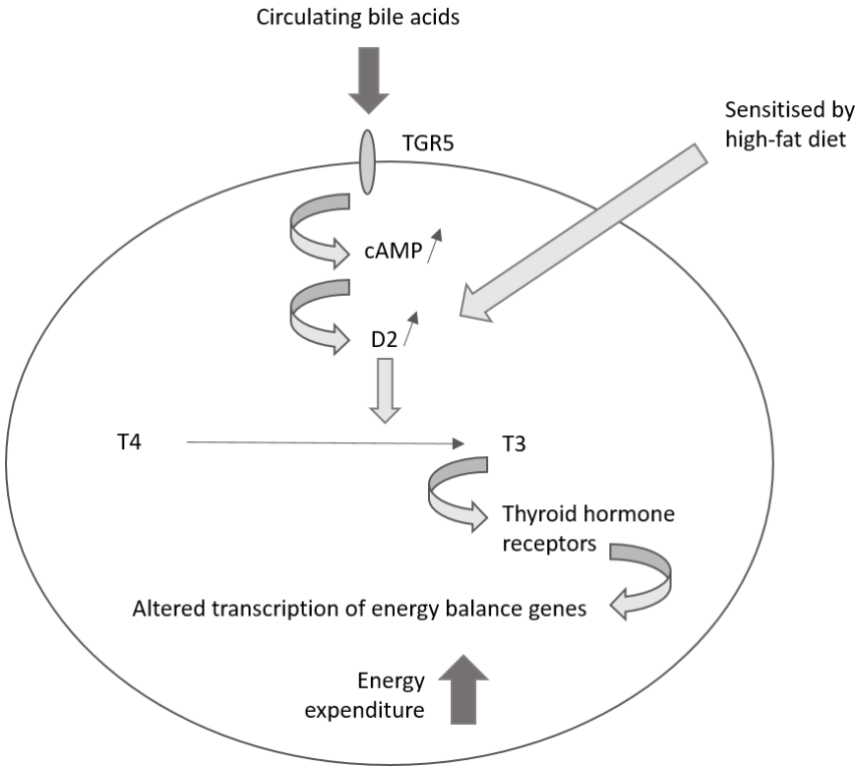

Fig. 7: The effect of BAs on energy expenditure. Circulating BAs bind to the G-protein-coupled BA receptor TGR5, which stimulates increased cAMP-PKA activation and increased expression of D2. This response is sensitized by a high-fat diet. D2 converts T4 to active T3, which stimulates thyroid hormone receptor binding to target genes. This leads to an altered expression of genes associated with energy balance and increased energy expenditure (adapted from Jenkins and Hardie, 2008).

Besides TGR5, BAs are also natural ligands for the farnesoid X receptor (FXR). FXR belongs to the nuclear hormone receptor family and is activated most potently by the hydrophobic BA CDCA, whereas hydrophilic UDCA demonstrates little activity (Makishima et al., 1999; Parks et al., 1999; Wang et al., 1999). FXR activation leads to a decreased endogenous BA production, and thereby protects liver cells against toxic high BA levels. Moreover FXR directly affects adipocyte differentiation and function and may play an important role in the regulation of systemic lipid metabolism and peripheral glucose homeostasis (Kalaany and Mangelsdorf, 2006). The loss of FXR using a gene knockout model results in impaired adipocyte differentiation, impaired glucose tolerance, insulin resistance and dyslipidemia (Cariou et al., 2007; Rizzo et al., 2006; Sinal et al., 2000). These data raise the possibility that targeted FXR activation may also be useful to manage various aspects of the metabolic phenotype including type-2 diabetes, dyslipidemia and adipocyte function (Jenkins and Hardie, 2008).

In summary, the findings of the recent years raised the possibility that targeting BA signaling pathways may ameliorate obesity and associated pathologies such as insulin resistance, impaired glucose tolerance and dyslipidemia and promise to be highly active areas of research in the future (Jenkins and Hardie, 2008). However, BAs are potent detergents that may disrupt cell membranes and can promote the generation of reactive oxygen species that, in turn, oxidatively modify lipids, proteins, and nucleic acids, and eventually cause hepatocyte necrosis and apoptosis. Toxic BAs, especially hydrophobic BAs, can activate hepatocyte death receptors directly and induce oxidative damage. Thereby mitochondrial dysfunction is caused, and endoplasmic reticulum stress is induced (Perez and Briz, 2009). For this reason, the direct impacts of a BA-supplementation always have to be calculated and its risks need to be balanced against its potential advantages.

1.6 Aims and scope

This study is based on the studies of Watanabe and colleagues from 2006, showing that a dietary BA-supplementation prevents and ameliorates diet-induced obesity in mice fed a high-fat diet by a mechanism dependent on type-2 deiodinase (Watanabe et al., 2006). However, the authors did not provide a substantive, direct proof of neither brown adipose tissue recruitment nor UCP1 activation within this context. In order to prove the reproducibility of their experiment, Watanabe's key experiment should initially be repeated. Afterwards, the Ucp1 ko mouse model was used to directly prove the role of UCP1 in BA-derived protection of obesity. Additionally, 129S6/SvEvTac mice were used to assess the potential anti-obesogenic effects of white adipose tissue browning within this context. With the help of the obtained findings, we would be able to further enlighten and investigate the underlying molecular mechanisms of BA-mediated DIO-prevention.

2 MATERIAL AND METHODS

2.1 Animals

We employed male mice of the C57BL/6J and 129S6/SvEvTac inbred strains bred in our specified pathogen-free facility (at TU München, *Kleintierforschungszentrum*, Freising, Germany) with regular hygiene monitoring according to FELASA (Federation of European Laboratory Animal Science Associations) criteria at 50-60 % relative humidity, 22 °C ± 1°C and a 12-hour light/dark cycle. All mice received standard rodent chow diet (V1124-300, Ssniff Spezialdiäten GmbH) prior to experiments. They were housed in individually ventilated cages (IVC, type II long, 540 cm², Tecniplast, USA) up to five animals per cage.

Uncoupling protein 1 (Ucp1) knockout (ko) mice on C57BL/6J background were generated by Leslie Kozak and coworkers (Enerback et al., 1997; Hofmann et al., 2001) and founder mice were kindly provided to establish our colony. Wildtype (wt) and Ucp1 ko mice obtained from heterozygous breeding were mated in homozygous wt/wt and ko/ko breeding pairs. These pairs were kept at 30 °C inside a climate cabinet (HPP749, Memmert), where offspring was born, raised and subjected to experiments. Homozygous breeding allowed a usage of averagely 50 % of the offspring (only male mice). This approach facilitated direct comparisons of littermates, as usually more than one male offspring was born in each litter (in contrast to this approach, breeding heterozygous mice results in only one male, homozygous mouse ($Ucp1^{+/+}$ or $Ucp1^{-/-}$) each litter on average). Up to five animals were kept in open cages (type II long, 540 cm², Tecniplast, USA) with a 12-hour light/dark cycle and relative humidity of 50-60 %. Procedures were carried out in accordance with the German animal welfare law and approved by the Regional Government of Oberbayern, Germany.

2.2 Diets

Data were collected in three independent experiments characterized by the administration of four diets. Mice received control (C, S5745-E702) or high-fat (H, S5745-E712) diet providing 13 % or 48 % of energy from fat, respectively. To investigate the effect of dietary BA administration, these diets were supplemented with 0.5 % (w/w) sodium cholate at the expense of cornstarch to generate C + cholate (CC, S5745-706) and H + cholate (HC, S5745-

716) diets. All diets were obtained from Ssniff Spezialdiäten GmbH, Germany and fed *ad libitum*:

1) C: low fat control diet (5 % soy oil, 5 % saccharose; ssniff order number S5745-E702)

2) CC: low fat control diet containing 0.5 % cholic acid (ssniff order number S5745-E706)

3) H: high-fat diet (20 % palm oil, 5 % soy oil, 5 % saccharose; ssniff order number S5745-E712)

4) HC: high-fat diet containing 0.5 % cholic acid (ssniff order number S5745-E716)

Cholic acid was mixed into the homogenized food powder as sodium compound [Na-Cholate: CAS: 361-09-1], which afterwards was pressed to feeding pellets. This procedure prevents demixing and assures homogenous distribution of cholic acid within the pellet.

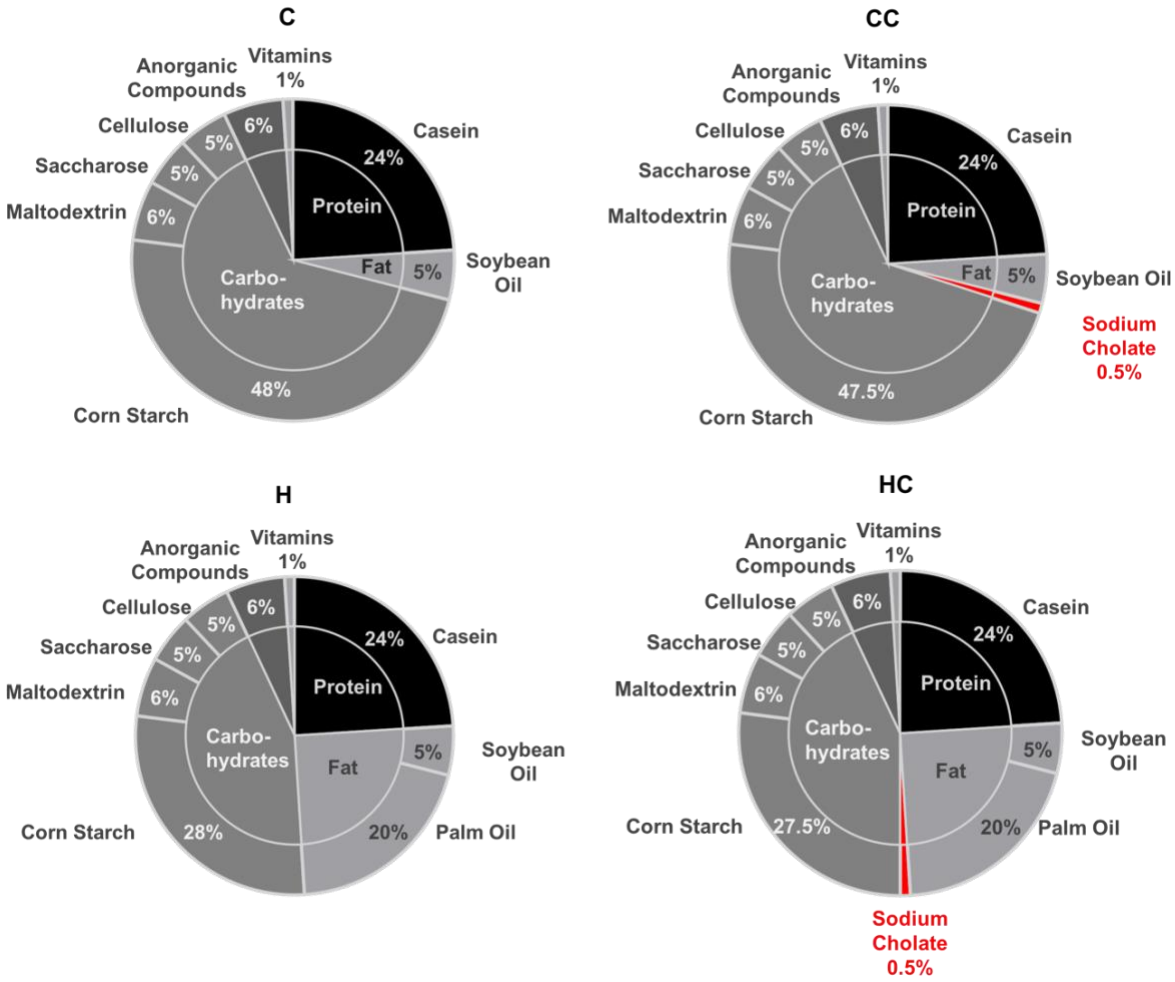

Fig. 8: Composition of experimental diets used in this thesis. The custom-made semi-purified diets were obtained from Ssniff Spezialdiäten GmbH, Soest, Germany: (A) C, S5745-E702, (B) CC, S5745–E706, (C) H, S5745-E712, (D) HC, S5745–E716. Macronutrients are given in percent by weight. Weight of supplemented sodium cholate was equalized by the percentage weight reduction of corn starch.

2.3 Cholic acid supplementation in C57BL/6J and 129S6/SvEvTac mice

Male C57BL/6J and 129S6/SvEvTac mice were assigned to one of the four diet groups (n=4-7 per diet group) at the age of 6-7 weeks and kept at room temperature for 4 weeks. Mice were housed individually. Body mass and food consumption were measured twice weekly. Body composition (fat mass and lean mass) was determined noninvasively using the time domain (TD-)NMR analyzer (MQ 7.5 NMR, Minispec, Bruker Optic GmbH, Germany) at the beginning, as well as after 2 and after 4 weeks of experiment. Data were analyzed with the MinispecPlus (Bruker Optic GmbH) and OPUS (OPUS Version 5.0, Bruker Optic GmbH) software. To determine assimilated energy, feces was collected of all individual mice during first and fourth week of experiment and its energy content subtracted from energy intake. Mice were euthanized with carbon dioxide. Plasma samples, iBAT, iWAT and enterohepatic organs (one sample containing small and large intestine, caecum, liver, gall bladder and pancreas) were removed during dissection and weighed. As two tissue locations exist from iWAT and iBAT at the left and on the right side of the body, the right-sided part was fixed for histologic examinations (see 2.5), the left-sided part as well as plasma and enterohepatic organs were shock frozen using liquid nitrogen and stored at -80 °C for further analyses.

2.4 Cholic acid supplementation in Ucp1 knockout and wildtype C57BL/6J mice

In order to challenge the hypothesis, that CA-derived resistance to DIO is due to increased thermogenic processes in BAT, we used Ucp1 ko C57BL/6J mice for a further feeding experiment. As body temperature is basically maintained via thermogenic processes, which should not be involved in these energy expenditure investigations, all animals (both wt and Ucp1 ko mice) were kept at thermoneutrality (30 °C) during pregnancy, breeding and the experimental phase. Except surrounding temperature, and open cages instead of IVC-cages, animals were kept under same conditions as for earlier experiments (as described above, part 2.1). At the age of 6 to 7 weeks, male mice were adapted to control diet for one week to circumvent an initial body mass drop that was observed in earlier experiments due to acclimatization problems to the harder texture of the semi-purified diets in comparison to chow diet. At the age of 7-8 weeks mice were assigned to one of the four experimental diets and kept at thermoneutrality for four further weeks (n=6 per group). Body mass and food

consumption were recorded twice weekly. At the day of diet switch (from control diet to the respective experimental diet) as well as after two and four weeks of experimental phase, body composition (fat and lean mass) was analyzed noninvasively as described above (2.3). At the end of the experiment, mice were euthanized with carbon dioxide.

2.4.1 Plasma collection and blood parameter measurement

Cardiac blood was collected from 6-8 hours fasted mice (fasting duration depended on dissection order) in a lithiumheparin-coated tube. The time window of blood collection did not exceed 2.5 hours during day time. Blood samples were centrifuged for 5 min at 2000 g. The plasma -appearing as supernatant- was removed, frozen in liquid nitrogen and stored at -80 °C. Plasma biomarker determination was performed with Piccolo Lipid Panel Plus Discs and the automated analyzer Piccolo xpress^{TM} (HITADO GmbH, Germany). Thereby plasma concentrations of cholesterol, HDL, triglyceride, glucose as well as liver enzymes alanine aminotransferase (ALAT) and aspartate aminotransferase (ASAT) were determined simultaneously.

2.4.2 Tissue dissection

After blood collection iWAT, eWAT, iBAT, liver, heart and kidneys were dissected and weighed. As two fat tissue locations exist from iWAT, eWAT and iBAT at the left and on the right side of the body, the right-sided part was fixed for histologic examinations (see 2.5). The left-sided part as well as liver, heart and kidneys were shock frozen using liquid nitrogen and stored at -80 °C for further analyses.

2.5 Tissue sample preparation for histologic analyses

2.5.1 Tissue fixation and paraffin embedding

Dissected tissues were fixed in 4 % paraformaldehyde solution with 0.0024 % picric acid for one week. Afterwards, fixated tissues were dehydrated in a series of increasing volume percent ethanol and xylene and infiltrated with Paraplast (Leica).

Table 1: Automated dehydration steps and respective incubation times for tissue paraffin embedding

Bin #	Content	Incubation time [min]
1	70 % EtOH	60
2	70 % EtOH	60
3	80 % EtOH	60
4	80 % EtOH	60
5	90 % EtOH	60
6	90 % EtOH	60
7	99 % EtOH	60
8	99 % EtOH	60
9	Xylene	60
10	Xylene	60
11	Paraplast	60
12	Paraplast	60

Afterwards, infiltrated tissue samples were paraffin embedded and cut with a rotary microtome (Leica). For that, about 1/3 of the tissue was discarded to reach interior tissue parts and be able to draw tissue-specific conclusions. Sections of 5 µm thickness were mounted on specimen slides (Carl Roth) and dried for 3 days at 55 °C.

2.5.2 Hematoxylin & Eosin (H&E) staining

For H&E staining, dried sections were transferred to a Multistainer (Leica) to ensure a standardized coloration. Hematoxylin and Eosin stains (Carl Roth) were used to color nuclei (Hematoxylin, blue stain) and cytosolic (Eosin, red/pink stain) structures. Stained sections were mounted in Roti-Mount (Carl Roth).

Table 2: Automated H&E staining steps

Bin #	Content	Incubation time [min]
1	Xylene	3
2	Xylene	3
3	100 % EtOH	2
4	96 % EtOH	2
5	70 % EtOH	1
6	distilled water	1
7	Hematoxylin	5
8	flow water	4
9	Eosin	2
10	70 % EtOH	1
11	96 % EtOH	1
12	100 % EtOH	1
13	100 % EtOH	1.5
14	Xylene	1.5
15	Xylene	2
16	Xylene	2

2.5.3 Immunohistochemistry (IHC)

In order to detect UCP1-positive cells, IHC staining was conducted (we were not able to conduct Western blots, as we used both iWAT parts for qPCR & histological analyses). For IHC analyses, dried H&E-stained tissue sections were heated at 70 °C for 10 min and deparaffinized in xylene and a decreasing ethanol gradient (99 %, 80 % and 70 %). Afterwards, sections were unmasked at 90 °C in 20 mM sodium-citrate for 20 min and in 10 mM sodium-citrate for 10 min. Next, the sections were rinsed with dH_2O three times, 5 min each, incubated in 3 % H_2O_2 for 10 min, rinsed in dH_2O for 5 min, incubated with 2.5 % blocking buffer (goat serum in PBS) for 1 h at room temperature and rinsed again three times for 5 min in dH_2O. Sections were incubated overnight with 1:500 diluted primary UCP1 antibody (Abcam, ab10983) in 0.25 % goat serum and 0.1 % PBS-T at 4 °C. After rinsing three times 5 min each in 0.1 % PBS-T, sections were incubated with 1:200 diluted HRP conjugated secondary antibody (Abcam, ab97051) for 1 h at RT. Afterwards, sections were rinsed three times in 0.1 % PBS-T, 5 min each and incubated with DAB enhanced mix (Leica) for 2 min. DAB reaction was stopped by rinsing the sections in ddH_2O. Subsequently sections were incubated for 3 min in hematoxylin

and rinsed with ddH_2O. Sections were then dehydrated in increasing ethanol concentrates (70%, 96% and 100%) and xylene for 2 min each. Sections were mounted in Roti-Mount (Roth).

2.6 Calculation of assimilated energy by balancing dietary energy intake and fecal energy loss

The part of dietary energy that is absorbed in the gut and not lost with feces is called assimilated energy. To estimate assimilated energy, dietary energy intake was opposed fecal energy loss. Energy intake and energy loss are calculated by multiplying food or feces mass with its corresponding energy content, respectively. Energy content of food and feces samples was determined by bomb calorimetry analysis. For that purpose, food intake and feces mass was recorded as stated above (2.3). Feces was separated from litter, dried at 55 °C for at least one week and homogenized with a bead mill (TissueLyser II, Retsch, Qiagen, Hilden, Germany). Around 1 g of the homogenized feces was used to press a pellet. The exact pellet weight was noted. As food samples already were homogenized, a food pellet of around 1 g (the exact weight was noted) was used for further analysis. To analyze the energy content of food and feces samples, a bomb calorimeter (Calorimeter 6300, Parr, Frankfurt, Germany) was used. Within the bomb calorimeter, the dried sample is burned under high pressure of excess pure oxygen. During combustion, energy is released as heat. The induced temperature rise (ΔT) is measured with a thermometer and used to calculate the energy content (J/g) of the sample:

$$Caloric\ value\ (J/g) = W * \frac{\Delta T}{G}$$

W = heat capacity of the calorimeter (J/K)
ΔT = temperature change (K)
G = sample weight (g)

The heat capacity is defined as the amount of heat needed to increase the temperature of the entire calorimeter by 1 °C.

2.7 Energy expenditure analysis by indirect calorimetry measurements

Energy expenditure of mice was determined by indirect calorimetry (CaloSys SPEC, LabMaster, TSE Systems, Bad Homburg, Germany). In subjects with aerobic metabolism dietary nutrients

are converted to energy under oxygen consumption and carbon dioxide production. The caloric equivalent, which corresponds to the energy per liter oxygen consumed, is used to determine energy expenditure. Depending on the substrate that is oxidized, the caloric equivalent ranges from 19-21 kJ*l O_2^{-1}.

Two weeks before experimental start and during the first two days of measurement all mice received the control diet to acclimate to the texture and taste of the experimental diet as well as the altered habitat. The diet change to either H or HC diet was conducted in the time period between 9 am and 1 pm (cohort 1: 9 am, cohort 2: 12 am, cohort 3: 1 pm). For indirect calorimetry measurements, up to eight mice were kept individually in special modified home cages and placed in a temperature-controlled climate chamber (Feutron) at 23 °C. Air was aspirated with a constant flow rate of 0.7 l*min^{-1}. The volumes of oxygen consumed (Δvol % O_2) and carbon dioxide produced (Δvol % CO_2) were determined automatically every nine minutes. Mice were kept in the indirect calorimetry chamber for seven days. After 48 hours in the climate chamber, diet was changed to high-fat diet with our without cholic acid supplementation, in each case to the half of all animals. Body weight was determined at five specific time points:

- Previous to indirect calorimetry measurements: 14, 7 and 2 days before diet change
- After indirect calorimetry measurements: 5 and 8 days after diet change, which corresponds to the beginning and the end of the subsequent FDA measurement

Body weight and food intake were not measured during indirect calorimetry phase, in order to not distort gas concentrations (overview experimental setup: see Fig. 2).

The respiratory exchange ratio (RER) was calculated for each data point every nine minutes according to the following equation:

$$RER = \Delta CO_2\ [\%] / \Delta O_2\ [\%]$$

The RER indicates, which substrate is mainly oxidized for energy generation. It ranges within the limits from 1.0 (carbohydrates), 0.81 (proteins) to 0.705 (lipids) (Even and Nadkarni, 2012).

Oxidation of one carbohydrate molecule:

$$6\ O_2 + C_6H_{12}O_6 \rightarrow 6\ CO_2 + 6\ H_2O + 38\ ATP$$

$$RER_{carbohydrate} = VCO_2/VO_2 = 6\ CO_2/6\ O_2 = 1.0$$

Oxidation of one fatty acid molecule:

$$23\ O_2 + C_{16}H_{32}O_2 \rightarrow 16\ CO_2 + 16\ H_2O + 129\ ATP$$

$$RER_{fatty\ acid}: VCO_2/VO_2 = 16\ CO_2/23\ O_2 = 0.7$$

$MeanRER_{24h}$ was assessed by calculating the mean RER value for 24 hours at the second day of measurement (the first day was discarded as acclimatization phase).

The caloric equivalent (CE), which is the number of kilojoules produced per liter of oxygen consumed, was calculated according to the following equation:

$$CE\ [kJ*l\ O_2^{-1}] = 16 + 5*meanRER_{24h,\ ad\text{-}lib}$$

The daily energy expenditure (DEE), which is the energy expended during 24 hours, was calculated according to the following equation:

$$Daily\ energy\ expenditure\ (DEE)\ [J/d] = CE\ [k*l\ O_2^{-1}] * meanVO_{2,\ 24h}\ [ml*d^{-1}]$$

Resting metabolic rate (RMR), which represents the minimum amount of energy required to maintain body functions at rest, under thermoneutrality (30 °C) and fasted, was calculated according to the following equation:

$$Resting\ metabolic\ rate\ (RMR)\ [J/h] = CE\ [kJ*l\ O_2^{-1}] * VO_{2,\ rest}\ [ml\ O_2*h^{-1}]$$

$VO_{2,\ rest}$ was specified by selecting the lowest VO_2 consumption rate during all days of measurement, which normally can be found during the resting phase of the animals at day times.

DEE and RMR were corrected for body composition. As lean mass is metabolically more active than fat mass, a correction formula, that involves fitting both lean mass and fat mass as independent variables and that weighs lean mass stronger than fat mass, was used: lean mass + 0.2 fat mass (Even and Nadkarni, 2012).

2.8 Feeding-drinking-activity measurements

Subsequent to indirect calorimetry measurements, mice were transferred to a feeding-drinking-activity system (TSE Systems), where food intake and spontaneous locomotor activity were measured automatically. Mice were kept in type III cages (820 cm^2) at room temperature with *ad libitum* access to food and water. Food intake was measured in 5-minutes intervals. Physical activity was identified via infrared photo sensors three-dimensionally (X, Y and Z directive light barriers). The first day of measurement was skipped as acclimatization phase of mice and analysis started at 0:00 a.m. at day 2. Food intake and activity (given as distance covered in meters) were analyzed cumulatively or in absolute numbers in 12-hours periods (light/dark phases), respectively.

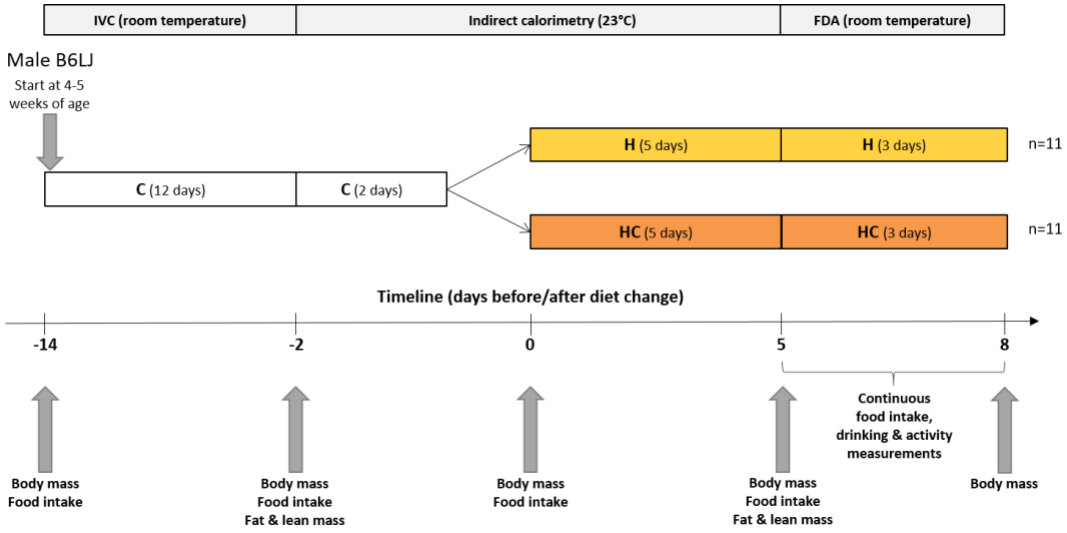

Fig. 9: Overview of experimental setup for indirect calorimetry and subsequent feeding-drinking-activity measurements (C: control diet, FDA: Feeding-drinking-activity measurement, H: high-fat diet, HC: high-fat diet supplemented with 0.5 % cholic acid, IVC: Individually ventilated cage).

2.9 RNA isolation from tissue samples, cDNA synthesis and quantitative real-time polymerase chain reaction (qRT-PCR)

Total tissue RNA was isolated by homogenizing tissue samples in 1000 µl TRIsure (Bioline) for 20 s using an Ultra-Turrax (IKA) and incubating for 5 min at room temperature. For tissues with high fat content, such as iWAT or eWAT, an intermediate centrifugation step of 2500 g for 5 min was inserted to separate the homogenate from the top lipid phase. Afterwards, the samples were mixed with 200 µl chloroform, incubated for further 3 min at room temperature

and centrifuged for 15 min, 12000 *g* at 4 °C. The clear top phase was mixed with 500 µl 75 % ethanol, transferred to columns of the SV Total RNA Isolation System (Promega) and proceeded according to the manual. RNA was eluted in 50 µl nuclease-free water and concentration was measured spectrophotometrically (Infinite® 200 NanoQuant, Tecan). RNA integrity was assessed on a 1.5 % DNA agarose gel (note: DNA gels were tested to assess rRNA samples and found to be equally suitable with RNA gels). 800 ng of isolated RNA (about 15 µl sample) were mixed with 10 µl nuclease free H_2O as well as 5 µl loading buffer and separated by length on the DNA agarose gel for approximately 40 min at 100 V to visualize the 28S and 18S rRNA bands. RNA was portioned into aliquots and stored at -80 °C.

loading buffer (6x concentrated):
10 mM Tris-HCl (pH 7.6), 0.2 % OrangeG, 60 % glycerol, 60 mM EDTA

1.5 % agarose gel:
3 g agarose, 200 ml TAE-Buffer (Roth), 10 µl Roti Safe (Roth)

Isolated RNA was reverse-transcribed into cDNA by means of the QuantiTect® Reverse Transcription Kit (Qiagen), which utilizes oligo-dT and random primers in a 10 µl reaction mixture containing 500 ng RNA, was used. cDNA was stored at -20 °C. Primer sequences were designed using the Primer3 algorithm (SDSC Biology Workbench) and tested in a non-quantitative PCR. Only primer pairs that generated a single, sharp product band were applied in the qRT-PCR analysis. Primers were produced by Eurofins Genomics and sequences were as follows:

Ucp1: for: 5’-TCT CTG CCA GGA CAG TAC CC-3’, rev: 5’-AGA AGC CCA ATG ATG TTC AG-3’

Cidea: for: 5’- TGC TCT TCT GTA TCG CCC AGT-3’, rev: 5’-GCC GTG TTA AGG AAT CTG CTG-3’

Cox7a1: for: 5’-CCG ACA ATG ACC TCC CAG TA-3’, rev: 5’-TGT TTG TCC AAG TCC TCC AA-3’

Otop1: for: 5’-ACT AGG ACC CCG TCG AAT CT-3’, rev: 5’-ACC ATG CTC TAC GTG CTG TG-3’

Hsp90: for: 5’-AGG AGG GTC AAG GAA GTG GT-3’, rev: 5’-TTT TTC TTG TCT TTG CCG CT-3’

ActB: for: 5’-AGA GGG AAA TCG TGC GTG AC-3’, rev: 5’-CAA TAG TGA TGA CCT GGC CGT-3’

Gene expression was determined from a standard curve consisting of pooled cDNA in 28-fold dilution. Expression levels of target genes were normalized to the mean of heat shock protein 90 (Hsp90) and beta-actin (ActB) expression.

For analysis of gene expression, the SYBR Green-based qRT-PCR was performed either on 96-well (Mastercycler® ep realplex epgradient S, Eppendorf) or 384-well format (Roche LightCycler® 480) according to tables 3 and 4. A melting curve was recorded at the end of the program to confirm the quality of the amplified product and identify possible non-specific reaction products.

Table 3: qRT-PCR reaction mixture for gene expression analysis

	Volume per reaction [µl]	
	96-well plate	**384-well plate**
Sensimix SYBR No-ROX (Bioline)	12.5	6.25
Primer forward	1.0 (10 pmol/µl)	1.0 (5 pmol/µl)
Primer reverse	1.0 (10pmol/µl)	1.0 (5 pmol/µl)
Nuclease-free water	9.5	3.25
cDNA	1.0	1.0
Total volume per well	**25.0**	**12.5**

Table 4: qRT-PCR program for gene expression analysis

Step	**Temperature [°C]**	**Time [s]**	**Cycles**
Initialization	95	420	
Denaturation	97	10	45x
Annealing	53	15	
Elongation	72	20	
Melting Curve	60 to 95	1200	

The samples' gene expression range was calculated with the help of a standard curve that was generated from pooled, undiluted cDNA of all samples (n=48) and diluted by 2^n in eight steps. On 96-well plates, standards and cDNAs were measured in duplicates, on 384-well format in triplicates. The mean expression of the technical replicates was normalized by the mean expression of the two housekeeping genes HSP90 and ActB.

2.10 Mass spectrometric analysis of bile acid composition and concentration

2.10.1 Bile acid extraction

Plasma

10 µl plasma were mixed 1:2 with 10 µl of 1 µM internal standard mix (bile acids that were used for external and internal standards: see appendix, table 10). To extract bile acids, 500 µl methanol was added, mixed and centrifuged at 12000 rpm for 10 min at 4 °C. 1.5 ml supernatant was transferred to a new reaction tube. The solvent was evaporated in a speed vac (SPD111V SpeedVac, Thermo Savant) at 40 °C. The residue was resuspended in 50 µl methanol and 50 µl LCMS water, vortexed at 40 °C for 5 min (Thermomixer compact, eppendorf). 10 µl of the final analyte, which contains a bile acid proportion of plasma : internal standard of 1:1, was transferred to HPLC vials.

Organs

Enterohepatic organ samples were ground in liquid nitrogen. Bile acids were extracted out of 40 mg tissue with 800 µl methanol. The supernatant was dried in speed vac at 40 °C. The extract was resuspended in 800 µl methanol. 20 µl of the resuspended extract were diluted 1:50 with 980 µl of a methanol and water mix (1:1). 100 µl were transferred to the LCMS vial and 10 µl stable isotope labeled standard added. As the proportion of extract and standard was 1:5 in vial (2 µl extract, 10 µl standard), the final bile acid concentration results were multiplied by 5.

Feces

20 mg of dried and pestled feces were extracted twice with 800 µl methanol and mixed at 700 rpm at 25 °C for 30 min and afterwards centrifuged at 12000 rpm for 10 min. The supernatant was transferred to a new reaction tube and dried in speed vac at 40 °C. The extract was resuspended in 1 ml methanol and diluted 1:50 (10 µl extract, 490 µl methanol). 50 µl of the diluted extract was combined with 10 µl stable isotope labeled standards and 60 µl LCMS water containing NH4Ac 10 mM and filtered. As the proportion of extract and standard was 1:10 in vial (1 µl extract, 10 µl standard), the final bile acid concentration results were multiplied by 10.

2.10.2 Analysis of bile acid concentration and composition

The mass spectrometer (ABSciex QTrap 5500) was operated in positive mode and mass spectra recorded using the multiple reaction monitoring (MRM) mode. Signal acquisition was performed using Analyst Software and quantitation with Multiquant Software (ABSciex, Framingham, MA, USA).

2.11 Blood lipids analysis

A quantitative determination of total cholesterol (CHOL), high-density lipoprotein cholesterol (HDL), triglycerides (TRIG), alanine aminotransferase (ALT), aspartate aminotransferase (AST), and glucose (GLU) in the plasma samples was conducted with Piccolo® Lipid Panel Plus Reagent Disc, used with the Piccolo xpress™ Chemistry Analyzer (Abaxis North America, USA). For that purpose, 110 µl of heparinized plasma samples were transferred to a lipid panel plus disc and analyzed according to the manufacturer's protocol in the automated Piccolo Analyzer. Low-density lipoprotein cholesterol (LDL) and very low-density lipoprotein cholesterol (VLDL) were automatically calculated out of the CHOL, HDL and TRIG concentrations by the analyzer.

2.12 Bile acid transporter sequencing & *in silico* PCR

RNA of enterohepatic organs (small & large intestine, liver, gall bladder) was isolated from a C57BL/6J as well as a 129S6/SvEvTac mouse, and qualitatively as well as quantitatively controlled as described in chapter 2.9 and reverse transcribed to cDNA.

Full length primers were designed with the help of the online platforms "Ensemble genome browser" (http://www.ensembl.org/index.html) and "Primer3" (http://workbench.sdsc.edu/), to cover the full length of the gene's coding region.

Oligo name	Forward primer sequence (5' → 3')	Reverse primer sequence (5' → 3')
ASBT	ATTTGCACAGCACAAGCAGT	TCTCATCAAATGATGGCCTG
OSTb	GGGCCAGAAACATCTCAATC	GGGCGTTATGGGGTACTCTC

The PCR products were transferred to a DNA gel, generated bands were cut. Sequencing of the bile acid transporters Ostb (Slc51b gene) and Asbt (Alc10A2 gene) was performed by a commercial provider (Eurofins Genomics GmbH, Germany).

2.13 Statistics

Statistical analyses were performed using the software GraphPad PRISM 6, SigmaPlot 12.3 (Systat Software Inc., San Jose CA/USA), and R (RStudio 2.14.1). Statistical tests were applied as specified in the respective figure legends. P-values <0.05 were considered as statistically significant.

For comparison of two normally distributed groups, significance was determined using the two-sided Student's t-test. Two or more normally distributed groups were compared by two-way Analysis Of Variance (ANOVA) with respect to two variables. Related samples were analyzed with Sidak's post-test for multiple comparisons. Two-Way Repeated Measures (RM) ANOVA and Sidak's post-test was used to compare one variable between two groups, that was repeatedly measured over time. A linear regression model was applied to compare a repeatedly measured variable among experimental groups that differed with respect to two characteristics. Data adjustment was performed to remove the influence of a disruptive factor. Regression lines are indicated for significant correlations only.

3 RESULTS

In the year 2006, Watanabe et al. described the prevention of diet-induced obesity (DIO) due to dietary cholic acid (CA) supplementation in C57BL/6J (BL6J) mice. They speculated that this phenomenon is based on a CA-derived increase of thermogenic processes in brown adipose tissue (BAT). However, the authors did not provide a substantive, direct proof of neither BAT recruitment nor UCP1 activation within this context. In order to prove their experiment's reproducibility, we initially repeated the key experiment of Watanabe et al., 2006. Moreover, we used the Ucp1 ko mouse to directly prove the role of UCP1. 129S6/SvEvTac (129Sv) mice were used to investigate the role of white fat browning within this regard. With the help of the obtained findings, we would be able to further enlighten the underlying molecular mechanisms and to investigate a possible contribution of white adipose tissue (WAT) browning to this effect.

Parts of this work have recently been published (Fromme et al., 2019).

3.1 Bile acid supplementation verifiably prevents C57BL/6J mice from diet-induced obesity

In our study male BL6J mice at the age of 6-7 weeks were fed a control (C) or high-fat diet (H), or one of the two diets with CA-supplementation (CC or HC), respectively. No differences in food intake were observed during the complete experimental phase (Fig. 10a). As experimental diets varied in energy content (Table 5), animal food intake was adjusted by energy content (kJ/g) of the respective diet. No differences in energy intake could be detected between non-supplemented and CA-supplemented diet groups (Fig. 10b). Despite these findings, H-fed BL6J mice significantly gained more body mass compared to control fed mice after 28 feeding days ($p=0.001$), whereas HC-fed mice showed a body mass development comparable to C-fed mice. Notably, CA-supplementation seems to prevent diet-induced obesity but does not lead to body mass loss in general: it maintains normal body weight in H-fed mice but does not further reduce body mass in C-fed mice (Fig. 10c). Thereby, a reduced fat mass fully accounted for the CA-mediated DIO-prevention (Fig. 10d), as lean mass was not affected by CA-supplementation (Fig. 10e). These observations proved the reproducibility of Watanabe's key finding and provided the basis for all further investigations.

We observed an initial body mass drop for C, CC and HC-fed mice within the first experimental week (Fig. 10c). This effect presumably resulted from the diet change from chow diet to experimental semi-purified diet, which has a different taste and comparatively hard texture. The H diet instead is pleasant-tasting and its texture is soft. Moreover, the related initial body mass loss of HC and CC-fed mice can eventually be attributed to the bitter taste that bile acids possess by nature. In order to circumvent adaption difficulties to the differing texture of the semi-purified experimental food, an intermediate phase was included in all following feeding experiments, where all animals first switched to C diet for one week and afterwards received the respective experimental diet.

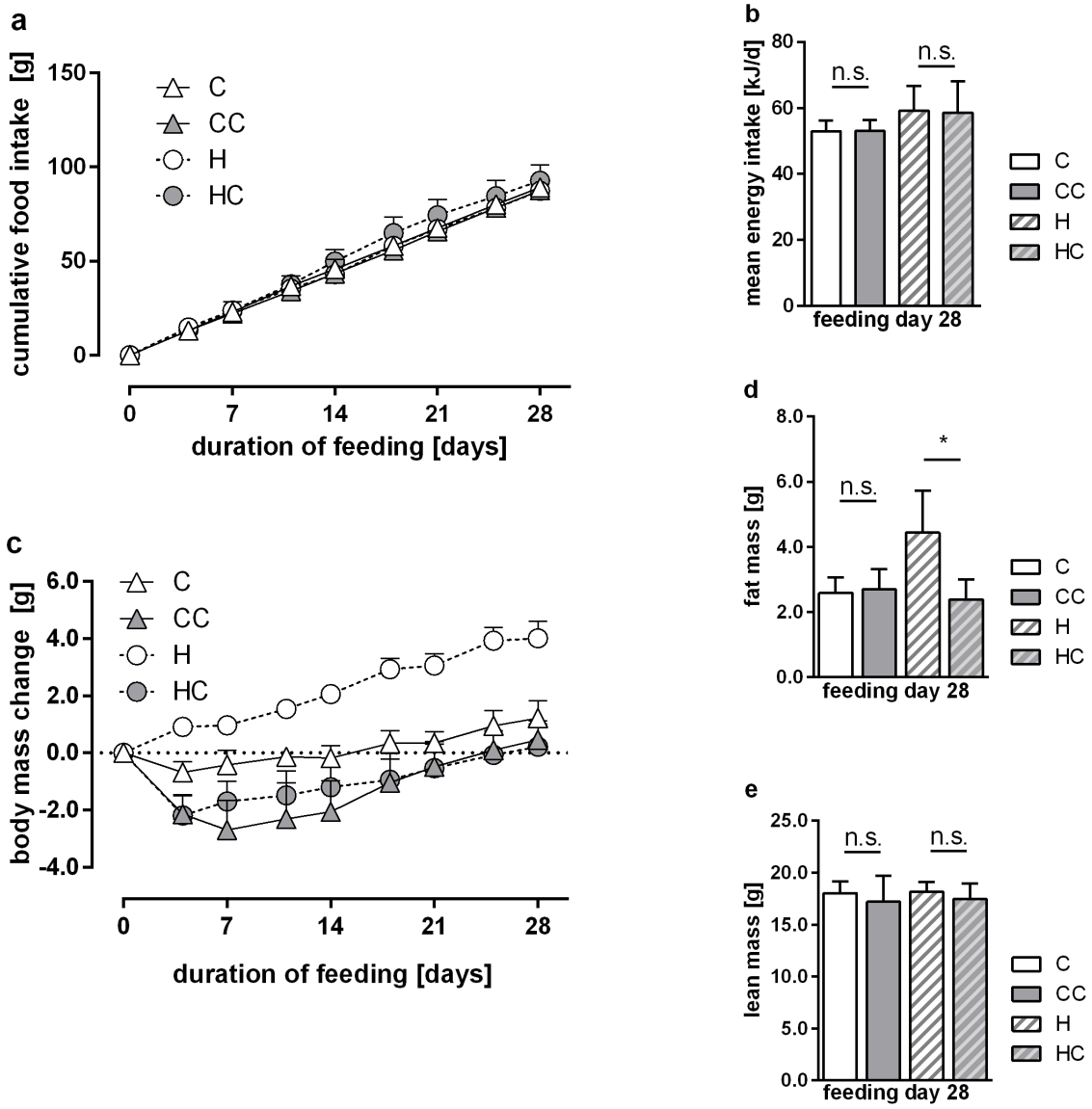

Fig. 10: Cholic acid supplementation prevents diet-induced obesity in C57BL/6J mice due to fat mass reduction (n=4-7). Figure modified from Fromme et al. (2019). a) Cumulative food intake during 28 experimental days. Note: Food intake of only four H-fed animals was analysed due to exclusion of three food spilling animals). b) Mean energy intake at experimental day 28. Differences between

supplemented and non-supplemented groups were t-tested. a) and b) Mean values with standard deviation are shown (n=4-7). c) Body mass development over 28 experimental days. CA-supplementation effectively prevented body mass gain of H-fed BL6J mice (BA main effect p=0.0024; Linear Mixed Effects Model), whereas supplementing CA to C diet does not affect body mass development (p=0.718). Mean values with standard error bars are shown (n=6-7). d) Total fat mass at experimental day 28. CA-supplementation impeded H feeding derived fat mass accumulation (p=0.0024). e) Total lean mass at experimental day 28. d) and e) Mean values with standard deviation are shown (n=6-7).

Table 5: Energy content of experimental diets analyzed by bomb calorimetry.

Diet	Energy [kJ/g]
C	17.2
CC	17.0
H	20.5
HC	21.2

To consider possible effects of CA-supplementation on energy assimilation, energy contents of food and feces samples of experimental week 4 were analyzed by bomb calorimetry. The energy of high-fat diets is assimilated more effectively than energy of low fat diets. However, no influence of CA-supplementation on assimilated energy and assimilation coefficient was observed, neither on C nor on H diet (Fig. 11). Thus, differences in body mass and body composition between non-supplemented and CA-supplemented diets were not caused by an altered energy intake.

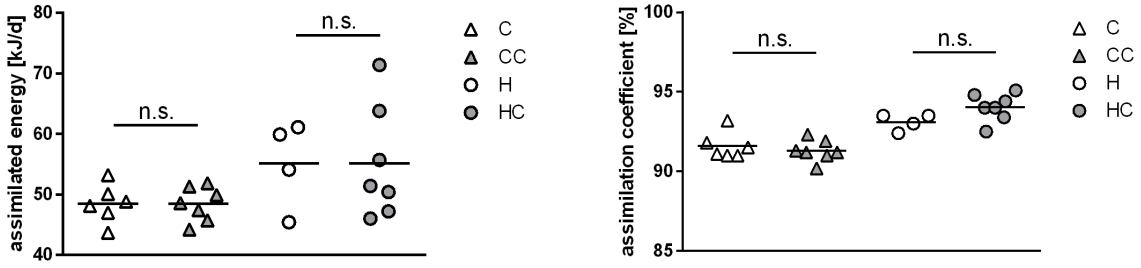

Fig. 11: Assimilated energy and assimilation coefficient in BL6J mice after 28 experimental days (n=4-7). Mean values are shown, data points represent individual animals.

3.2 Influence of dietary cholic acid supplementation on C57BL/6J mice

At experimental day 28, animals were sacrificed and dissected. Amongst others, inguinal white adipose tissue (iWAT) and interscapular brown adipose tissue (iBAT) were weighed, the left-sided fat pad was shock frozen for qPCR experiments, the right-sided part was fixed for H&E-staining and subsequent microscopic analyses.

3.2.1 Altered iBAT morphology and Ucp1 mRNA expression

Mean total iBAT mass was significantly reduced due to CA-supplementation in H-fed mice (Fig. 12a). This effect, however, presumably is not caused by the reduction of pure brown adipocytes but mainly by a reduction of the size and number of white adipocytes residing in iBAT. This effect was not only observed during animal dissection by comparing iBAT appearance visually, whereby iBAT of H-fed mice was larger and pale compared to the more consolidated and darker iBAT of HC-fed mice. Moreover, microscopic analyses revealed enlarged iBAT adipocyte sizes of H-fed BL6J mice. This effect was reversed by CA-supplementation, as iBAT lipid storage of HC-fed mice was comparable to C-fed mice (Fig. 12b).

As it was hypothesized, that the DIO-protective effect of CA-supplementation to H diet is due to increased thermogenic processes in BL6J mice, we analyzed iBAT Ucp1 mRNA expression. The qPCR measurements revealed a decrease of relative iBAT Ucp1 expression in HC-fed mice compared to H-fed mice ($p=0.0302$). CA-supplementation did not affect Ucp1 expression in C-fed mice ($p=0.4862$) (Fig. 12c). Therefore, we cannot confirm a CA-caused Ucp1 recruitment in BL6J iBAT on transcript levels. Moreover, we analyzed mRNA expression of the cAMP-dependent thyroid hormone activating enzyme type 2 iodothyronine deiodinase (D2), as it was presented to be essential to the DIO-protective effect of CA (Watanabe et al., 2006). However, we found no effect of CA-supplementation on D2 mRNA expression (comparing non-supplemented with the respective supplemented diet group with Student's t-test, data not shown).

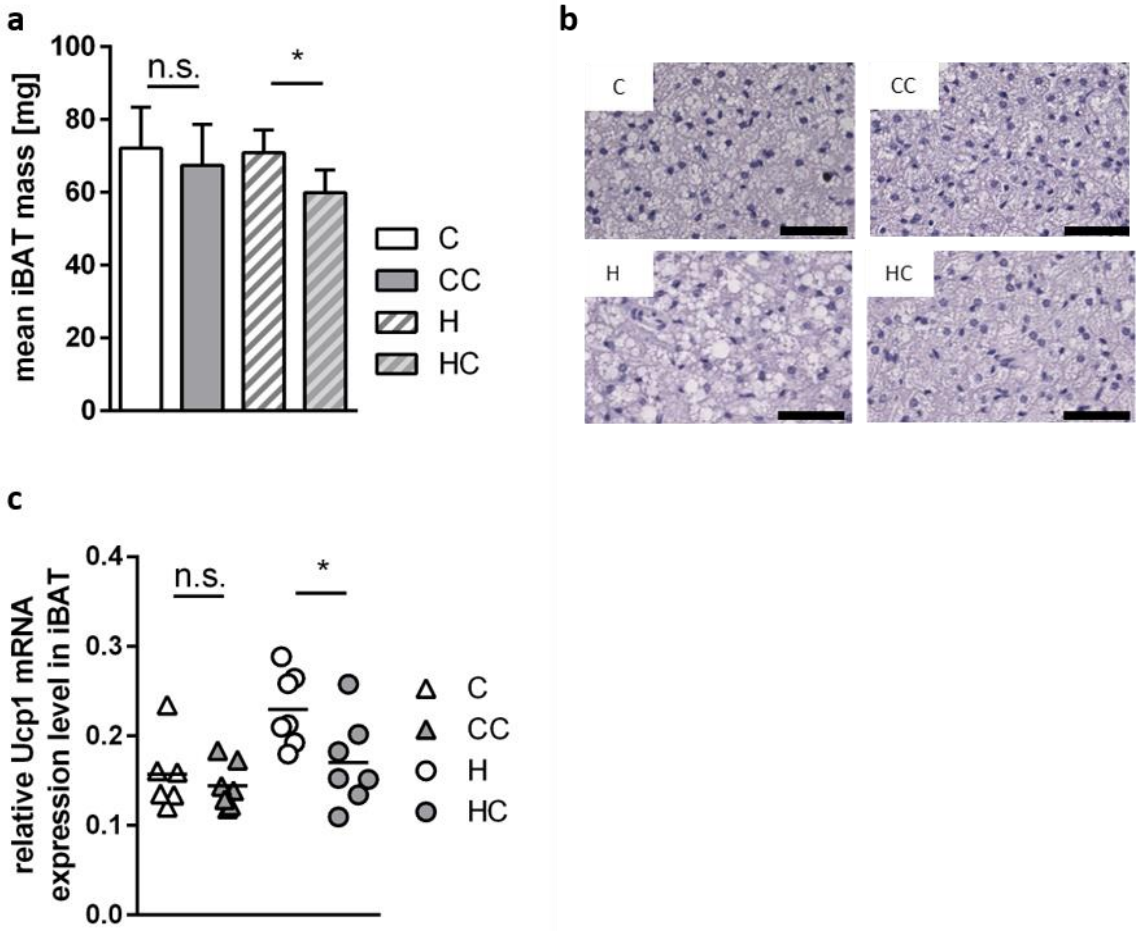

Fig. 12: Effects of CA-supplementation on BL6J iBAT mass, morphology and Ucp1 mRNA expression (n=6-7). Figure modified from Fromme et al. (2019). a) Mean BL6J iBAT mass: Comparison of interscapular brown adipose tissue (iBAT) masses according to different diets. Mean values with standard deviation are shown. b) Microscopic specimen of exemplary H&E-stained iBAT tissue slides. Scale bar: 50 µm. c) Relative BL6J Ucp1 mRNA expression in iBAT after 28 days of experimental diet feeding with or without cholic acid supplementation. Ucp1 gene expression measured by quantitative PCR. Transcript levels were normalized to the mean expression of Hsp90 and ActB. Means are shown, data points represent individual animals. Statistical significance between non-supplemented and CA-supplemented diet groups was tested using Student's t-test.

3.2.2 Reduced iWAT mass and potential recruitment of brite adipocytes in HC-fed C57BL/6J mice

Bile acids effectively impede white adipocyte hypertrophy caused by H feeding in BL6J mice. Congruently to total fat mass, CA-supplementation reduced mean iWAT mass of H-fed mice ($p<0.001$) but not C-fed mice (Fig. 13a). Analyzing histologic specimens of iWAT derived from HC-fed BL6J mice, we did not only observe a reduced adipocyte hypertrophy, but also the occurrence of multilocular cells (Fig. 13b). In order to decide, whether these cells potentially

contribute to thermogenic processes, we analyzed the expression of the brown adipocyte markers Ucp1, CideA, Cox7A1 and Otop1 in BL6J iWAT using two separate two-way ANOVAs, for each C and H diets, with the two factors “CA-supplementation” and “gene”.

The results of these qPCR measurements support the hypothesis that BAs cause brite adipocyte formation in BL6J iWAT, as CA-supplementation significantly increases brown fat marker expression in H-fed mice ($p=0.0034$). Moreover, we detected a significant interaction between both factors ($p=0.0021$), showing that the effect of CA-supplementation differs between the several brown fat markers of H-fed mice. In order to elucidate the strength of this effect on the different brown fat markers we conducted a Post-Hoc Sidak’s multiple comparisons test, which revealed a significant increase of Ucp1 expression due to CA-supplementation of H diet.

In C-fed animals, CA-supplementation did not affect brown fat marker expression, but we found an interaction between both factors “CA-supplementation” and “gene” ($p=0.0232$). However, this effect could not be confirmed for a single brown fat marker with Sidak’s multiple comparisons test (Fig. 13c).

To corroborate these observations on protein level, we IHC-stained UCP1-positive cells in iWAT and observed a browning effect of HC-fed BL6J mice (Fig. 13d). With the help of IHC-staining, we were able to proof, that the multilocular cells, which occurred in iWAT of HC-fed Bl6J mice, were UCP1-positive. Thus, CA-supplementation of BL6J mice in combination with a high-fat diet leads to a browning effect in iWAT.

In summary, CA-supplementation significantly decreases iWAT mass, significantly increases brown fat marker expression and leads to recruitment of UCP1-positive multilocular cells in H-fed BL6J mice but has none of these effects in C-fed BL6J mice (Fig. 13).

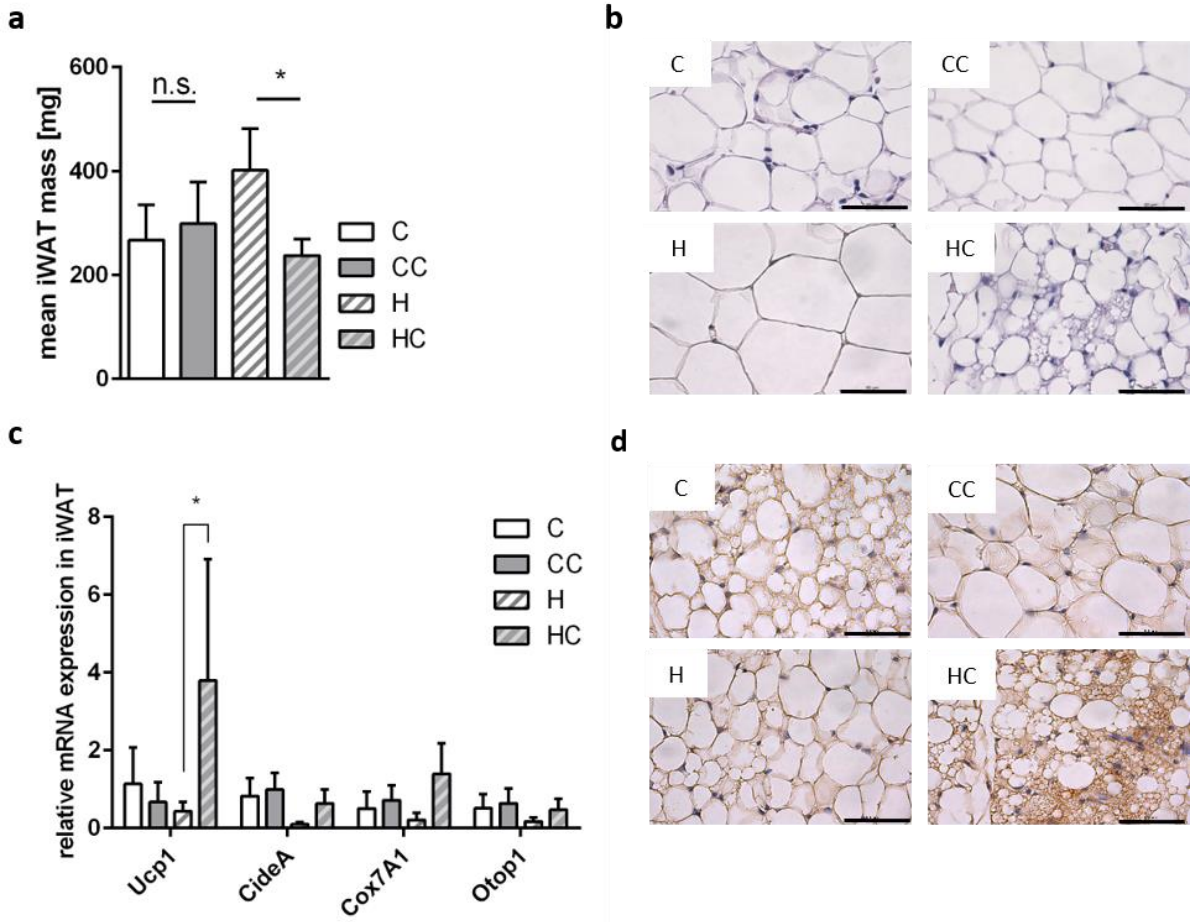

Fig. 13: Effects of CA-supplementation on BL6J iWAT mass, morphology, brown adipocyte marker mRNA expression and occurrence of UCP1-positive cells (n=5-7). Figure modified from Fromme et al. (2019). a) Mean BL6J iWAT masses: Comparison of inguinal white adipose tissue masses according to different diets. Mean values with standard deviation are shown (n=5-7). Statistical significance between non-supplemented and CA-supplemented diet groups was tested using Student's t-test. b) Microscopic specimen of exemplary H&E-stained iWAT tissue slides. Scale bar: 50 µm. c) Compilation of relative mRNA expression levels of different brown adipocyte markers in iWAT after 28 days of experimental diet feeding with or without CA-supplementation. Transcript levels were normalized to the mean expression of Hsp90 and ActB (n=6-7). Statistical significance was tested group-wise for C and H groups, respectively, using two-way RM ANOVA and Sidak's multiple comparisons test for Post-Hoc testing. d) Exemplary specimen of IHC-stained UCP1-positive cells in BL6J iWAT. Scale bar: 50 µm.

3.2.3 Cholic acid supplementation does not increase energy expenditure

With the help of indirect calorimetry (IC) measurements, it was possible to analyze the effect of CA-supplementation on energy expenditure. Therefore, IC measurements were performed with a further cohort of male BL6J mice. Twenty-two animals were set on control diet at the age of 4-5 weeks. After 12 days on C diet, the animals were singly caged and carried over into the indirect calorimetry measurement chamber for two further days on C diet, to adapt to the

climate chamber. Afterwards, at the age of 6-7 weeks (which corresponds to the age of the mice of the initial experiment) the animals were assigned to either H or HC group (n=11). After five consecutive measurement days on the experimental diets, the animals switched to a feeding-drinking-activity (FDA) measurement system for further 3 days (experimental design: see Fig. 9). All animals had free access to food and water during the whole experimental phase.

The animals were randomly assigned to one of the two diet groups. Before the switch from C to H/HC diet, both diet groups did not significantly differ in mean body mass ($p=0.98$, Student's t-test). After diet change mean body mass significantly differed between the two groups already after 5 days ($p<0.001$). This difference persisted after transferring the mice from indirect calorimetry to FDA device ($p<0.01$) (Fig. 14).

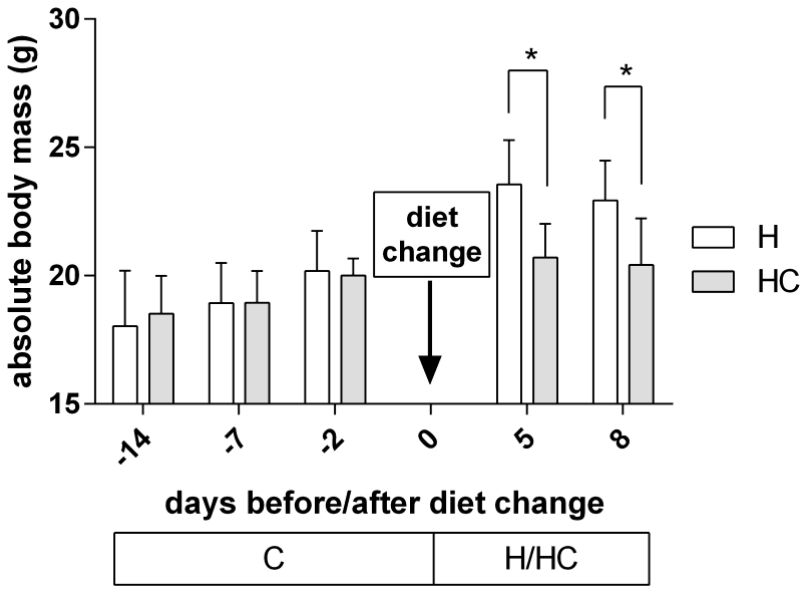

Fig. 14: Absolute body mass of BL6J mice during IVC housing (days -14 to -2) and indirect calorimetry (days -2 to 0) on C diet as well as on indirect calorimetry (days 0 to 5) and feeding-drinking-activity measurements (days 5 to 8) on H or HC diet, respectively (n=11). Means with standard deviation are shown. Two-way RM ANOVAs were used for statistical testing.

Food intake did not differ between the groups at all time points during the experiment (Fig. 15).

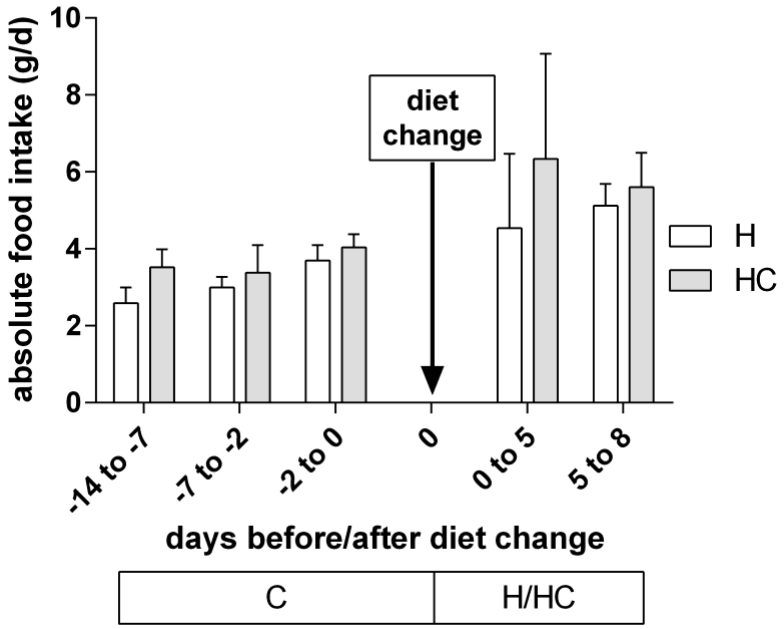

Fig. 15: Food intake of BL6J mice during IVC housing (days -14 to -2) and indirect calorimetry (days -2 to 0) on C diet as well as on indirect calorimetry (days 0 to 5) and feeding-drinking-activity measurements (days 5 to 8) on H or HC diet, respectively (n=11). Means with standard deviation are shown. Two-way RM ANOVAs were used for statistical testing. Note: Standard deviation of food intake mass of period 0 to 5 was comparatively high due to food spilling animals. Excluding spilling animals from statistical testing does not alter food intake comparability between both diet groups.

Fat and lean mass were determined before (at day -2) and after (at day 5) indirect calorimetry measurement via NMR spectrometry (Fig. 16, experimental design: see Fig. 9). The high-fat diet-induced increase in fat mass was prevented by CA-supplementation, two-way RM ANOVA analyses of fat masses before and after indirect calorimetry (factor “time-point”) revealed a significant variation due to CA-supplementation (factor “diet”) of H-fed BL6J mice ($p=0.0045$), as well as a significant interaction between time-point and diet ($p<0.0001$). Sidak’s multiple comparisons testing identified a significant reduction of HC-fed mice’s fat mass, five days after diet change (“after IC”), as H-fed mice gained 1.5 g fat mass, but HC-fed mice did not accumulate further adipose tissue.) No fat mass difference was detected between both diet groups before IC.

H-fed mice also gained lean mass, probably in line with the higher weight of fat mass they had to cope with (Fig. 16). Two-way RM ANOVA analysis of lean mass before and after indirect

calorimetry (factor "time-point) revealed a significant variation due to CA-supplementation (factor "diet") of H-fed BL6J mice (p=0.0235), as well as a significant interaction between time-point and diet (p=0.0008). Sidak's multiple comparisons testing identified, that lean mass was significantly increased in H-fed BL6J mice after IC, as they gained 1.5 g of lean mass during IC measurement, whereas HC-fed mice did not. These results are comparable to the results obtained in earlier experiments.

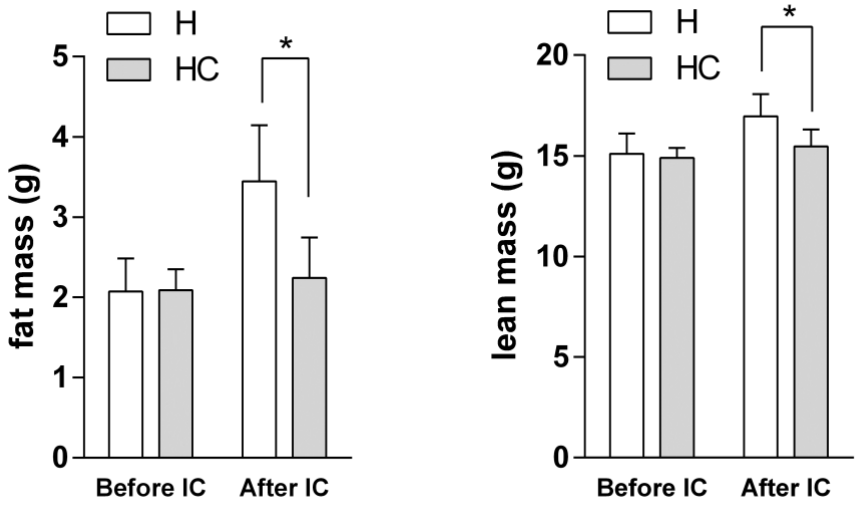

Fig. 16: Fat mass and lean mass before and after indirect calorimetry measurements (at day -2 and day 5 of experiment) (n=11). Figure modified from Fromme et al. (2019). Values are means with standard deviation. Body composition was assessed via NMR spectrometry (Minispec, Bruker). Two-way RM ANOVAs were used for statistical testing.

Energy expenditure analysis

Analyzing the indirect calorimetry results, both groups on C diet show parallel mean respiratory exchange ratios initially (Fig. 17). During dark phase from 5 pm (17:00) to 5 am (5:00) the mean RER is kept at levels around 1.0 and starts to fall at late dark phase. During light phase from 5 am (5:00) to 5 pm (17:00) mean RER initially falls and finally reaches lowest values around 0.8 at 10-12 am. After that, RER rises again constantly and reaches levels around 1.0 in the following dark phase. At time points where RER exceeds 1.0, animals probably exercised intensely, CO_2 production by the working muscles rises. All mice displayed the typical circadian rhythm of nocturnal activity accompanied by high heat production and preferred carbohydrate usage as compared to lower heat production and preferred lipid usage during daytime at rest.

However, after switching the diet from C to H or HC, respectively, RER courses alter and clearly differ between diet groups at a progressive rate. In contrast to C-feeding, RER of H-fed mice is flattened with far lower peaks during active phases. They only reach levels between 0.9 at the beginning of dark phase and 0.8 at the beginning of light phase. This curve progression is typical for H feeding, as animals primarily metabolize lipids but not carbohydrates. HC fed mice however show phases during light phase, where very low RER levels, partly below 0.8 are reached for several hours. Moreover, the whole RER course seems to be shifted in comparison to H-fed mice. Especially from day two after diet change on, clear differences between diet groups were observed. HC-fed animals did not only maintain RER levels of around 0.8 during light phase, they also reach RER values of about 0.9 around two hours later compared to their H-fed mates (around 17:00 for H-fed mice, 19:00 for HC-fed mice) (Fig. 17). These observations suggest, that HC-fed mice either start feeding at later time-points compared to H-fed mice, probably due to unfavorable flavor of CA, which is known to exhibit a bitter taste, or that CA-supplementation leads to an altered metabolism, where lipid metabolism is prolonged and the change to carbohydrate metabolization is delayed. Differences in RER between the supplemented and the non-supplemented diet group appeared rapidly after diet change and were thus not secondary to changes in body mass and composition.

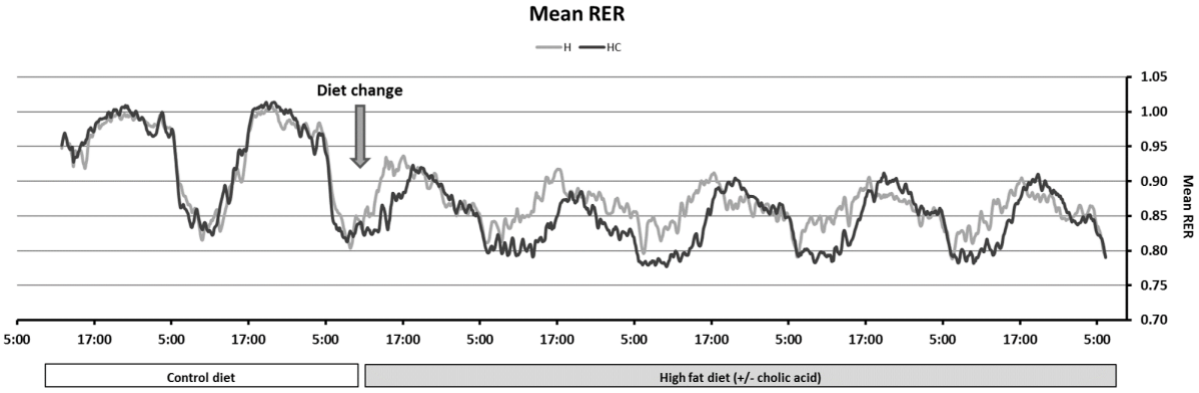

Fig. 17: Mean RER over one week, before and after diet change from C to H or HC diet, respectively (n=11). Figure modified from Fromme et al. (2019).

Contradicting to our hypothesis, calculations of mean energy expenditure revealed decreased rates for HC-fed mice compared to H-fed mice. Both H and HC-fed mice showed highest energy expenditure levels at the beginning of dark phase, as they are comparatively active directly after resting phase, typically start searching for food and show increased food intake. Energy

expenditure slightly decreases during dark and active phase (17:00-5:00). H-fed animals seemed to expend slightly more energy compared to HC-fed during dark. This difference distinctly appears during light, resting phase (5:00-17:00), where HC-fed animals constantly expended less energy (HC: ~2.9 Watt compared to H: ~3.3 Watt) (Fig. 18).

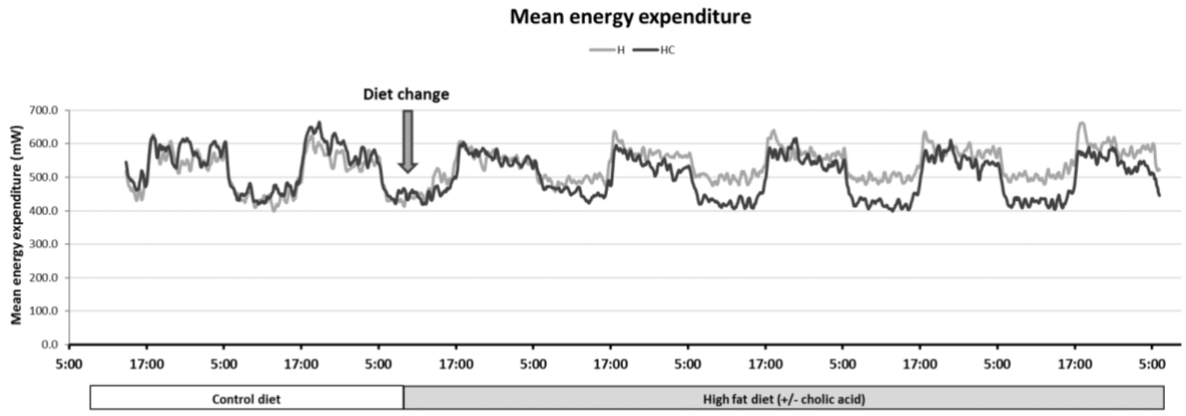

Fig. 18: Mean energy expenditure over one week, before and after diet change from C to H or HC diet, respectively (n=11). Figure modified from Fromme et al. (2019).

With the help of IC and FI data, we were able to balance energy over two days of C feeding (days -2 to 0) as well as five days of H and HC feeding (days 0 to 5). FI (g/d) was multiplied by energy content of respective diet type (C: 17.2 kJ/g before diet change, and H: 20.5 kJ/g or HC: 21.2 kJ/g after diet change). Approximately half of all animals spilled food (probably due to single caging). Therefore, we conducted energy balance calculations twice. Calculations including all animals resulted of a positive energy balance before and after diet change. There were no differences in mean energy intake or energy expenditure during C feeding (Figs. 19a and 19b). After diet change to H or HC diet, respectively, two-way RM ANOVA revealed a significant increase of energy intake after diet change to H diets ($p=0.0002$), as well as a significantly higher energy intake of HC-fed compared to H-fed BL6J mice ($p=0.0443$). Energy expenditure also was significantly increased after diet change to H or HC diet ($p<0.0001$). Besides, we fund a significant interaction between both factors “time” and “CA-supplementation” (despite no effect for CA-supplementation alone) ($p= 0.0061$). Sidak’s multiple comparisons testing showed a significant difference between CA-supplemented and non-supplemented H diet after diet change. As HC fed BL6J mice exhibited an increased energy intake, but a decreased energy expenditure compared to H-fed animals, the positive energy balance was significantly greater in these animals ($p=0.0317$) (Fig. 19c). These results

contradict body mass observations, at which body mass was significantly reduced by HC-feeding.

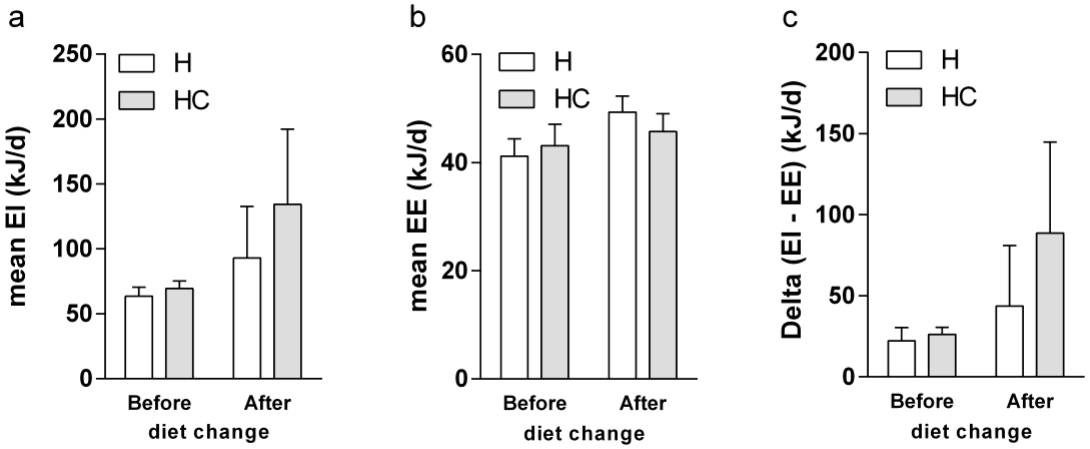

Fig. 19: Energy intake (kJ/d), energy expenditure (kJ/d) and their respective delta, before (days -2 to 0) and after diet change (days 0 to 5) during IC measurements, including spilling animals (n=11). Figure modified from Fromme et al. (2019). Two-way RM ANOVAs were used for statistical testing.

As these calculations were adulterated due to spilling animals, we exemplary excluded food intake data of these animals (spillage limit was set to a food consumption of >5g/d). By extracting these data, neither mean energy intake (p=0.9196), nor delta energy (p=0.3537) differed between H and HC-fed animals, anymore. Energy expenditure was not altered, as it is not affected by food spillage (Fig. 20).

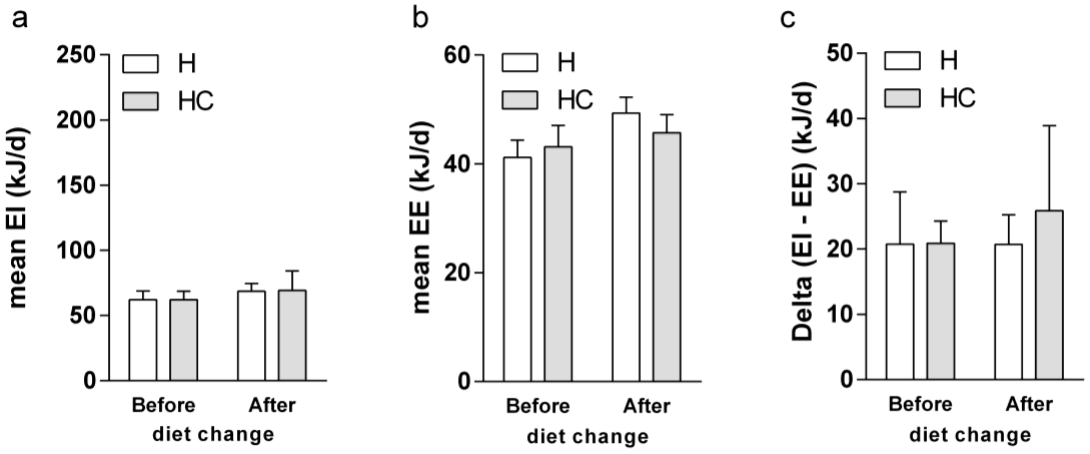

Fig. 20: Energy intake (kJ/d) (n=3-9), energy expenditure (n=11) and their respective delta (n=3-9), before (days -2 to 0) and after diet change (days 0 to 5) during IC measurements, excluding spilling animals. Figure modified from Fromme et al. (2019). Student's t-tests were applied to compare H to HC diet group after diet change.

Calculations of daily energy expenditure (DEE) and resting metabolic rate (RMR) revealed similar results: Both mean DEE and mean RMR did not differ between groups before diet change but increased due to H feeding and decreased due to CA-supplementation in the HC diet group, respectively. Both DEE and RMR significantly differed between non-supplemented and CA-supplemented H diets (Figs. 21b and 22b).

As H-fed animals significantly gained body mass during five days of indirect calorimetry measurements, we adjusted both DEE and RMR, respectively for body composition according to the formula LM + 0.2 FM (Even and Nadkarni, 2012) in order to accommodate for the different body compositions of both diet groups.

Both DEE and RMR significantly correlated with adapted body composition. As both DEE and RMR fitted to the regression line, H-fed animals seemingly just adapted their energy metabolism appropriate to their higher body mass. After body composition adjustment, both DEE and RMR did not differ between diet groups (Figs. 21 and 22). Consequently, we can conclude that any variations for DEE and RMR are due to body mass differences between diet groups.

DEE and RMR adjustment was additionally done for full body mass in comparison to the body mass correction formula LM + 0.2 FM (data not shown). Both types of calculation yielded the same result, leaving the basic statement identical.

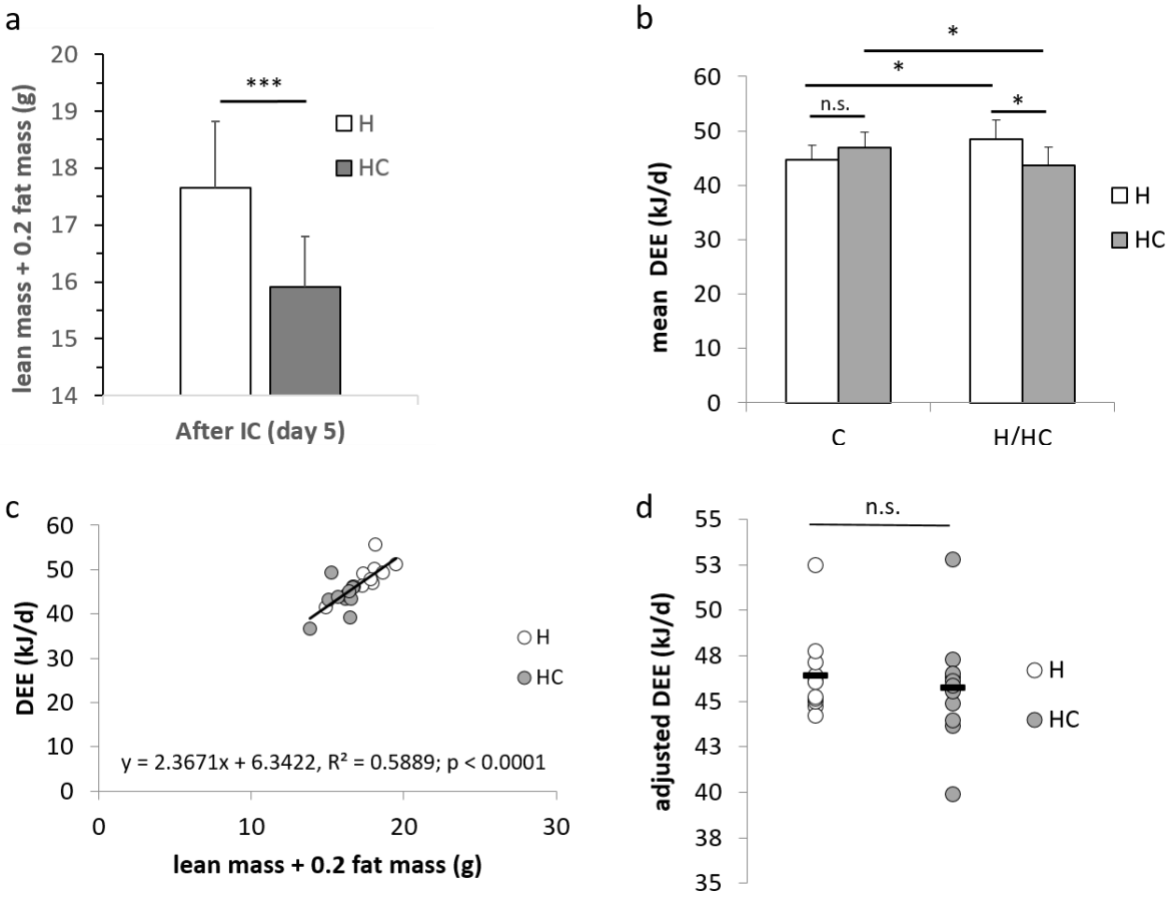

Fig. 21: Daily energy expenditure of H and HC-fed BL6J mice (n=11). Figure modified from Fromme et al. (2019). a) Body composition according to correction formula (LM + 0.2 FM) after five days on H or HC diet, respectively. b) Mean daily energy expenditure before (C) and after (H or HC) diet change. a) and b) Means with standard deviation are shown. c) Scatterplot showing a significant correlation of DEE and corrected body composition. d) DEE adjusted for corrected body composition. Both diet groups exhibit a comparable DEE, adapted to different body compositions. Mean values are shown, data points represent individual animals.

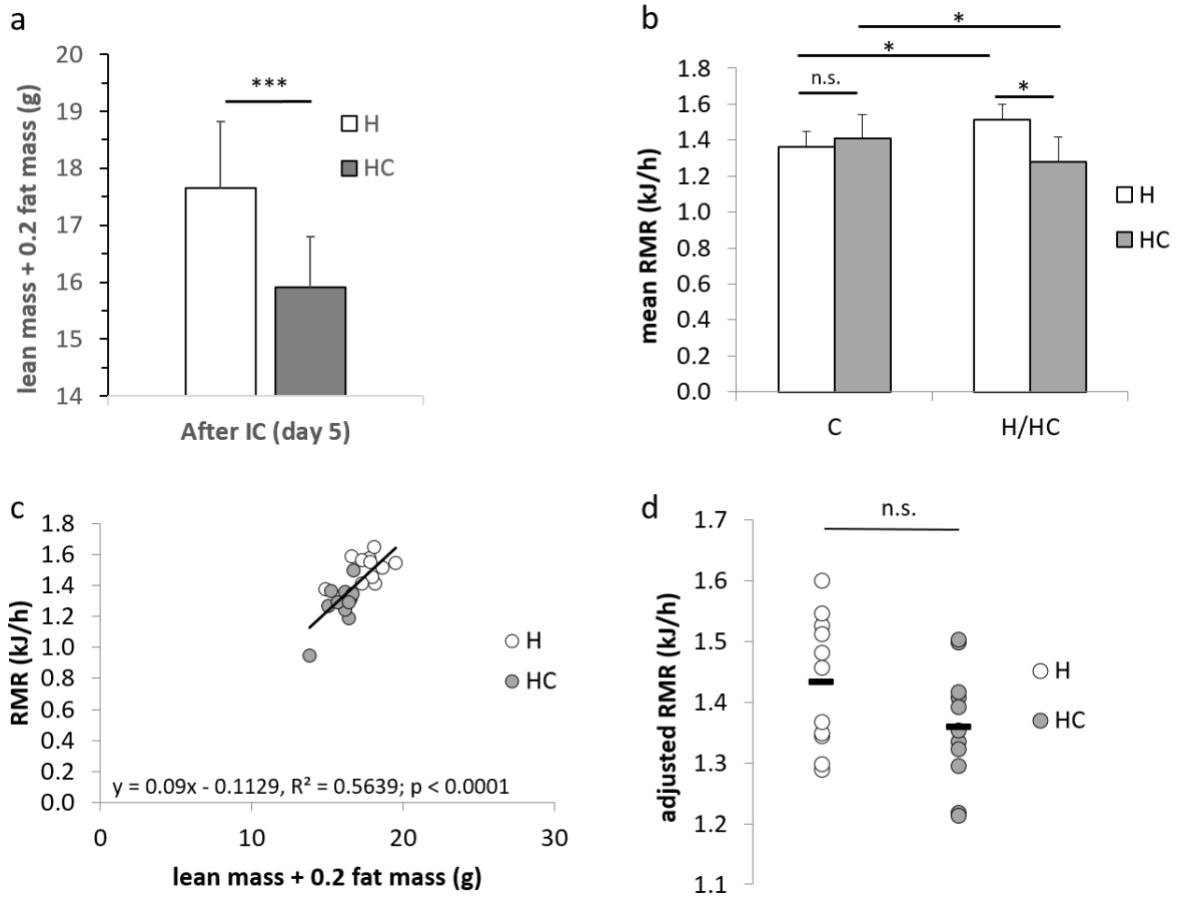

Fig. 22: Resting metabolic rate of H and HC-fed BL6J mice (n=11). Figure modified from Fromme et al. (2019). a) Body composition according to correction formula (LM + 0.2 FM) after five days on H or HC diet, respectively. b) Mean resting metabolic rate before (C) and after (H or HC) diet change. a) and b) Means with standard deviation are shown. c) Scatterplot showing a significant correlation of RMR and corrected body composition. d) RMR adjusted for corrected body composition. Both diet groups exhibit a comparable RMR, adapted to different body compositions. Mean values are shown, data points represent individual animals.

Feeding-drinking-activity-measurements

Subsequent to indirect calorimetry measurements, animals were transferred to the FDA measurement system in order to automatically measure food intake as well as physical activity in 5-minutes intervals per animal (drinking frequency was not observed within this setting). Mice were kept in the FDA measurement system at room temperature (22 ± 1 °C) on a 12 hours light/dark cycle and were further fed their respective experimental diet, which they were assigned to (H or HC diet, *ad libitum*) for 3 days. The first day was used for acclimatization of animals and therefore all measurements discarded. Measurement analyses were started with the first light phase at day 2.

Both non-supplemented and CA-supplemented groups showed similar cumulative food intakes. During the first 12 hours of light phase HC-fed mice showed a slightly reduced cumulative food intake compared to H-fed mice. At the end of the first light phase the HC-fed mice ate significantly less compared to H-fed mice. During dark phase however, HC-fed mice absolutely ate more than H-fed mice, so cumulative food intake was comparatively similar for both diet groups at the end of the first day. During the second light phase, cumulative food intake stayed fairly constant for both groups, so no differences were observed for absolute or cumulative food intake between both diet groups. During second dark phase however, HC-fed mice significantly ate more compared to H-fed mice. This difference however was not significant when cumulative food intake was examined. In summary, HC-fed mice seem to eat more during dark phases when they are active. However, this difference is compensated during light phases, in which H-fed mice eat more (Fig. 23). In order to verify these results, longer measurement periods of several days have to be performed and an overestimation of food intake due to spilling needs to be controlled.

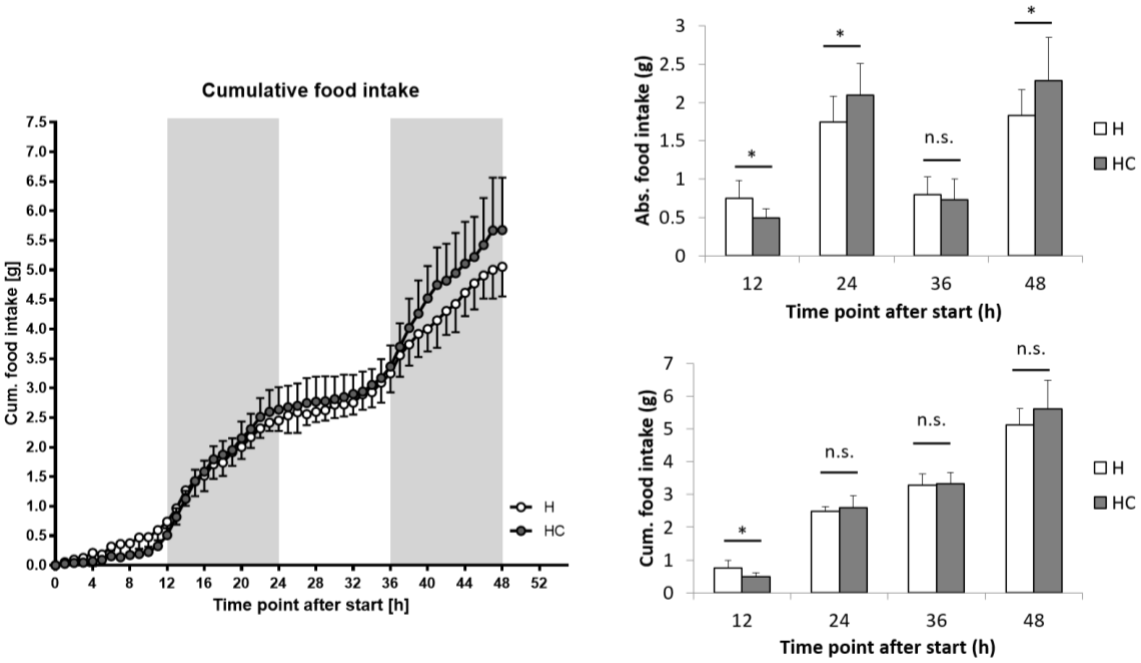

Fig. 23: Cumulative and absolute food intake of H and HC-fed BL6J animals during FDA-measurements over 48 hours (n=11). Food intake was compared between diet groups for every time-point separately with Student's t-test. Values are means with standard deviation.

Feed consumption of individual animals was comparatively high due to spillage. Therefore, energy could not be balanced perfectly. Nevertheless, energy expenditure measurements (as follows) provided clear evidence.

Activity rate was determined by measuring the distance that all mice covered during the second and third day after transferring them to the FDA system. Analysis of absolute distance showed no significant difference between the diet groups, whereas HC-fed mice tend to run longer distances, however statistically not significant (Fig. 24). Analysis of cumulative distance only was significant at the end of dark phase one, 24 hours after start of measurement.

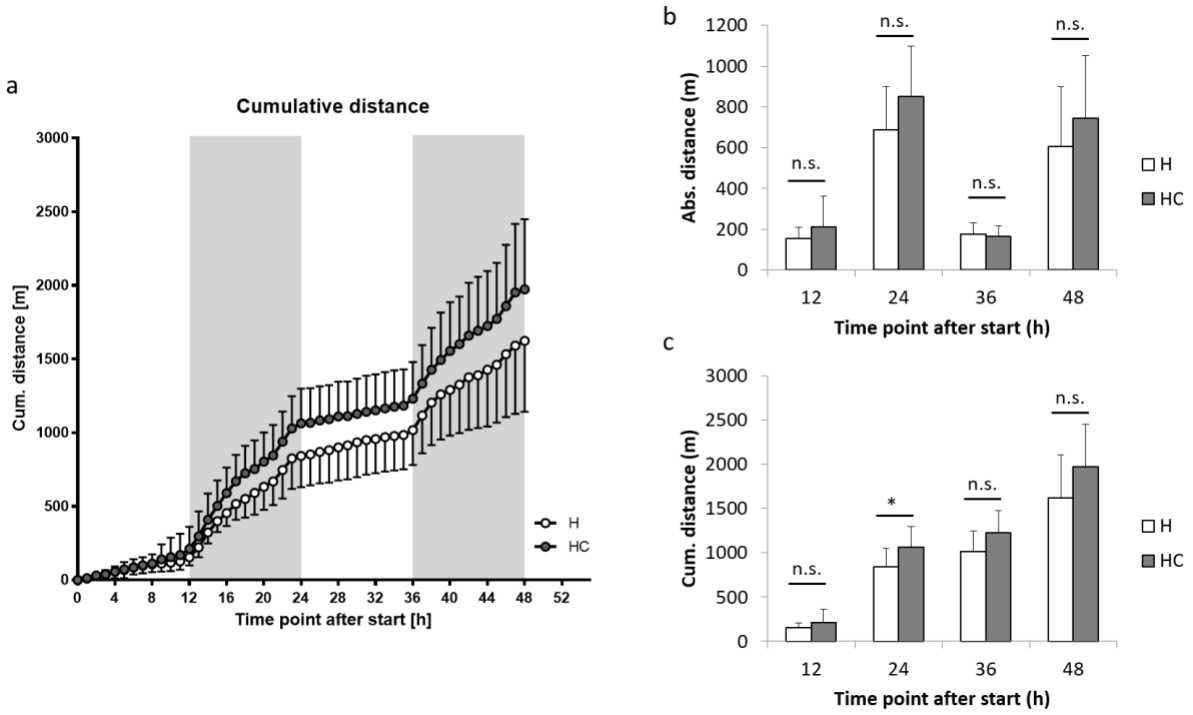

Fig. 24: Cumulative and absolute distance, that H and HC-fed BL6J animals covered during FDA-measurements over 48 hours (n=11). Food intake was compared between diet groups for every time point separately with Student's t-test. Values are means with standard deviation.

All results from IC and FDA system measurements suggest, that the CA-derived DIO-resistance of BL6J mice is not due to increased energy expenditure. Energy expenditure was rather decreased due to HC feeding. This effect however was merely caused by an adaption to a decreased body mass, as it disappeared after adjusting energy expenditure data to body composition.

3.3 Influence of dietary cholic acid supplementation on 129S6/SvEvTac mice

It was hypothesized, that body mass changes in BL6J mice could also result of brite adipocyte recruitment by CA-supplementation. 129S6 mice were used to verify this hypothesis. The

129S6 mouse strain is well known for its high capacity to recruit brite adipocytes. If CA-supplementation really affects body mass by brite adipocyte recruitment and enlargement of thermogenic capacity, stronger effects of CA-supplementation on body mass development were expected in 129S6 mice.

Mice of the 129S6 strain were kept and fed similar and in parallel to BL6J mice. At the age of 6-7 weeks mice received a diet switch from standard chow to the respective experimental diet. The animals received C or H diet either with or without 0.5 % CA-supplementation and were kept for four weeks on the experimental diet. Body mass and food intake were recorded twice a week. After 28 days mice were dissected and different tissues sampled for further analyses (at the same time and identical to BL6J mice).

3.3.1 Bile acid supplementation does not alter 129S6/SvEvTac body mass

Comparable to BL6J mice, 129S6 mice showed mean food as well as energy intakes, which were not affected by CA-supplementation (Figs. 25a and 25b). All diet groups continuously gained body mass (in accordance with age specific development) and H-fed 129S6 mice gained significantly more body mass compared to C-fed mice ($p=0.047$). In contrast to BL6J mice, CA-supplementation did not affect body mass of 129S6 mice, neither of C-fed nor H-fed mice (BA main-effect $p=0.3925$). Mean body mass of CA-supplemented and non-supplemented animals never differed significantly during the whole experimental phase (Fig. 25c).

Concordant with body mass development, no differences were observed in fat mass between control groups and supplemented diet groups: CA-supplementation did not influence body mass in both C and H diets and did not reduce fat mass of H-fed mice (Fig. 25d), as detected in BL6J mice. Furthermore, no differences between CA-supplemented and non-supplemented animals were seen in lean mass at the end of experiment (Fig. 25e).

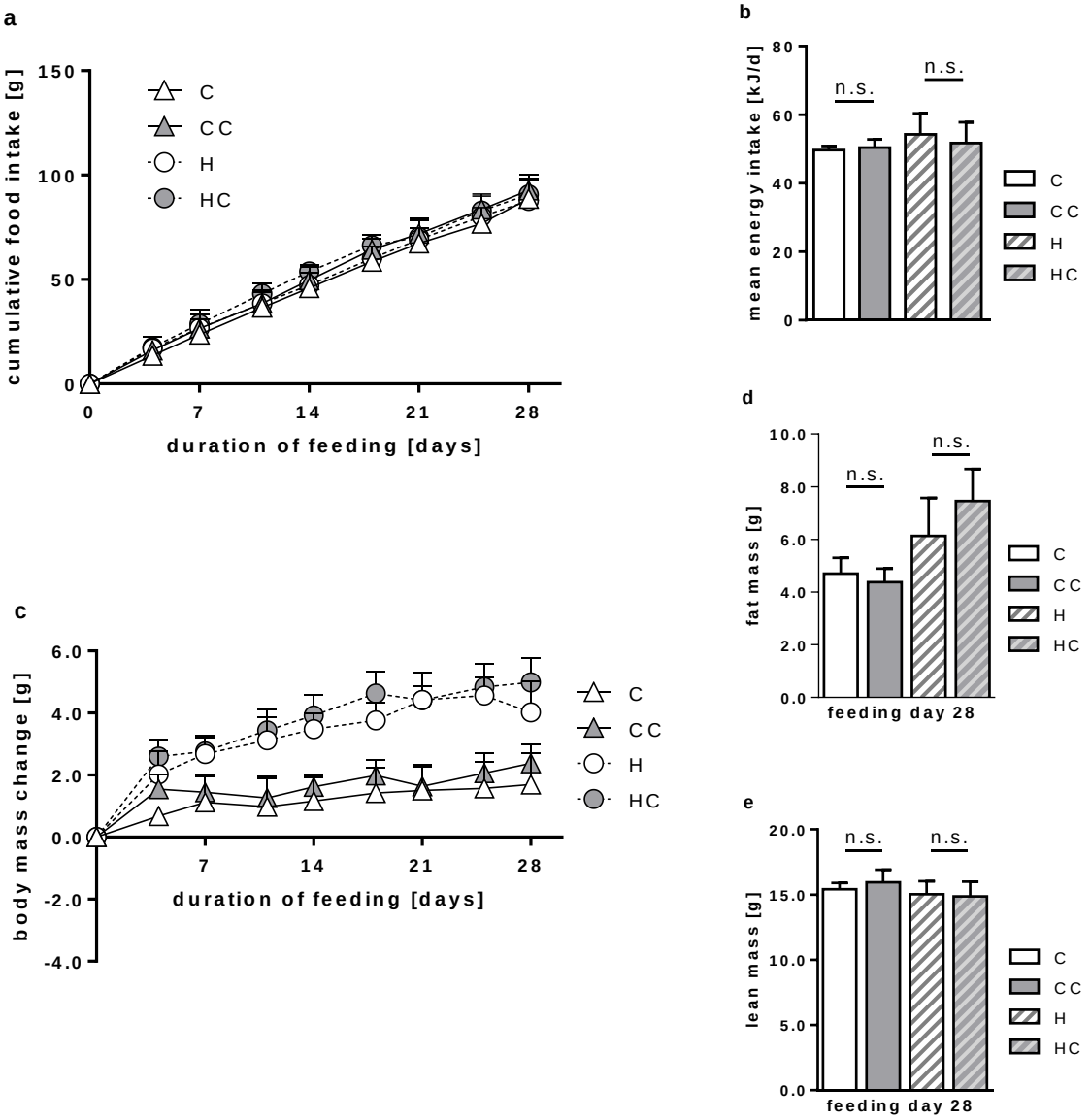

Fig. 25: Cholic acid supplementation has no influence on 129S6 body mass or composition (n=4-6). Figure modified from Fromme et al. (2019). a) Cumulative food intake during 28 days. b) Mean energy intake at experimental day 28. Differences between supplemented and non-supplemented groups were t-tested. a) and b) Mean values with standard deviation are shown. c) 129S6 body mass development after diet change. CA-supplementation does not affect 129S6 body mass development (BA main effect p=0.3925; Linear Mixed Effects Model). Mean values with standard error bars are shown. d) and e) Mean values with standard deviation are shown.

Similar to BL6J mice, energy intake (Fig. 25b), assimilated energy as well as assimilation efficiency (Fig. 26) were slightly increased in both H compared to C-fed groups, but CA-supplementation did not affect energy assimilation or assimilation coefficient, respectively, in 129S6 mice (Fig. 26).

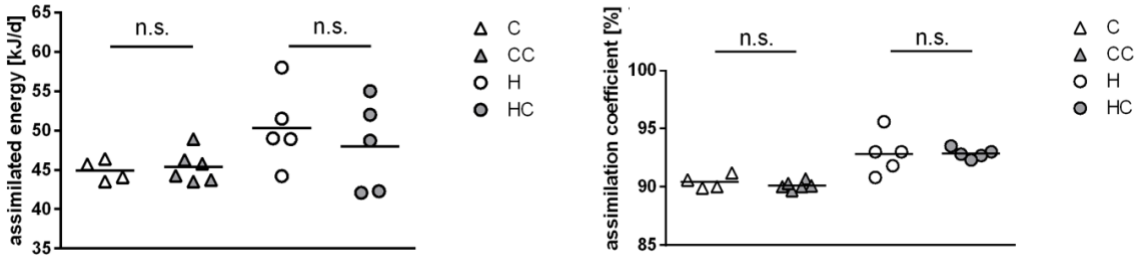

Fig. 26: Assimilated energy and assimilation coefficient in 129S6 mice after 28 experimental days (n=4-6). Mean values are shown, data points represent individual animals. Student's t-tests were applied to compare non-supplemented to CA-supplemented diets.

3.3.2 No influence on neither iBAT nor iWAT mass, morphology or brown fat marker mRNA expression, respectively

Mean iBAT mass of 129S6 mice was higher in H-fed mice compared to C-fed mice (p=0.0182). However, CA-supplementation did not alter iBAT mass in 129S6 mice (Fig. 27a). Microscopic analyses of 129S6 iBAT specimen revealed, that the increase of iBAT mass due to H feeding is mainly caused by the increase of lipid accumulation within adipocytes. This effect is not prohibited by CA-supplementation, as it was observed in BL6J mice (Fig. 27b).

Relative iBAT Ucp1 expression was not affected by CA-supplementation (Fig. 27c). Moreover, no differences between CA-supplemented and non-supplemented 129S6 animals were detected for relative iBAT Cox7a1, CideA, or Otop1 expression (not shown).

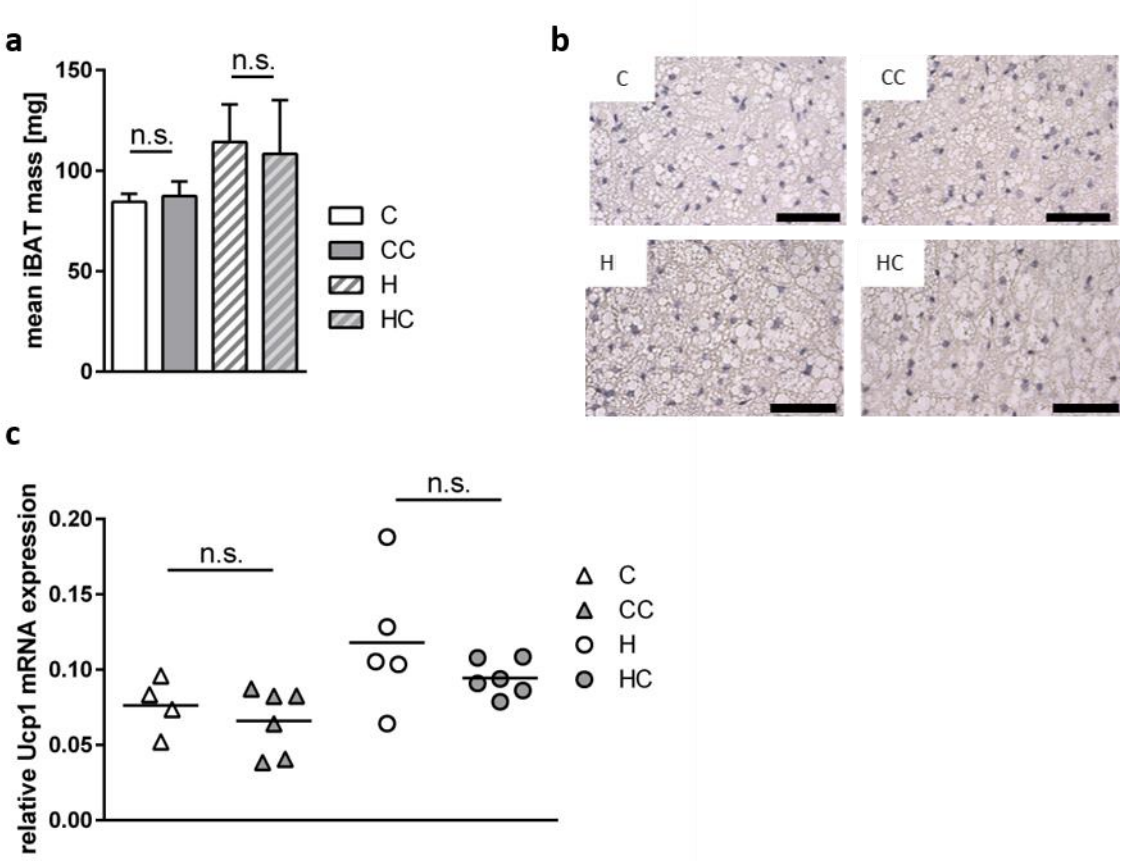

Fig. 27: 129S6 iBAT analyses (n=4-6). Figure modified from Fromme et al. (2019). a) Mean iBAT mass after 28 experimental days. CA-supplemented groups were compared to non-supplemented diets using Student's t-test. Means with standard deviation are shown. b) Exemplary iBAT specimen taken from 129S6 mice after 28 experimental days. H&E staining, scale bar 50 µm. c) Relative Ucp1 mRNA expression after 28 experimental days. Means are shown, data points represent individual animals.

Congruently, iWAT mass was increased due to H feeding (p=0.0155), however not affected by CA-supplementation (Fig. 28a). iWAT adipocyte morphology did not obviously differ between diet groups. Adipocyte size was not (as obviously as in BL6J mice) altered by different diets or CA-supplementation. The observed H diet-caused increase of iWAT mass did not seem to result in adipocyte hypertrophy primarily (Fig. 28b). Eventually adipocyte hyperplasia accounted for iWAT mass increase in H-fed mice. This hypothesis however was not investigated within this study.

Quantitative PCR analyses of brown adipocyte marker expression in 129S6 iWAT did not show a specific trend towards gene expression alterations due to CA-supplementation (Fig. 28c). As for BL6J mice, C and H groups were compared separately using two separate two-way ANOVAs, for each C and H diets, with the factors "CA-supplementation" and "gene".

In contrast to BL6J mice, CA-supplementation did not affect brown fat marker expression in H-fed animals. The same results were obtained for the C diet group.

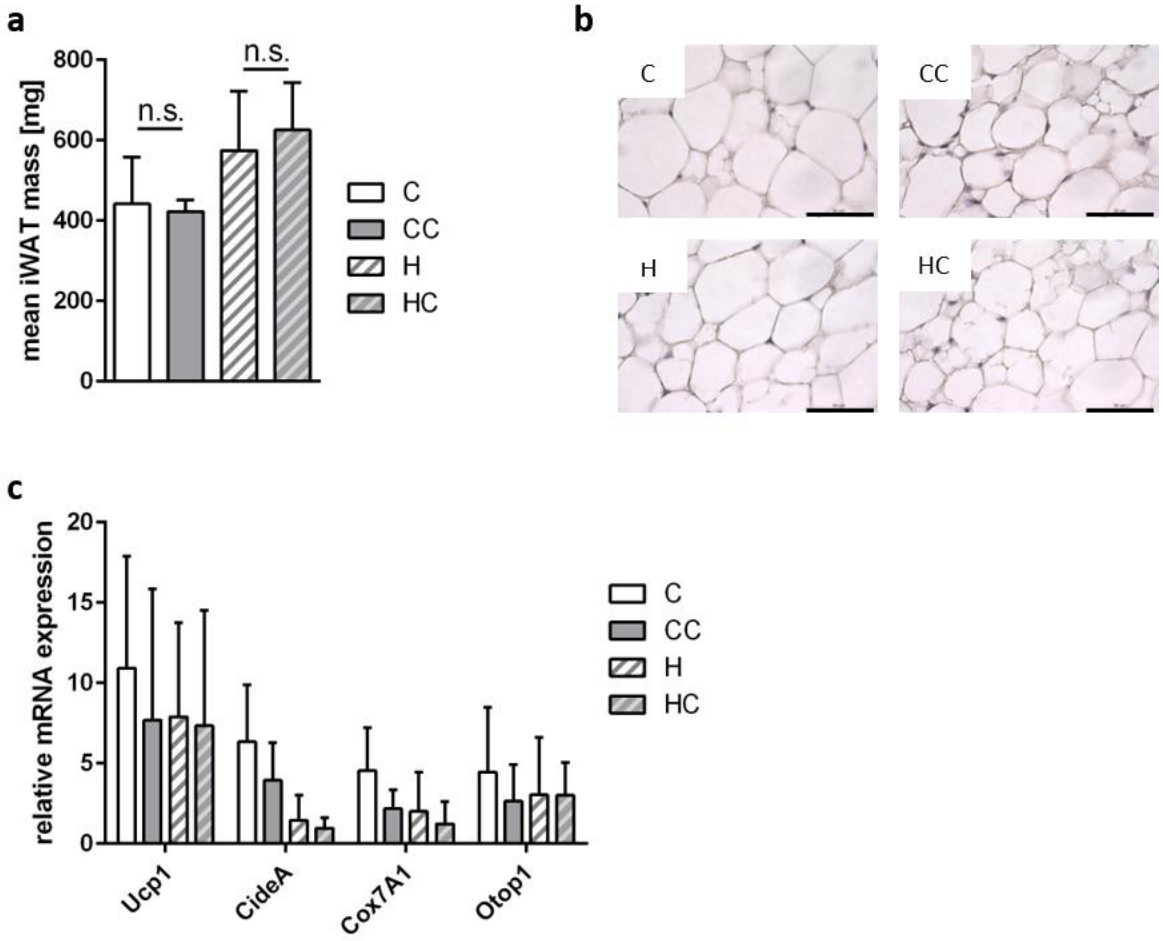

Fig. 28: 129S6 iWAT analyses (n=4-6). **Figure modified from Fromme et al. (2019).** a) Mean 129S6 iWAT masses after 28 experimental diets. Mean values with standard deviation are shown. Statistical significance between non-supplemented and CA-supplemented diet groups was tested using Student's t-test. b) Exemplary 129S6 iWAT specimen after 28 experimental diets. H&E stains, scale bar 50 µm. c) Compilation of relative mRNA expression levels of different brown adipocyte markers in iWAT after 28 days of experimental diet feeding with or without CA-supplementation. Transcript levels were normalized to the mean expression of Hsp90 and ActB. Statistical significance was tested group-wise for C and H groups, respectively, using two-way RM ANOVA and Sidak's multiple comparisons test for Post-Hoc testing.

We can conclude that the CA-derived prevention of DIO is strain specific. Moreover, there is a strain specific difference between BL6J and 129S6 mice concerning the influence of CA-supplementation on iWAT morphology and iWAT brown fat marker expression. With the help of this result, we further studied the different mouse strains to narrow down the relevant site of action by successive strain comparisons.

3.4 Searching for the relevant strain difference

3.4.1 Bile acid transporter sequencing

The data we have raised did not argument for a decreased food intake, which might have accounted for a body mass drop of HC-fed animals. As food intake seemed to be unchanged by CA-supplementation, we investigated subsequent sites of action that might account for the observed strain differences between BL6J and 129S6 mice.

In order to elucidate the strain specific variations, we initially sequenced the genes of the two BA transporters apical sodium dependent bile acid transporter (ASBT), and organic solute transporter β (OSTb) that are responsible for the uptake of BAs from gut and their efflux to portal blood.

The ASBT transporter is located at the terminal ileum, where it is responsible for the uptake of BAs from the gut lumen into enterocytes. The coding region of the corresponding gene was sequenced in large parts (codons for >320 amino acids). However, the start codon and the codons for the first eight amino acids as well as the stop codon and the codons for the last 20 amino acids were missing. Within the sequenced region ten stem specific differences were identified. Five of these nucleotide sequence differences lead to stem specific differences in amino acid sequence, whereby three of those are located N-terminal within a region of only 12 amino acids.

The OSTb transporter is primarily located at the basolateral membrane of enterocytes from the ileum and responsible for the efflux of bile acids into portal blood (as heteromer in interaction with OSTa). The coding region of the OSTb transporter gene was sequenced completely. Sequencing revealed one single strain specific position, which is known as rs29931408. A nucleotide replacement C/A leads to an amino acid switch of Q (glutamine) to A (alanine).

Accordingly, these two transporters are prime candidates to further investigate the strain specific phenotypic differences that were observed after CA-supplementation of H diet.

3.4.2 Balancing bile acid levels in C57BL/6J and 129S6/SvEvTac mice

In contrast to mice of the C57BL/6J strain, 129S6/SvEvTac mice did not react to dietary cholate supplementation in any parameter measured in this study. To clarify whether this discrepancy is caused by differences in intestinal bile acid absorption, metabolism or tissue sensitivity, we determined BA concentration and composition in several organismic compartments.

As food intake did not differ between strains and was not influenced by CA-supplementation, CA intake also was expected to be similar between diet groups as well as strains. CA was mixed into food pellets by a specialized food manufacturer (Ssniff), who guarantees for homogenous distribution of CA within the food pellets as well as prevention of demixing or separation. Both mouse strains were fed with pellets of the same batch. As food intake was comparable between strains and diet groups, the calculated CA intake amounts to averagely 40 µmol/day in all supplemented groups (Table 6, Fig. 29).

Calculation of mean CA intake [µmol/day]:
Mean food intake [g*day^{-1}] * 0.005 (CA percentage in CC and HC diet) * 408.58 [g*mol^{-1}]$^{-1}$ (molecular weight of CA)*10^{6}.

Table 6: Mean daily food intake (n=4-7).

Diet	Strain	Mean daily food intake [g/day]
C	B	3.2
	S	3.0
CC	B	3.1
	S	3.3
H	B	3.1
	S	3.1
HC	B	3.3
	S	3.2

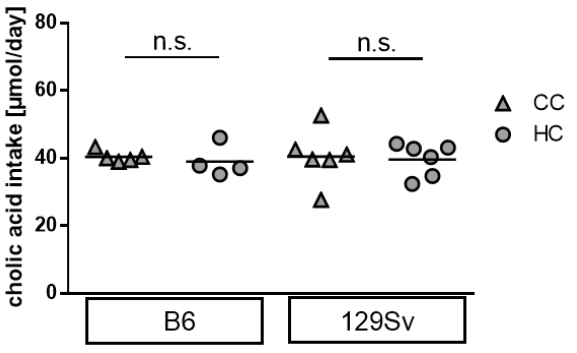

Fig. 29: Calculated cholic acid intake (n=4-7). Figure modified from Fromme et al. (2019).

In plasma, organ and feces samples, bile acids were mass spectrometrically quantified and qualified by using radiolabelled standards. With this procedure, the 17 physiologically most abundant bile acids could be detected (15 single BAs +2 groups of murine BAs) in plasma. Due to supply difficulties, fewer standards were available during subsequent BA analysis in organs and feces: Nine single BAs and the two BA-groups could be detected in enterohepatic organs

and 13 single BAs and the two BA-groups in feces. The amount of total BAs was calculated by adding masses of individual BAs.

Plasma

The quantified plasma BA levels were adjusted to the calculated individual plasma volume of each animal. Therefore, the following plasma BA concentrations relate to total plamsa levels within experimental animals.

Plasma BA levels of BL6J mice were massively increased due to CA-supplementation, both in C diet group (14-fold increase) and in H diet group (45-fold increase). In 129S6 mice, this increase was only seen in C-fed animals, as their mean plasma BA level was raised 53-fold, but was not in H-fed animals.

In plasma of C-fed BL6J mice, a more than 10-fold higher BA level was found compared to C-fed 129S6 mice (BC/SC=15.8 µM/1.4 µM). This difference could hint at a generally higher BA concentration in BL6J plasma compared to 129S6 mice. This strain difference was not observed in the H-fed group, as one SH animal exhibited extraordinary high plasma BA levels. Without this animal, H-fed BL6J animals would have shown 4.4-times higher BA plamsa levels compared to 129S6 mice. Bile acid concentration in H-fed BL6J (BH) mice was approximately 70 % less than their C-fed (BC) counterparts (BC/BH=15.8 µM/4.4 µM). This difference was also mainly caused by a single C-fed BL6J animal. Removing this animal would lead to similar BA levels in BC and BH mice. BL6J mice seem to naturally have higher plasma BA levels compared to 129S6 mice, except during H diet, where we found similar mean BA levels for both strains.

Notably, there have been individual mice, that showed exceptional high plasma BA levels, which were much higher compared to their counterparts of the same diet and strain. For example, one H-fed 129S6 animal had 20-fold higher plasma BA levels compared to the other H-fed 129S6 mice. Without this animal, we would also have seen an increase of BA levels due to CA-supplementation in H-fed 129S6 animals, as well as a difference of H-fed BL6J mice compared to 129S6 mice (Table 7, Fig. 30).

Table 7: Plasma BA levels (n=4-7).

Diet	Strain	Mean plasma bile acid levels [µM]
	B	15.8
	S	1.4
CC	B	227.6
	S	37.6
H	B	4.4
	S	5.0
HC	B	196.1
	S	4.8

In order to receive statistical evidence, we used two separate two-way ANOVAs for each C and H diet group separately with the two factors “CA-supplementation” and “strain”. (As no matched data was imposed, like in analyses of e.g. gene expressions, Post-Hoc testing was not conducted.)

Plasma BA levels of all C-fed animals of both strains neither showed a statistically significant strain effect nor an influence of CA-supplementation.

In contrast to this, plasma BA levels of H-fed animals were significantly increased due to CA-supplementation ($p=0.0088$). Moreover, strains significantly differed in H diet groups ($p=0.0090$), with BL6J mice showing a higher plasma BA concentration compared to 129S6 mice, above all with CA-supplemented H diet. We also detected a significant interaction between both factors ($p=0.0087$) in this group, confirming a higher plasma BA-raising effect for supplemented H-fed BL6J compared to 129S6 animals.

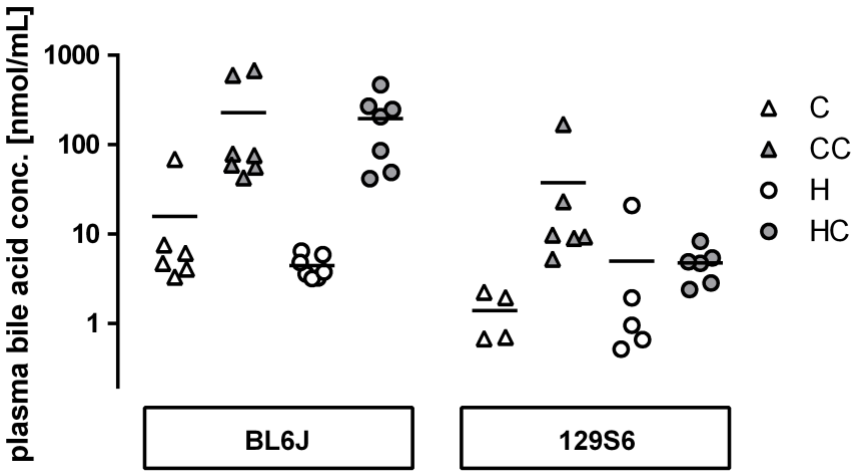

Fig. 30: Plasma bile acid concentration [µM] on log-scale, analyzed by HPLC/MS quantification (n=4-7). Figure modified from Fromme et al. (2019). Means are depicted on log-scale, data points represent individual animals. Statistical analyses were conducted using separate two-way ANOVAs for C and H diets, with the two factors "CA-supplementation" and "strain". C diets: no effect due to CA-supplementation, no strain effect. H diets: effect due to CA-supplementation (p=0.0088), strain effect (p=0.0090), and strain-diet-interaction (p=0.0087).

In conclusion, BL6J mice generally exhibit higher plasma BA levels compared to 129S6 mice. Plasma BA levels were found to be influenced by both CA-supplementation and strain, respectively, in H diet groups.

Enterohepatic organs

For BA analyses in organs, mice were dissected and all organs that are part of the enterohepatic circulation (including small and large intestine, caecum, liver, and gall bladder; collectively called enterohepatic organs (EO) in the following) were removed, shock frozen in liquid nitrogen, homogenized and processed for HPLC analysis as described above (see paragraph 2.10). As hypothesized, BA pool was enlarged in CA-supplemented animals compared to non-supplemented animals. BL6J mice naturally show higher BA pool sizes compared to 129S6 mice, with C-fed 129S6 mice having only an organ BA pool size of 55 % compared to C-fed BL6J mice and 42 % in H-fed animals. H-feeding slightly increases organ BA pool size in in BL6J animals but not in 129S6 animals.

Despite equal CA-uptake with food, supplemented 129S6 mice showed a far less BA pool size compared to BL6J mice (CC: 78 % less, HC: 67 % less). Due to CA-supplementation, 129S6 mice only reach organ BA pool concentrations that are comparable to BL6J organ BA pool

concentrations without CA-supplementation. Moreover, the fold-change of mean organ BA pool due to CA-supplementation is higher in BL6J (C → CC: 5.3-fold, and H → HC: 3.5-fold) compared to 129S6 mice (C → CC: 2.2-fold and H → HC: 2.7-fold) (Table 8).

Table 8: Mean BA pool [µmol/animal] in enterohepatic circulation of BL6J and 129S6 mice, adjusted to individual EO weight.

Diet	Strain	Mean organ BA pool
C	B	5.3
	S	2.9
CC	B	28.1
	S	6.3
H	B	7.3
	S	3.1
HC	B	25.5
	S	8.4

Statistical analyses were also conducted using two separate two-way ANOVAs for each C and H diet group separately with the two factors “CA-supplementation” and “strain”.

In both diet groups, EO BA concentration significantly differed due to CA-supplementation (C: $p<0.0001$, H: $p<0.0001$), with higher BA concentrations in CA-supplemented diet groups. Moreover, EO BA concentration significantly differed between strains in both diet groups (C: $p<0.0001$, H: $p<0.0001$). We also found a significant strain-diet-interaction in both diet groups (C: $p<0.0001$, H: $p=0.0016$), demonstrating a stronger BA pool raising effect in supplemented BL6J compared to 129S6 animals (Fig. 31).

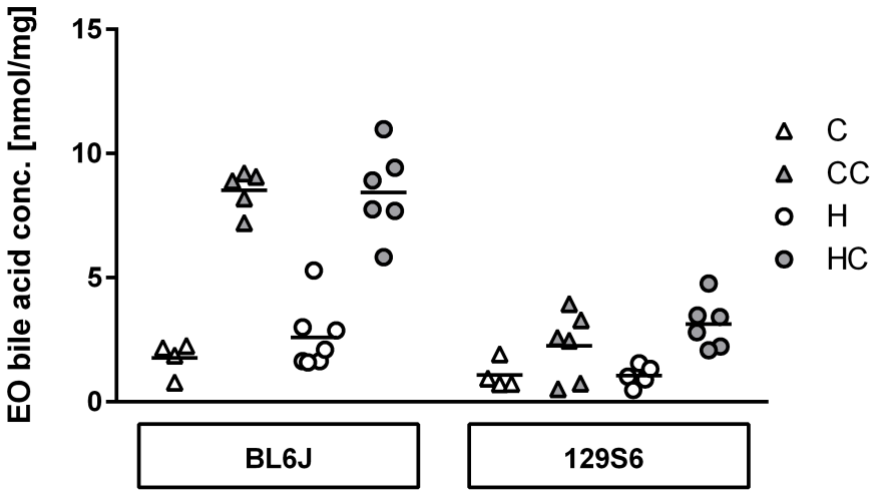

Fig. 31: Bile acid concentration [nmol/mg] in enterohepatic organs, analyzed by HPLC/MS quantification (n=4-7). Figure modified from Fromme et al. (2019). Means are depicted, data points represent individual animals. Statistical analyses were conducted using separate two-way ANOVAs for C and H diets, with the two factors "CA-supplementation" and "strain". C diets: effect due to CA-supplementation ($p<0.0001$), strain effect ($p<0.0001$), strain-diet-interaction ($p<0.0001$). H diets: effect due to CA-supplementation ($p<0.0001$), strain effect ($p<0.0001$), strain-diet-interaction ($p=0.0016$). Cave: Not all BAs that were quantified in plasma were also quantified in EO (missing bile acids: Dehydro-CA, CDCA, UDCA, GCDCA, GUDCA, TUDCA).

Feces

To estimate daily fecal bile acid loss, excreted feces mass was determined and its BA concentration analyzed using HPLC/MS. For that, feces were sampled at week four of experiment for three days, pooled, homogenized and processed for HPLC/MS analysis as stated above (methods, paragraph 2.10.1).

The total amount of BAs in feces was drastically increased by CA-supplementation. The observed strain difference in plasma and organ BA concentrations could also be seen in fecal bile acid concentrations, as 129S6 mice exhibited slightly lower BA concentrations (statistically significant for C/CC-fed animals) (Table 9, Fig. 32).

Table 9: Mean fecal bile acid excretion [µmol/g] of BL6J and 129S6 mice.

Diet	Strain	Mean fecal BA excretion [µmol/g]
C	B	6.2
	S	4.8
CC	B	69.0
	S	46.2
H	B	17.7
	S	7.9
HC	B	73.5
	S	68.3

For statistical analyses we pooled animals of both strains and conducted two-way ANOVAs for each diet group separately: BA excretion significantly differs between strains in C diet groups ($p=0.0074$), with 129S6 animals excreting less BAs compared to BL6J animals. Moreover, we found a statistically significant increase of fecal BA excretion due to CA-supplementation ($p<0.0001$) as well as a significant interaction between both factors ($p=0.0150$), hinting at a stronger increase in BA excretion due to CA-supplementation in BL6J animals. Additionally, CA-supplementation also significantly increases BA excretion in H-fed animals ($p<0.0001$). In contrast to C-fed mice, we did not observe a strain difference in H diet groups (Fig. 32).

As there were no differences in feces mass between strains or diet groups, similar results were obtained for daily fecal BA excretion mass (not shown).

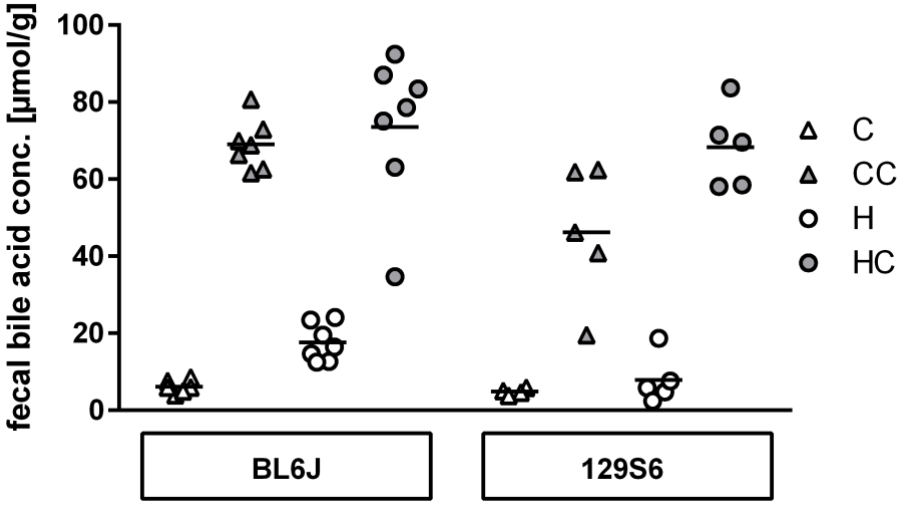

Fig. 32: Fecal bile acid excretion [µmol/g], analyzed by HPLC/MS quantification (n=4-7). Figure modified from Fromme et al. (2019). Means are depicted, data points represent individual animals. Statistical analyses were conducted using separate two-way ANOVAs for C and H diets, with the two factors "CA-supplementation" and "strain". C diets: effect due to CA-supplementation ($p<0.0001$),

strain effect (p=0.0074), and strain-diet-interaction (p=0.0150). H diets: effect due to CA-supplementation (p<0.0001). Cave: Not all bile acids that were quantified in plasma were also quantified in EO (missing bile acids: Dehydro-CA, TCDCA).

Bile acid composition

Bile acid composition is compartment (feces, enterohepatic organ, plasma) specific and similar in both strains (Fig. 33). Interestingly, despite differences in absolute plasma concentration (Fig. 30), the contribution of individual bile acids to the total pool was comparable in both strains and differed only as a consequence of supplementation and compartment (feces, enterohepatic organ, plasma) (Fig. 33).

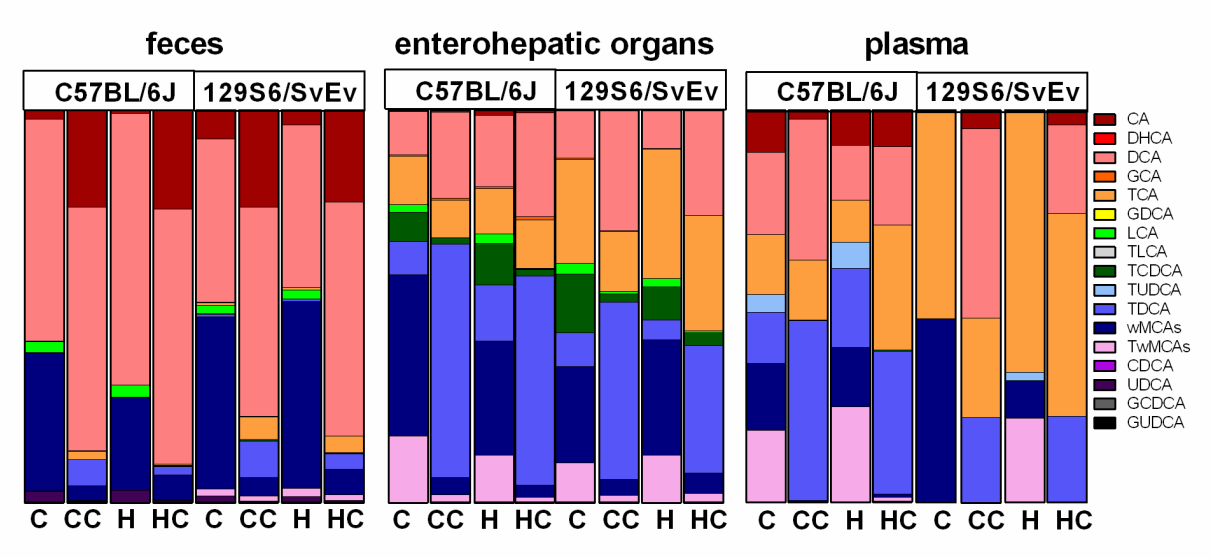

Fig. 33: Composition of bile acid pools in feces, enterohepatic organs and plasma (n=4-7). Figure taken from Fromme et al. (2019). Every bar section represents the median molar concentration as a fraction of total pool size. CA: cholate, DCA: deoxycholate, TCA: taurocholate, GDCA: glycodeoxycholate, LCA: lithocholate, TCDCA: taurochenodeoxycholate, TDCA: taurodeoxycholate, wMCAs: omega-muricholates, CDCA: chenodeoxycholate, UDCA: ursodeoxycholate, TUDCA: tauroursodeoxycholate, DHCA: dehydrocholate, GCA: glycocholate, TLCA: taurolithocholate , TwMCAs: tauro-omega-muricholates, GCDCA: glycochenodeoxycholate, GUDCA: glycoursodeoxycholate.

Taking together all results of plasma, organ, and fecal bile acid quantification, we can conclude, that the spillover of BAs from enterohepatic circulation into plasma does not seem to be responsible for the strain difference in the DIO-preventive effect of CA, as it was hypothesized in literature before (Watanabe et al., 2006).

3.5 Ucp1 is not responsible for the adiposity-preventive effect of cholic acid

Increased energy expenditure in brown adipose tissue was made responsible for the DIO-preventive effect of dietary CA-supplementation in published literature (Watanabe et al., 2006). In a first approach, only indirect proofs were used, e.g. the use of D2 ko mice.

In order to directly challenge the hypothesis that resistance to diet-induced obesity conferred by bile acid supplementation is due to increased thermogenic processes in BAT, we used Ucp1 ko C57BL/6J mice for a further feeding experiment. Male Ucp1 ko and wildtype BL6J mice, respectively, at the age of 6-7 weeks were fed C diet for one week in order to acclimatize to the experimental diet. In order to extract the potential CA-derived increase in thermogenic processes, we impeded thermogenic processes for body temperature maintenance by keeping all animals at thermoneutrality (30 °C). All mice were assigned to one of four diet groups: C or H diet, with or without cholic acid (0.5 % w/w) supplementation, respectively. Body mass, food intake and body composition were determined in frequent intervals. After four weeks of feeding the experimental diet, mice were sacrificed and dissected. Amongst others, iBAT, iWAT and eWAT were taken for further analyses.

3.5.1 No genotype effect on body mass development or body composition

Seven days before diet change and assignment to one of four experimental diets all mice received control diet in order to acclimatize to the texture and composition, which the semi-purified experimental diets have in comparison to a regular chow diet. During that week, no differences in body mass development were observed between diet groups. After assignment to one of the four particular diet groups, clear differences occurred already after one week of experiment.

Due to the insertion of one week adaption phase, all BL6J wildtype diet groups absolutely gained more weight compared to the mice of the previous experiment.

At thermoneutrality, H-fed BL6J mice also gained more weight compared to C-fed mice and this effect was prevented by CA-supplementation in both wt ($p<0.0001$) and Ucp1 ko mice ($p<0.0001$), without statistical significant differences due to Ucp1 ko. Sidak's multiple comparisons testing showed that the observed BM restriction significantly affects wt mice

from the first week after diet change on. In Ucp1 ko mice this difference becomes significant from two weeks after diet change on (Fig. 34).

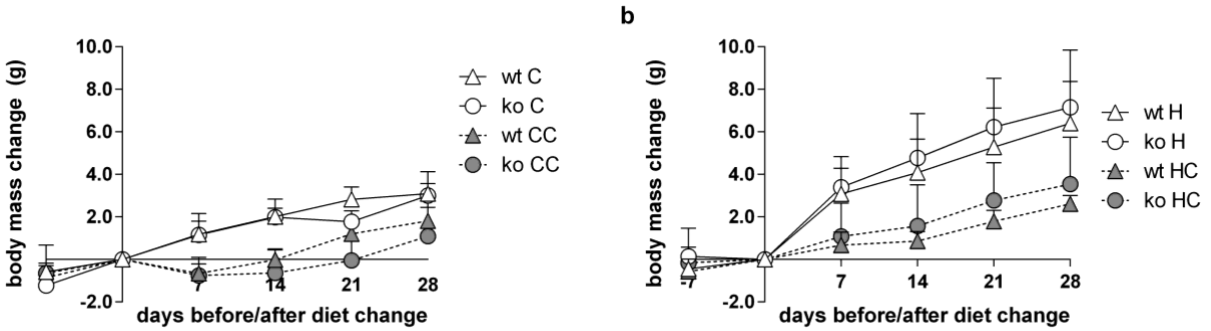

Fig. 34: Body mass development of wt and Ucp1 ko mice on C or H diet, with or without cholic acid supplementation (n=6). Figure modified from Fromme et al. (2019). Body mass development during 28 days of C and CC (a) or H and HC (b) feeding, respectively. Statistical analysis was conducted for each diet group separately. Four separate two-way RM ANOVAs were used with the two factors "time-point" and "genotype". In all diet groups, genotype did not affect body mass development. Means with standard deviation are shown.

In contrast to earlier experiments at room temperature, we also observed a significant BM gain restriction due to CA-supplementation in C-fed mice at thermoneutrality (taking together all C-fed mice of both genotypes): CA-supplementation restricts absolute BM gain of C-fed mice (p=0.0025), but no genotype effect was detected. Comparably, in H diet groups CA-supplementation restricts BM gain of H-fed mice (p=0.0002), as observed in earlier experiments at room temperature, but no genotype effect was observed (Fig. 35).

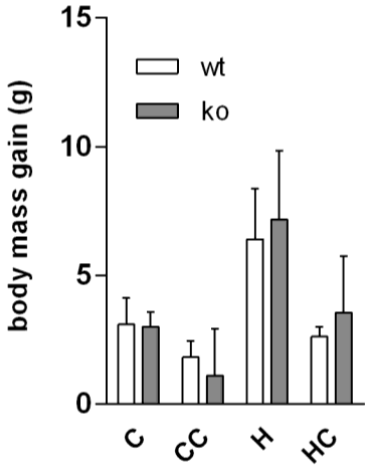

Fig. 35: Total body mass gain after 28 experimental days (n=6). Statistical analysis was conducted for C and H diets separately. Two separate two-way ANOVAs were used with the two factors "CA-supplementation" and "genotype". No genotype effect was detected. Means with standard deviation are shown.

Body composition analyses revealed that CA-supplementation significantly reduced fat mass accumulation in H-fed mice in both diet groups (p=0.0245 in C, and p=0.0013 in H-fed mice) after 28 days of experimental diet feeding. However, no genotype difference was detected. Lean mass of H-fed animals significantly differed between both genotypes (p=0.0302), and was only affected by CA-supplementation in C-fed animals (p=0.0083). As Ucp1 ko mice generally possess less body mass, fat mass and lean mass compared to wt mice, body composition parameters were depicted as delta, relating to the start of the experiment (day 0) (Fig. 36).

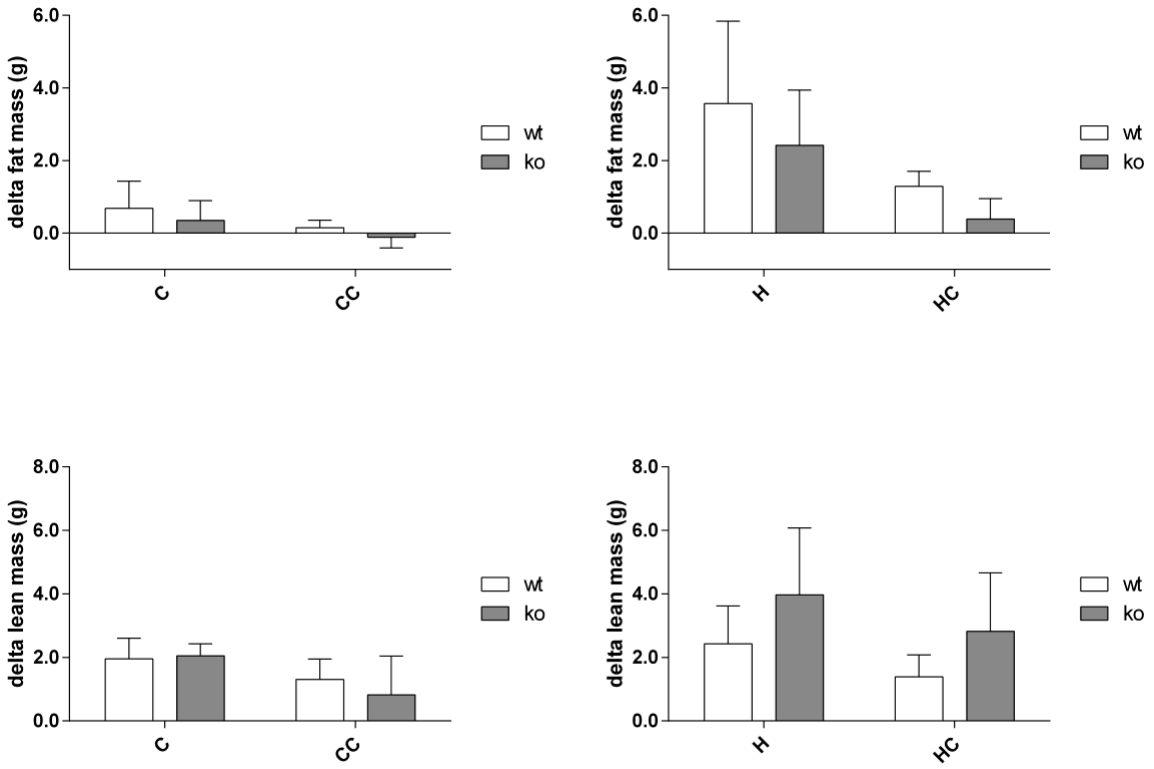

Fig. 36: Delta fat mass and delta lean mass (related to baseline values at the start of the experiment day 0) of BL6J wt and Ucp1 ko mice after 28 days of experimental feeding (n=6). Figure modified from Fromme et al. (2019). Means with standard deviation are shown.

The observed differences in body weight and fat mass conferred by cholic acid supplementation cannot be attributed to differences in food intake, as absolute food intake at week four did not differ, neither between diet groups nor between genotypes (Fig. 37).

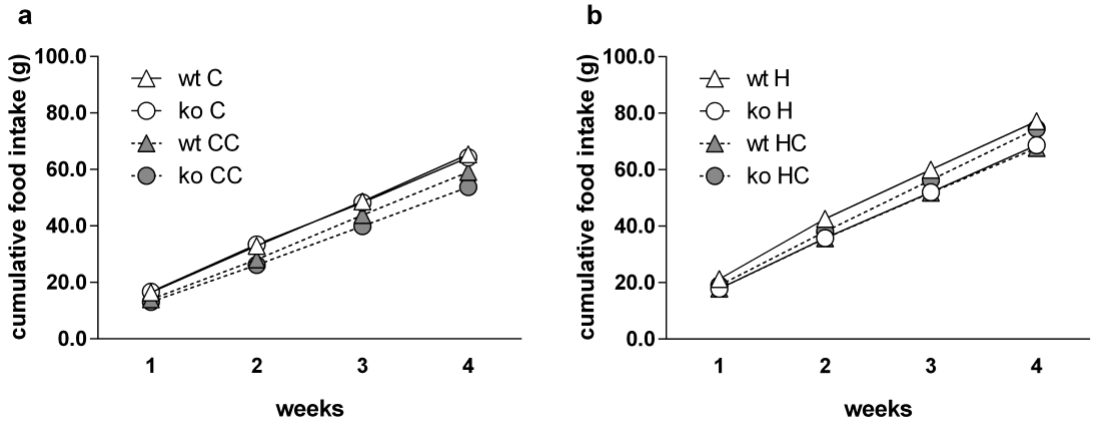

Fig. 37: Cumulative food intake of C57BL/6J wt and Ucp1 ko mice during four weeks of C and CC (a) or H and HC (b) diet feeding, respectively (n=6).

3.5.2 Brown and white adipose tissue weight analyses

Cholic acid supplementation did not affect iBAT mass of neither wt nor Ucp1 ko BL6J mice. It tended towards reducing iBAT mass of H-fed wt and ko mice, however statistically not significant. iBAT activity or function is not predicated on iBAT mass. Probably, the slight reduction of iBAT mass in H-fed animals, as it was also seen in earlier experiments, is only a cause of cholic acid induced body fat reduction, whereupon embedded white adipocytes within iBAT are reduced in size (Fig. 38).

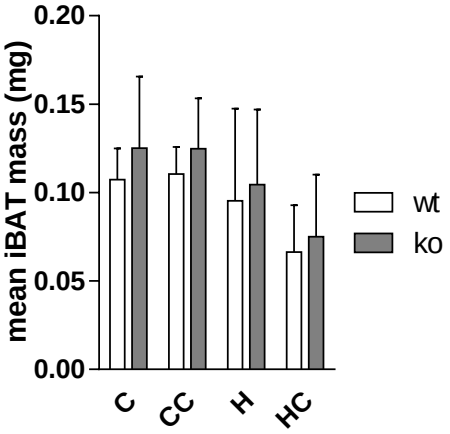

Fig. 38: iBAT mass after 28 experimental days (n=6). Means with standard deviation are shown. Statistical significance was tested using two separate two-way ANOVA analyses, each for C and H diets, respectively, with the two factors “CA-supplementation” and “genotype”. None of the two factors influenced iBAT mass.

Epididymal and inguinal WAT masses were analyzed both separately and pooled. Congruent with former experiments (and body mass/ other results obtained in this trial) the H feeding induced increase of WAT weight is abrogated by cholic acid supplementation in wt, but also in ko mice. To analyze the influence of the two factors “CA-supplementation” and “genotype” on eWAT and iWAT masses, we used two separate two-way ANOVAs for each C and H diets. In C diets, CA-supplementation was found to significantly influence pooled WAT mass (p=0.0062), whereas genotype does not. In H diets, both CA-supplementation (p=0.0023) as well as genotype (p=0.0085) significantly influenced pooled WAT mass, but no interaction between both factors was detected (Fig. 39). These observances point towards generally reduced WAT mass increase due to H feeding in Ucp1 ko mice, as well as a reduction of WAT mass in both genotypes due to CA-supplementation. However, CA-driven prevention of pooled WAT accumulation due to H feeding is equally potent in both genotypes.

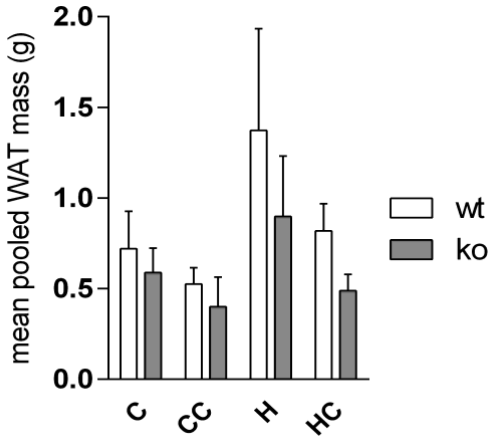

Fig. 39: Pooled WAT (both iWAT and eWAT) mass in wt and ko mice after 28 experimental days (n=6). Means with standard deviation are shown. Statistical significance was tested using two separate two-way ANOVA analyses, each for C and H diets, respectively, with the factors “CA-supplementation” and “genotype”.

Similar results were obtained, if iWAT and eWAT data were analyzed separately:

CA-supplementation significantly reduced iWAT mass of C-fed mice (p=0.0261) and of H-fed mice (p=0.0042) in both genotypes. Moreover, iWAT mass significantly differed between both genotypes (p=0.0334). There was no interaction between both factors in none of the two different diet groups (Fig. 40a). eWAT mass of C-fed mice was significantly influenced by both factors genotype (p=0.0105) and CA-supplementation (p=0.0029). The same result was obtained for eWAT mass of H-fed mice, as it was significantly reduced by CA-supplementation

(p=0.0016) and Ucp1 ko (p=0.0028). There was no interaction between both factors in none of the two different diet groups (Fig. 40b).

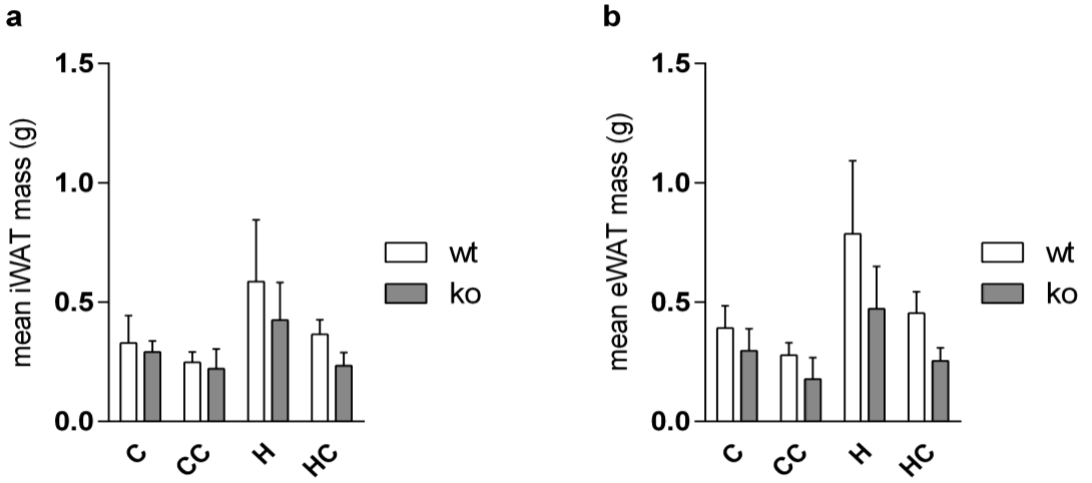

Fig. 40: Separate analyses of iWAT and eWAT mass in wt and ko mice after 28 experimental days (n=6). Means with standard deviation are shown. Statistical significance was analyzed for iWAT and eWAT separately. For each iWAT and eWAT, there were used two separate two-way ANOVA analyses, for C and H diets, respectively, with the two factors "CA-supplementation" and "genotype".

3.5.3 Blood parameter analysis

Piccolo Lipid Panel Plus Reagent Discs (Abaxis, Inc.) were used for the *in vitro* quantitative determination of total cholesterol, high-density lipoprotein cholesterol (HDL), triglycerides, as well as glucose, respectively, in heparinized plasma samples. Moreover, we determined plasma levels of the liver enzymes alanine aminotransferase (ALAT) and aspartate aminotransferase (ASAT), which are biomarkers for liver health.

We targeted on revising beneficial effects of dietary CA-supplementation, which is supposed to partially revert the pathological impact of H diet, and to generally compare plasma parameters of BL6J wt to Ucp1 ko mice.

As described in literature, the collected data patterns a general trend towards improving the H diet caused negative impact on blood parameters. The H diet-caused increase of cholesterol (p=0.0033), glucose (p=0.0014) and HDL (p=0.0132) levels was reduced by CA-supplementation. There was also seen a certain reduction of the respective plasma levels of C-fed animals. This trend was significant for cholesterol and HDL. We also observed a statistically significant genotype difference for cholesterol of C-fed animals (p=0.0260). In

summary, CA-supplementation partially causes improvement of blood parameters in H-fed mice (Fig. 41).

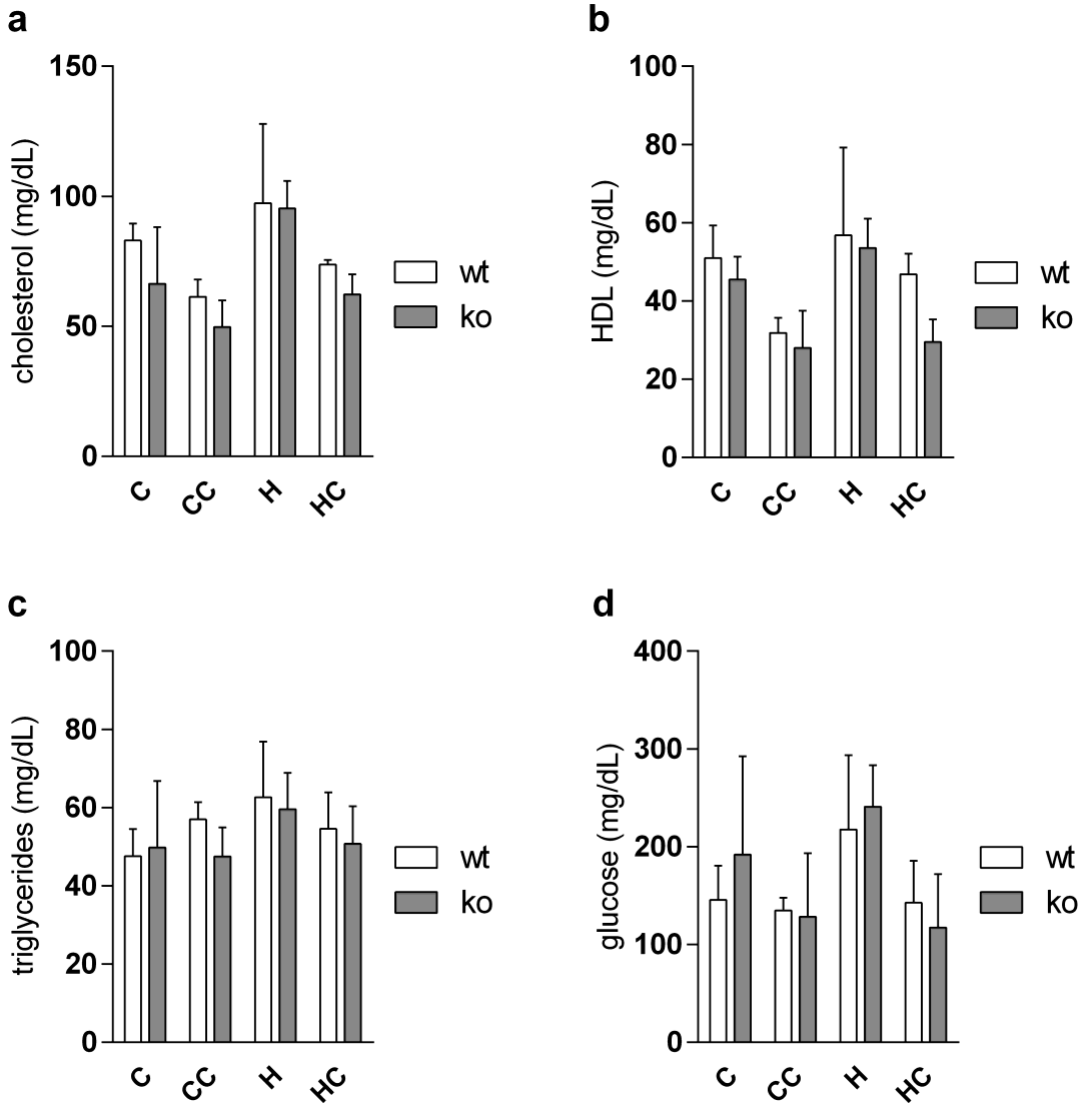

Fig. 41: Plasma parameter analysis in BL6J Ucp1 ko and wt mice, separated for diets (n=6). Plasma cholesterol (a), HDL (b), triglycerides (c), and glucose (d), means with standard deviation are shown. Two separate two-way ANOVAs were conducted for C and H diets, factors "CA-supplementation" and "genotype".

In contrast to these rather beneficial impacts, we also observed pathological side effects of CA-supplementation, as liver enzyme levels were increased in both CA-supplemented diets. Especially in H-fed animals, mean ALAT levels were increased 10-fold in wt and 8-fold, and ASAT levels were increased 6-fold in wt and 4-fold in ko mice due to CA-supplementation (Fig. 42). These increases were especially pronounced in single animals, resulting in high standard deviations. Therefore, the observed increase was only significant for ALAT of H-fed animals

(p=0.0179, two-way ANOVA over both wt and ko mice on H diet, factors “CA-supplementation” and “genotype”). If both genotypes are analyzed separately, the CA-supplementation-caused increase of ASAT and ALAT in H-fed ko mice is statistically significant (ALAT: p=0.0046, and ASAT: p=0.0186; unpaired t-tests).

C and CC-fed Ucp1 ko mice generally seemed to obtain higher ALAT and ASAT levels compared to H-fed animals as well as compared to wt mice. However, these observances only are significant for ALAT levels of C-fed animals.

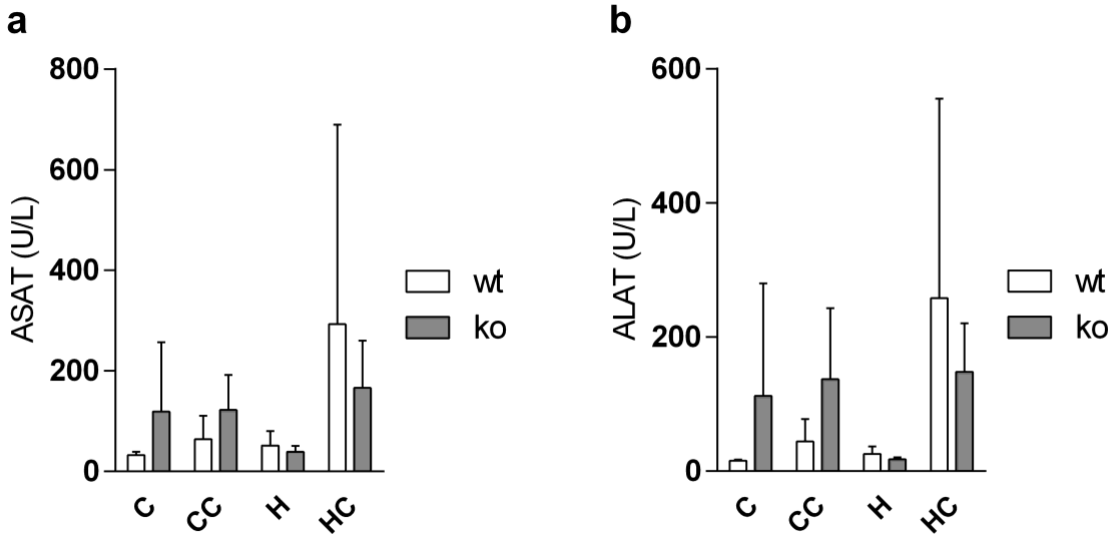

Fig. 42: Liver enzyme analysis in BL6J Ucp1 ko and wt mice, separated for diets (n=6). ASAT (a) and ALAT (b), means with standard deviation are shown. Two separate two-way ANOVAs were conducted for C and H diets, factors “CA-supplementation” and “genotype”.

Summarizing all results from the plasma metabolic marker analysis, we observed a CA-supplementation induced trend towards improvement of H diet caused impairment of selected plasma parameters. However, this improvement goes hand in hand with pathologically elevated liver enzyme levels (ASAT and ALAT), which points towards an impairment of liver functionality in both genotypes.

Taking together all results obtained from Ucp1 ko mouse studies, the Ucp1 gene knockout did not lead to a loss of the DIO-preventive effect of CA-supplementation in this experiment, as Ucp1 ko mice in all diet groups showed BM developments as well as body compositions, that are comparable to those of wt mice. These results stand in clear contrast to published literature. In conclusion, the DIO-preventive effect of dietary cholic acid supplementation must be independent of the Ucp1 gene.

4 DISCUSSION

During the last years, a new role for circulating bile acids has emerged, as bile acids do not only solubilize dietary lipids, cholesterol or fat-soluble vitamins, but also function as signaling molecules and thereby mediate various metabolic effects. Bile acids activate nuclear receptors like FXR (Makishima et al., 1999; Parks et al., 1999; Wang et al., 1999), the G-protein coupled receptor TGR5 (Kawamata et al., 2003; Maruyama et al., 2002) and cell signaling pathways in hepatocytes or enterocytes (Dent et al., 2005; Fang et al., 2007). Thereby bile acids influence e.g. glucose or fatty acid metabolism and contribute to the prevention or amelioration of characteristic features of the metabolic syndrome, as they e.g. protect mice against hepatic lipid accumulation, increased plasma triacyl glycerol and glucose levels (Liaset et al., 2011) and can prevent as well as reverse diet-induced obesity (Watanabe et al., 2006). The inverse correlation between systemic bile acid levels and body fat mass was not only observed in mice, but also was proved in men (Suzuki et al., 2014).

In order to increase the understanding how BAs mediate body mass stabilization, we investigated BA derived effects on two different inbred mouse strains, with a special focus on the generation of brite adipocytes in iWAT as well as energy expenditure analyses. Furthermore, we used Ucp1 knockout mice to clarify the participation of non-shivering thermogenesis at this effect.

4.1 Cholic acid derived prevention from diet-induced obesity in C57BL/6J mice

In our study we were able to reproduce the DIO-protective effect of cholic acid (CA) in BL6J mice, that has been described previously (Teodoro et al., 2014; Watanabe et al., 2011; Watanabe et al., 2006; Watanabe et al., 2012; Zietak and Kozak, 2016), as HC-fed mice showed a significantly lower body mass increase compared to H-fed mice without differences in energy intake. Body mass stabilization in HC-fed BL6J mice could be fully explained by a significant fat mass reduction due to CA-supplementation, whereas lean mass was not affected. Intriguingly, body mass was not further reduced in CC-fed animals compared to C-fed mice. This phenomenon is already confirmed on cell level by *in vitro* experiments, where isolated BAT cells were treated with TCA and cells from H-fed mice were more sensitive to the addition of

TCA than cells from chow fed mice (Watanabe et al., 2006). Yet it needs to be clarified why this effect is only present in relation to high-fat diets.

As CA-supplementation did not affect energy assimilation, we hypothezised, that energy expenditure was the site to analyze BA effects on body mass stabilization. Due to a spillover from liver into blood circulation, BAs reach peripheral sites of action. Thus it was hypothesized, that BAs bind TGR5 in BAT and initiate a signaling cascade, where cAMP-dependent thyroid hormone activating enzyme type 2 iodothyronine deiodinase (D2) is induced. Thereby D2 converts inactive thyroxine (T_4) into the active 3,5,3'-tri-iodothyronine (T_3) (Bianco et al., 2002). Besides, other key genes in energy expenditure were reported to be increasingly expressed in BAT after BA feeding, amongst others PGC-1α, which is the main regulator of mitochondrial biogenesis (Weitzel et al., 2003), and UCP1, which mediates non-shivering thermogenesis in BAT. Thereby energy expenditure in BAT and skeletal muscle shall activated, leading to adiposity prevention and insulin sensitization(Watanabe et al., 2006). In BAT, this mechanism is proposed to be driven by an enhanced Ucp1 mRNA expression (Watanabe et al., 2006).

In order to assess the influence of BA-supplementation on BAT, we investigated iBAT mass and morphology as well as Ucp1 mRNA expression levels of BL6J mice, which were fed either a low fat control diet (C) or a high-fat diet (H) non-supplemented or supplemented with cholic acid (CC and HC). Comparable to previously published results, iBAT of HC-fed mice weighed significantly less than iBAT of their H-fed counterparts. Microscopic analyses confirmed that not only surrounding WAT mass, but also lipid content of brown adipocytes was reduced due to CA-supplementation. This effect could not be observed in iBAT of CA-supplemented C-fed mice. Besides reduction of adipocyte hypertrophy, it has already been shown by electron microscopic analyses, that CA-supplementation leads to an increase in the number of lamellar cristae in iBAT mitochondria. This effect goes along with an increase of iBAT Ucp1 mRNA expression (Watanabe et al., 2006). Moreover, it was shown, that also CDCA-supplementation to H diet increases iBAT Ucp1 mRNA expression as well as UCP1 protein content in C57BL/6J mice (Teodoro et al., 2014). In contrast to that, we were not able to confirm this effect, as we observed a significant reduction of iBAT Ucp1 mRNA expression levels in HC-fed mice. In order to approve and further explain our result, iBAT UCP1 measurements on protein level need to be performed. However, HC-feeding showed to significantly reduce iWAT mass as well as

adipocyte lipid content in BL6J mice. Microscopic analyses revealed the occurrence of multilocular cells in iWAT of HC-fed BL6J mice. With respect to browning, we used qPCR measurements to confirm the induction of the BAT-selective genes Ucp1, Cox7A1, CideA and Otop1. We found an overall increase of BAT-selective gene expression in iWAT due to CA-supplementation to H diet, as well as a moderate, but significant increase of Ucp1 transcript abundance as reported earlier (Teodoro et al., 2014; Zietak and Kozak, 2016), an effect probably caused by direct interaction of bile acids with TGR5 (Velazquez-Villegas et al., 2018). Moreover, immunohistochemical staining for UCP1-positive cells in iWAT showed a relative browning effect of CA-supplementation in H-fed BL6J mice. The bile acid-derived promotion of fat oxidation was not only proved after dietary bile acid supplementation, but also after continuous intracerebroventricular bile acid infusion, (Eggink et al., 2017), showing that bile acids may exert metabolic effects on fat metabolism via the brain. Besides, supplementing a gut-restricted agonist for the bile acid sensor farnesoid X receptor (FXR) induces enteric fibroblast growth factor 15 (FGF15) and thereby alters BA composition, reduces DIO, enhances thermogenesis and WAT browning (Fang et al., 2015). Therefore, the influence of BAs on metabolism seems to have different sites of action, as cerebral as well as peripheral-mediated BA signals lead to similar effects like DIO-resistance or WAT browning.

We can confirm that CA-supplementation effectively prevents BL6J mice from DIO by significantly decreasing WAT mass. Moreover, CA-supplementation significantly increases brown fat marker expression and leads to a recruitment of UCP1-positive multilocular cells in iWAT of H-fed BL6J mice, but has none of these effects in C-fed BL6J mice.

4.2 Cholic acid supplementation does not induce energy expenditure in C57BL/6J mice

We hypothesized, that energy expenditure must be responsible for the DIO-preventive effect of CA-supplementation, as it neither affected food nor energy intake. In order to analyze the influence of CA-supplementation on energy expenditure, indirect calorimetry as well as feeding-drinking-activity measurements were performed on C57BL/6J mice. Already one day after diet change, clear differences between H and HC-fed animals were observed. Mean RER of both diet groups was lowered. All mice displayed the typical circadian rhythm of nocturnal activity accompanied by high heat production and preferred carbohydrate usage as compared

to lower heat production and preferred lipid use during daytime. However, CA-supplementation stimulated an accentuation of the H-diet-induced decrease of RER, which verifies that BA-supplementation increases fat oxidation, as already described in earlier publications (Teodoro et al., 2014; Watanabe et al., 2006). Furthermore, we observed a time-delayed shift of mean RER pattern in HC-fed mice, which has not been shown or discussed before. This shift suggests that HC-fed mice either start feeding at later time points compared to H-fed mice, probably due to an unpleasant flavor of CA, which is known to exhibit a bitter taste, or that CA-supplementation leads to an altered metabolism, where lipid metabolism phase is prolonged and the change to carbohydrate metabolization is delayed.

Despite body mass and body composition developments that were comparable to the results of our former experiments, as well as the observed differences in mean RER, daily energy expenditure as well as resting metabolic rate did not differ between H and HC-fed mice after body mass adjustment. Thus, mice displayed a DEE appropriate for their individual body mass regardless of dietary bile acid supplementation at all times and only differences in body mass accounted for the differences in energy expenditure. Nevertheless, our data can not be resolved high enough to explain the minor differences in energy balance, that accumulate to the final differences in body weight and composition. Food intake measurements potentially were not accurate enough to reveal the relevant changes in energy intake that might account for the observed phenomenon. Previous studies stated that BA-mediated prevention of DIO could not be traced back by a decreased food intake. However, food intake oftentimes was adjusted to the animals' BW (Watanabe et al., 2011; Watanabe et al., 2006; Watanabe et al., 2012). Thereby a decrease in absolute food intake could be disguised with a decreased BW, which occurred after CA-supplementation. In studies, where a food intake per mouse was considered, a transient decrease in food intake could be observed at the beginning of the intervention (Teodoro et al., 2014). During these studies, pair-feeding experiments were conducted in order to dissect the effect of BA-supplementation on body mass *per se*. Pair-feeding revealed that the DIO-preventive effect of BAs mostly traces back to a reduced food intake. However, a relatively mild and food intake-independent reduction in adiposity (not detectable on body weight level) could be observed, as well (Teodoro et al., 2014).

Our data cannot support the hypothesis that dietary bile acid supplementation increases energy expenditure as described before (Ockenga et al., 2012; Watanabe et al., 2006; Zietak

and Kozak, 2016). However, none of these observations doubtlessly proved that bile acid supplementation to mice causes an increase in energy expenditure. Data of Watanabe et al., 2006 is only based on a 15 hours indirect calorimetry measurement and normalized to body mass (Watanabe et al., 2006), a procedure not advisable in animals of different body mass and composition (Butler and Kozak, 2010; Tschop et al., 2011). Ockenga et al., 2012 did not show original data on O_2-consumption or VO_2-production, but only presented calculated values of energy expenditure, whose basis of calculation is not explained within this article (Ockenga et al., 2012). Zietak and Kozak, 2016 only consulted an indirect prove by estimating total energy expenditure with the help of a formula, that basically subtracts change in body energy stores from caloric intake (Ravussin et al., 2013; Zietak and Kozak, 2016). Moreover, two independent studies by other laboratories measuring the impact of dietary bile acid supplementation found no effect on energy expenditure (da-Silva et al., 2011; Teodoro et al., 2014).

To sum up, we cannot confirm an increase in energy expenditure in response to cholate supplementation, neither in absolute terms nor adjusted and neither at rest nor as a daily budget. As this conclusion was also drawn in other laboratories (da-Silva et al., 2011; Teodoro et al., 2014), we conclude that the contribution of brown fat thermogenesis to DIO-resistance conferred by cholate supplementation is questionable.

4.3 Cholic acid derived prevention from diet-induced obesity is strain specific

As bile acid derived prevention of DIO is claimed to result from increased BAT activity, we speculated that brite adipocyte recruitment may have an important influence and additionally contributes to the body mass stabilizing outcome. We used 129S6 mice to study the browning potential observed in BL6J mice by CA supplementation and eventually to potentiate it within this strain, as 129S6 mice have a higher propensity to recruit brite adipocytes. The 129S6 mice received the same diets and experimental treatments as the BL6J mice.

In contrast to our hypothesis, 129S6 mice were not at all responsive for CA-supplementation, as no differences emerged between non-supplemented and supplemented diet groups. All metabolic consequences of the CA-supplementation observed in C57BL/6J animals are

completely absent in 129S6 mice: Neither body mass development, nor iBAT or iWAT mass, morphology and gene expression profile was influenced by CA-supplementation. These results clearly exhibit the novel finding, that the prevention of DIO by BAs is mouse strain specific. With the help of this phenomenon, we obtained the possibility to specifically study strain specificities and thereby elucidate the adiposity protective effects of BAs in BL6J mice.

We started to compare both mouse strains by the enteral bile acid transporters ASBT and OST. ASBT is located at the apical membrane of ileal enterocytes and responsible for the uptake of bile acids from gut lumen across the apical brush border membrane of the enterocyte (Shneider, 2001). An Asbt knockout results in a down-regulation of FXR target genes such as Fgf15. The decreased Fgf15 expression as well as the reduced return of BAs to the liver results in an increased Cyp7a1 expression, thus resulting in an increased translation of the rate-limiting enzyme in the classical BA synthesis pathway. Accordingly, BA synthesis is increased by the Asbt gene knockout (Dawson, 2015). The heteromeric BA transporter OSTα-OSTβ is located at the enterocyte's basolateral membrane. Ostα and Ostβ actually are expressed in most tissues, but are most abundant in tissues involved in bile acid and steroid homeostasis (Ballatori et al., 2009). In Ostα knockout mice, Fgf15 expression is increased due to an increased BA storage in the enterocyte. Thereby Cyp7a1 gene expression is decreased and BA synthesis limited (Dawson, 2015; Rao et al., 2008). We were in fact able to identify strain specific differences, which might be jointly responsible for the varying bile acid absorption.

For this reason, and as we could not observe a difference in food intake and thereby CA uptake between both strains, we suspected differences in CA uptake within gut and spillover into circulation or in CA excretion. Therefore, BA analyses were conducted to determine BA concentration and composition in plasma, enterohepatic organs and feces.

Plasma BA analysis revealed that BL6J mice generally exhibit higher plasma BA levels compared to 129S6. Plasma BA levels were found to be influenced by both CA-supplementation and strain, respectively, in H diet groups. Additionally, we confirmed a higher plasma BA-raising effect for supplemented H-fed BL6J compared to 129S6 animals. There were not found major differences in plasma BA composition between strains or diet groups.

Organ bile acid pool was significantly influenced by strain and CA-supplementation: BL6J mice naturally possess a higher organ BA pool size compared to 129S6 mice, and CA-

supplementation led to a significant increase in organ pool size in both strains. Thereby, organ BA pool was stronger raised in BL6J compared to 129S6 animals. Compositional differences were merely seen due to CA-supplementation and not due to strain.

Fecal BA excretion mass also was increased due to CA-supplementation in both strains and diets. A strain effect as well as a diet-strain interaction was observed in C-fed animals, with a stronger increase of BA excretion in CA-supplemented BL6J mice compared to 129S6 mice. Similar to the other compartments, no differences were observed in fecal BA composition.

Taking together all results we can conclude that the spillover of BAs from enterohepatic circulation into plasma might account for the BA-derived effects itself, but does not seem to be responsible for the strain difference. As the relevant strain specific differences of H-fed animals were already seen in organ BA concentrations, and strain-specific differences in plasma BA levels only reflect those in enterohepatic organs, the CA-derived prevention of DIO must originate from a site of action, which is located downstream of plasma circulation.

Differences in plasma BA levels might be responsible for the CA-derived DIO-preventive effect in H diets only. As no effect of neither strain nor CA-supplementation was found in plasma BA levels in C-fed animals, but plasma BA levels were stronger increased in CA-supplemented H-fed BL6J mice, the relevant site of action might be along plasma circulation.

4.4 Using C57BL/6J Ucp1 knockout mice to challenge the hypothesis of UCP1-derived prevention of diet-induced obesity by cholic acid

In the absence of increased energy expenditure, the contribution of brown fat thermogenesis to DIO resistance conferred by CA-supplementation is questionable. We nevertheless conducted the appropriate experiment to investigate this possibility by including Ucp1 ko mice into a feeding trial, according to the initial experiments with BL6J and 129S6 mice.

In general, iBAT Ucp1 expression is decreased under thermoneutral conditions (Freeman et al., 1989; Rippe et al., 2000), as UCP1 is not needed to maintain body temperature. Moreover, Ucp1 ko mice were described to be DIO-resistant at room temperature (20° C), as they have to maintain normal body temperature without non-shivering thermogenesis, but by using less efficient, more energy consumptive pathways of metabolism (Liu et al., 2003). It has been

described that only UCP1 can mediate adaptive non-shivering thermogenesis in the cold and Ucp1-deficient mice shiver to maintain their body temperature (Golozoubova et al., 2001; Nedergaard et al., 2001). For this reason, and in order to subtract the energy expenditure used for body temperature maintenance as well as to distinctly quantify the BA-derived increase of energy expenditure, the experiment was conducted at thermoneutrality.

At room temperature, mice approximately use one third of the consumed calories to maintain body temperature (James and Trayhurn, 1981). Under thermoneutral conditions, no energy has to be expended to maintain body temperature. Accordingly, if food intake is not limited, excess energy from a high-fat diet is stored in adipose tissue and animals show an increased body mass gain compared to keeping at room temperature (Cui et al., 2016; Stemmer et al., 2015). In contrast, low-fat diet fed animals are able to regulate their appetite, resulting in a maintained body weight balance (Enerback et al., 1997). Under high-fat diet, however, it has already been described that food intake is not reduced, resulting in an increased body weight of high-fat diet fed animals at thermoneutrality (Rippe et al., 2000). During our thermoneutral experiment, the animals indeed reduced their food intake compared to the experiments at room temperature, but this reduction was not great enough to compensate for the decreased need of energy intake.

As described before, we used Ucp1 ko mice to investigate its necessity to mediating BA-derived DIO-resistance and thereby clearly demonstrate that UCP1-dependent, non-shivering thermogenesis in brown or brite adipocytes is not required for bile acid mediated protection against DIO. This conclusion, however, is in disagreement with the results of a very similar experiment with the same mouse strain conducted unknowingly in parallel in L. Kozak's laboratory (Zietak and Kozak, 2016). Here, Ucp1 ko mice were not protected against DIO by CA-supplementation. However, even the role of UCP1 itself in the development of DIO is not fully resolved. In different studies, the identical Ucp1 ko mouse strain is more (Feldmann et al., 2009; Rowland et al., 2016; von Essen et al., 2017), less (Liu et al., 2003) or similarly prone to DIO (this study, Maurer, 2016; Winn et al., 2017; Zietak and Kozak, 2016), even from cohort to cohort within the same colony (Von Essen, 2017).

For example, the studies of Liu et al. revealed that Ucp1-deficient mice are DIO-resistant at room temperature. Control wildtype mice significantly gained more body mass on a high-fat

diet. This difference, however, was reverted if ambient temperature was raised to 27 °C. Moreover, Ucp1 ko mice generally possessed lower RER values and it was shown, that this effect is not dependent on the ambient temperature, but on the diet's fat content. Moreover, Ucp1 ko mice apparently had a basic difference in substrate utilization compared to wt mice. From all their findings, Liu et al. hypothesized, that thermogenesis in Ucp1 ko mice is metabolically more expensive and for these reasons Ucp1 kos paradoxically are protected against obesity (Liu et al., 2003). Nevertheless, investigations failed to demonstrate an obese phenotype in Ucp1 ablated mice (Enerback et al., 1997; Liu et al., 2003).

In contrast to that, Feldmann and colleagues showed that an Ucp1 ablation in itself is sufficient to induce obesity under thermoneutral conditions (Feldmann et al., 2009). In their experiments, body fat depots' weights were significantly increased in both low fat and high-fat diet fed mutant mice, respectively. In conformity with Liu et al., they speculated that under thermoneutral conditions, there is no longer a need for a chronically elevated metabolism, as it is normally required at room temperature to maintain body temperature. Room temperature actually is a chronic thermal stress for mice, as they have to defend their body temperature at a low grade constantly. This is ensured by an increased food intake (Feldmann et al., 2009).

In our hands, no difference in neither body weight, fat nor lean mass development was detected between wildtype and Ucp1 ko BL6J mice under thermoneutral conditions. Both genotypes accumulated excess adipose tissue due to H-feeding. Comparable to experiments on wt BL6J mice at room temperature, CA-supplementation also leads to DIO-resistance and reduced accumulation of WAT depots in both BL6J wt and Ucp1 ko mice at thermoneutrality. Compared to room temperature, BL6J wt mice absolutely gained more body mass under thermoneutral conditions, as shown in earlier experiments (Rippe et al., 2000), but were also prevented from DIO, independently of their genotype. For this reason, we conclude, that the DIO-protective effect of CA-supplementation is independent of Ucp1.

4.5 Relevance in humans

To this day it has not been investigated whether cholic acid also exerts all of these positive effects on metabolic outcomes in men. If the findings obtained in rodent studies relating to weight control or glucose and lipid metabolism can be confirmed in human studies, such drugs would be highly attractive (Jenkins et al., 2008).

It has been proposed, that the DIO-preventive effect exerted by CA-supplementation might also be present in men, as the treatment of brown adipocytes and human skeletal myocytes with BA were shown to increase D2 activity and oxygen consumption *via* the activation of UCP1. It was postulated, that this effect is also mediated by TGR5-activation (Watanabe et al., 2006). However, the mere co-expression of the ubiquitously expressed BA receptor TGR5 and D2 in human skeletal muscle cells does not necessarily implicate a direct link of BA-D2-Ucp1 pathway in human BAT.

Since metabolically active brown adipose tissue has been identified in adult humans (Cypess et al., 2009; van Marken Lichtenbelt et al., 2009; Virtanen et al., 2009) brown adipose tissue activity has become an interesting target for the treatment of obesity, especially as the amount and activity of BAT in men is inversely correlated with body-mass index (Cypess et al., 2009) and percentage of body fat, but positively correlated with resting metabolic rate (van Marken Lichtenbelt et al., 2009). In addition, BAT-positive subjects are of comparatively younger age, have lower fasting insulin levels and insulin resistance, but a greater level of high-density lipoprotein cholesterol than individuals without BAT (Zhang et al., 2013).

In a study supplementing the primary bile acid chenodeoxycholic acid (CDCA) and investigating BAT activity via PET/CT examinations, it was shown that CDCA-supplementation indeed increases human BAT activity. However, the authors could not exclude, that BAs increase energy expenditure via BAT-independent mechanisms (Broeders et al., 2015). Nevertheless, as CDCA showed to be BAT-activating in humans, the other primary bile acid CA might be a promising BAT-activator, as well.

Humans have long been treated with the tertiary bile acid ursodeoxycholic acid (UDCA), which is formed in the liver by epimerization of the secondary bile acid lithocholic acid and naturally occurring in high concentration in the bile of the Chinese black bear (Gray). UDCA improves

fat digestion and absorption in cystic fibrosis patients with mild liver involvement (Drzymala-Czyz et al., 2016). Moreover, UDCA is used in the therapy on gallstone formation (Worobetz et al., 1993), or chronic liver disease (Guslandi, 1990) and has shown chemopreventive potential in colon cancer (Solimando et al., 2011). However, the respective studies have not focused on whether the often accompanying weight loss was more pronounced in the UDCA-treated group, or whether UDCA drugs used to prevent gallstone formation had an effect beyond that of bariatric surgery itself (Worobetz et al., 1993).

After Roux-en-Y gastric bypass (RYGB) surgery, in which the stomach's small upper pouch is directly connected to the small intestine (Andalib et al., 2015), total fasting BAs are increased compared to preoperative levels. This effect was not observed after purely restrictive procedures like adjustable gastric banding (Kohli et al., 2013; Patti et al., 2009; Pournaras et al., 2012). RYGB is the most effective treatment for morbid obesity and diabetes (Kashyap et al., 2013; Schauer et al., 2012). However, the resolution of diabetes and other comorbid conditions typically occurs before significant weight loss. As bile acid homeostasis is a tightly regulated process, and bile acid level and composition are rapidly adapted after RYGB, BAs have been identified as one class of putative compounds involved in the weight-independent effects of bariatric surgery. Overall findings on bile acid changes after bariatric surgery propose that especially bacterially derived, secondary BAs may mediate the early improvements after RYGB (Albaugh et al., 2015; Lutz and Bueter, 2014). These observations suggest an important influence of not only BA concentration, but also composition on metabolic outcomes. Moreover, an inverse correlation between postprandial bile acid concentration and body fat mass in healthy normal-weight subjects has been proven (Suzuki et al., 2014). The underlying mechanisms, however, have not been elucidated, yet.

Besides their positive metabolic impacts, bile acids may also exert deleterious effects if supplemented. As bile acids are potent detergents and cytotoxic at higher concentrations, their synthesis is normally tightly controlled and bile acid concentration normally maintains within narrow limits, to avoid cellular injury. Bile acids themselves are known to be cytotoxic to hepatocytes (Malhi et al., 2010) and early human studies confirm bile acid toxicity in primary human hepatocytes e.g. using GCDCA (Galle et al., 1990). Therefore, increased bile acid concentrations that for example are caused by bile acid supplementation can also generate a series of problems: Bile acids can induce arrhythmias (Desai and Penny, 2013), not

only in adults but also in fetuses. Intrahepatic cholestasis of pregnancy, where bile acid concentrations are pathologically raised in the mothers circulation, causes fetal arrhythmia and sudden intrauterine death (Sheikh Abdul Kadir et al., 2010). Besides, dietary lithocholic acid supplementation was shown to result in intrahepatic cholestasis and bile infarcts. This hepatotoxic effects went in line with a significant increase in plasma ALAT levels (Woolbright et al., 2014), an effect that we also observed in response to dietary cholic acid supplementation in BL6J mice. For this reason, the currently known positive effects of a dietary bile acid supplementation are not great enough to legitimate the negative consequences accompanying a bile acid treatment in humans.

4.6 Conclusion and perspective

In summary, we here report that the DIO-protective effect of a dietary cholic acid supplementation is mouse strain specific, does not increase energy expenditure and does not require UCP1-dependent, non-shivering thermogenesis.

The black and white strain difference observed in the metabolic response of C57BL/6J and 129S6/SvEvTac mice certainly proves a valuable model to elucidate molecular mechanistic determinants of these processes. However, it remains to be clarified which of the two strains is more representative for other mouse strains, other commonly used animal models and humans. Disconcertingly, a large body of literature on effects of dietary cholate supplementation relies on experiments with the C57BL/6J mouse strain (da-Silva et al., 2011; Teodoro et al., 2014; Watanabe et al., 2011; Watanabe et al., 2006; Watanabe et al., 2012; Zietak and Kozak, 2016). Past conclusions will have to be reviewed in the light of the very specific genetic background leading to exceptionally high bile acid sequestration and spillover in this strain and the new finding that all of these effects may be strain-specific.

Furthermore, dietary cholic acid supplementation also seems to recruit brite adipocytes in C57BL/6J iWAT. However, its underlying thermogenic capacity is not great enough to explain the prevention of adipose tissue accumulation during H diet. Moreover, indirect calorimetry measurements did not hint at an increased energy expenditure mediated by the CA-supplementation. We were not able to detect differences in energy intake, energy expenditure or energy loss with feces, respectively. Nevertheless, substantial body weight

differences were observed between CA-supplemented and non-supplemented H-fed BL6J animals. Our analytical apparatuses either were not sensitive enough to explain the minor differences in energy balance that in the end account for the DIO-protection of CA-supplementation, or more likely, CA-supplemented H-fed animals consume less food compared to non-supplemented mice. This would not explain why CA-supplemented C-fed animals do not loose further weight compared to non-supplemented C-fed mice, yet.

In the end, we clearly showed that the DIO-preventive effect of bile acids is independent of UCP1, as the respective knockout animals are protected in the same manner as wildtype animals. This is in line with the results obtained from indirect calorimetry measurements that also did not provide a basis for an increased non-shivering energy expenditure mediated by UCP1.

Data on the effects of bile acids is diversely discussed in literature. The underlying mechanisms of bile acid-derived effects on energy expenditure still are not doubtlessly elucidated. Bile acids in general display a wide range of steroid compounds that are not well studied up to date, but might be promising metabolic active effectors.

Despite all the positive impacts that are described in literature and assigned to bile acids, we must not forget that bile acids are potent detergents and cytotoxic at higher concentrations. Under physiologic conditions, bile acid synthesis is tightly controlled and BA concentration normally maintains within narrow limits to avoid cellular injury (in healthy objects, without BA-supplementation). A bile acid supplementation that e.g. prevents from diet-induced obesity also elevates systemic bile acid concentrations to cytotoxic levels. Therefore, the currently known positive effects of a dietary bile acid supplementation are not great enough to legitimate the negative consequences accompanying a bile acid treatment in human. In the future, any advantages and disadvantages of bile acid supplementation must be carefully considered.

LITERATURE

Ailhaud, G. (2000). Adipose tissue as an endocrine organ. Int J Obes Relat Metab Disord *24 Suppl 2*, S1-3.

Albaugh, V.L., Flynn, C.R., Cai, S., Xiao, Y., Tamboli, R.A., and Abumrad, N.N. (2015). Early Increases in Bile Acids Post Roux-en-Y Gastric Bypass Are Driven by Insulin-Sensitizing, Secondary Bile Acids. The Journal of clinical endocrinology and metabolism *100*, E1225-1233.

Alpini, G., Glaser, S., Baiocchi, L., Francis, H., Xia, X., and Lesage, G. (2005). Secretin activation of the apical Na+-dependent bile acid transporter is associated with cholehepatic shunting in rats. Hepatology *41*, 1037-1045.

Andalib, I., Shah, H., Bal, B.S., Shope, T.R., Finelli, F.C., and Koch, T.R. (2015). Breath Hydrogen as a Biomarker for Glucose Malabsorption after Roux-en-Y Gastric Bypass Surgery. Dis Markers *2015*, 102760.

Angelin, B., Bjorkhem, I., Einarsson, K., and Ewerth, S. (1982). Hepatic uptake of bile acids in man. Fasting and postprandial concentrations of individual bile acids in portal venous and systemic blood serum. The Journal of clinical investigation *70*, 724-731.

Ballatori, N., Christian, W.V., Wheeler, S.G., and Hammond, C.L. (2013). The heteromeric organic solute transporter, OSTalpha-OSTbeta/SLC51: a transporter for steroid-derived molecules. Mol Aspects Med *34*, 683-692.

Ballatori, N., Li, N., Fang, F., Boyer, J.L., Christian, W.V., and Hammond, C.L. (2009). OST alpha-OST beta: a key membrane transporter of bile acids and conjugated steroids. Frontiers in bioscience : a journal and virtual library *14*, 2829-2844.

Barbatelli, G., Morroni, M., Vinesi, P., Cinti, S., and Michetti, F. (1993). S-100 protein in rat brown adipose tissue under different functional conditions: a morphological, immunocytochemical, and immunochemical study. Exp Cell Res *208*, 226-231.

Barbatelli, G., Murano, I., Madsen, L., Hao, Q., Jimenez, M., Kristiansen, K., Giacobino, J.P., De Matteis, R., and Cinti, S. (2010). The emergence of cold-induced brown adipocytes in mouse white fat depots is determined predominantly by white to brown adipocyte transdifferentiation. Am J Physiol Endocrinol Metab *298*, E1244-1253.

Berry, W., and Reichen, J. (1983). Bile acid metabolism: its relation to clinical disease. Semin Liver Dis *3*, 330-340.

Bianco, A.C., Salvatore, D., Gereben, B., Berry, M.J., and Larsen, P.R. (2002). Biochemistry, cellular and molecular biology, and physiological roles of the iodothyronine selenodeiodinases. Endocr Rev *23*, 38-89.

Brauer, R.W., Leong, G.F., and Holloway, R.J. (1954). Mechanics of bile secretion; effect of perfusion pressure and temperature on bile flow and bile secretion pressure. The American journal of physiology *177*, 103-112.

Brendel, C., Schoonjans, K., Botrugno, O.A., Treuter, E., and Auwerx, J. (2002). The small heterodimer partner interacts with the liver X receptor alpha and represses its transcriptional activity. Molecular endocrinology (Baltimore, Md.) *16*, 2065-2076.

Broeders, E.P., Nascimento, E.B., Havekes, B., Brans, B., Roumans, K.H., Tailleux, A., Schaart, G., Kouach, M., Charton, J., Deprez, B., et al. (2015). The Bile Acid Chenodeoxycholic Acid Increases Human Brown Adipose Tissue Activity. Cell metabolism *22*, 418-426.

Butler, A.A., and Kozak, L.P. (2010). A recurring problem with the analysis of energy expenditure in genetic models expressing lean and obese phenotypes. Diabetes *59*, 323-329.

Cannon, B., and Nedergaard, J. (2004). Brown adipose tissue: function and physiological significance. Physiol Rev *84*, 277-359.

Cariou, B., Bouchaert, E., Abdelkarim, M., Dumont, J., Caron, S., Fruchart, J.C., Burcelin, R., Kuipers, F., and Staels, B. (2007). FXR-deficiency confers increased susceptibility to torpor. FEBS Lett *581*, 5191-5198.

Chiang, J.Y. (2013). Bile acid metabolism and signaling. Compr Physiol *3*, 1191-1212.

Coleman, R., Iqbal, S., Godfrey, P.P., and Billington, D. (1979). Membranes and bile formation. Composition of several mammalian biles and their membrane-damaging properties. The Biochemical journal *178*, 201-208.

Cousin, B., Munoz, O., Andre, M., Fontanilles, A.M., Dani, C., Cousin, J.L., Laharrague, P., Casteilla, L., and Penicaud, L. (1999). A role for preadipocytes as macrophage-like cells. FASEB J *13*, 305-312.

Cui, X., Nguyen, N.L., Zarebidaki, E., Cao, Q., Li, F., Zha, L., Bartness, T., Shi, H., and Xue, B. (2016). Thermoneutrality decreases thermogenic program and promotes adiposity in high-fat diet-fed mice. Physiol Rep *4*.

Cypess, A.M., Lehman, S., Williams, G., Tal, I., Rodman, D., Goldfine, A.B., Kuo, F.C., Palmer, E.L., Tseng, Y.H., Doria, A., et al. (2009). Identification and importance of brown adipose tissue in adult humans. N Engl J Med *360*, 1509-1517.

da-Silva, W.S., Ribich, S., Arrojo e Drigo, R., Castillo, M., Patti, M.E., and Bianco, A.C. (2011). The chemical chaperones tauroursodeoxycholic and 4-phenylbutyric acid accelerate thyroid hormone activation and energy expenditure. FEBS Lett *585*, 539-544.

Dawson, P.A. (2015). Impact of Inhibiting Ileal Apical versus Basolateral Bile Acid Transport on Cholesterol Metabolism and Atherosclerosis in Mice. Digestive diseases *33*, 382-387.

Dawson, P.A., Lan, T., and Rao, A. (2009). Bile acid transporters. Journal of lipid research *50*, 2340-2357.

Dent, P., Fang, Y., Gupta, S., Studer, E., Mitchell, C., Spiegel, S., and Hylemon, P.B. (2005). Conjugated bile acids promote ERK1/2 and AKT activation via a pertussis toxin-sensitive mechanism in murine and human hepatocytes. Hepatology *42*, 1291-1299.

Desai, M.S., and Penny, D.J. (2013). Bile acids induce arrhythmias: old metabolite, new tricks. Heart *99*, 1629-1630.

Drzymala-Czyz, S., Jonczyk-Potoczna, K., Lisowska, A., Stajgis, M., and Walkowiak, J. (2016). Supplementation of ursodeoxycholic acid improves fat digestion and absorption in cystic fibrosis patients with mild liver involvement. Eur J Gastroenterol Hepatol *28*, 645-649.

Duboc, H., Tache, Y., and Hofmann, A.F. (2014). The bile acid TGR5 membrane receptor: from basic research to clinical application. Dig Liver Dis *46*, 302-312.

Eggert, T., Bakonyi, D., and Hummel, W. (2014). Enzymatic routes for the synthesis of ursodeoxycholic acid. J Biotechnol *191*, 11-21.

Eggink, H.M., Tambyrajah, L.L., van den Berg, R., Mol, I., van den Heuvel, J.K., Koehorst, M., Groen, A.K., Boelen, A., Kalsbeek, A., Romijn, J.A., et al. (2017). Chronic infusion of taurolithocholate into the brain increases fat oxidation in mice. J Endocrinol.

Enerback, S., Jacobsson, A., Simpson, E.M., Guerra, C., Yamashita, H., Harper, M.E., and Kozak, L.P. (1997). Mice lacking mitochondrial uncoupling protein are cold-sensitive but not obese. Nature *387*, 90-94.

Even, P.C., and Nadkarni, N.A. (2012). Indirect calorimetry in laboratory mice and rats: principles, practical considerations, interpretation and perspectives. Am J Physiol Regul Integr Comp Physiol *303*, R459-476.

Eyssen, H.J., Parmentier, G.G., and Mertens, J.A. (1976). Sulfated bile acids in germ-free and conventional mice. European journal of biochemistry *66*, 507-514.

Fahey, D.A., Carey, M.C., and Donovan, J.M. (1995). Bile acid/phosphatidylcholine interactions in mixed monomolecular layers: differences in condensation effects but not interfacial orientation between hydrophobic and hydrophilic bile acid species. Biochemistry *34*, 10886-10897.

Fang, S., Suh, J.M., Reilly, S.M., Yu, E., Osborn, O., Lackey, D., Yoshihara, E., Perino, A., Jacinto, S., Lukasheva, Y., et al. (2015). Intestinal FXR agonism promotes adipose tissue browning and reduces obesity and insulin resistance. Nature medicine *21*, 159-165.

Fang, Y., Studer, E., Mitchell, C., Grant, S., Pandak, W.M., Hylemon, P.B., and Dent, P. (2007). Conjugated bile acids regulate hepatocyte glycogen synthase activity in vitro and in vivo via Galphai signaling. Mol Pharmacol *71*, 1122-1128.

Feldmann, H.M., Golozoubova, V., Cannon, B., and Nedergaard, J. (2009). UCP1 ablation induces obesity and abolishes diet-induced thermogenesis in mice exempt from thermal stress by living at thermoneutrality. Cell Metab *9*, 203-209.

Freeman, K.B., Heffernan, M., Dhalla, Z., and Patel, H.V. (1989). Effects of exposure temperature on brown adipose tissue uncoupling protein mRNA levels. Biochem Cell Biol *67*, 147-151.

Fromme, T., Huttinger, K., Maurer, S., Li, Y., Gantert, T., Fiamoncini, J., Daniel, H., Westphal, S., and Klingenspor, M. (2019). Bile acid supplementation decreases body mass gain in C57BL/6J but not 129S6/SvEvTac mice without increasing energy expenditure. Scientific reports *9*, 131.

Galle, P.R., Theilmann, L., Raedsch, R., Otto, G., and Stiehl, A. (1990). Ursodeoxycholate reduces hepatotoxicity of bile salts in primary human hepatocytes. Hepatology *12*, 486-491.

Gerk, P.M., and Vore, M. (2002). Regulation of expression of the multidrug resistance-associated protein 2 (MRP2) and its role in drug disposition. J Pharmacol Exp Ther *302*, 407-415.

Giralt, M., and Villarroya, F. (2013). White, brown, beige/brite: different adipose cells for different functions? Endocrinology *154*, 2992-3000.

Golozoubova, V., Hohtola, E., Matthias, A., Jacobsson, A., Cannon, B., and Nedergaard, J. (2001). Only UCP1 can mediate adaptive nonshivering thermogenesis in the cold. FASEB J *15*, 2048-2050.

Goodwin, B., Jones, S.A., Price, R.R., Watson, M.A., McKee, D.D., Moore, L.B., Galardi, C., Wilson, J.G., Lewis, M.C., Roth, M.E., et al. (2000). A regulatory cascade of the nuclear receptors FXR, SHP-1, and LRH-1 represses bile acid biosynthesis. Molecular cell *6*, 517-526.

Gray, S.G. Epigenetic cancer therapy.

Guerra, C., Koza, R.A., Yamashita, H., Walsh, K., and Kozak, L.P. (1998). Emergence of brown adipocytes in white fat in mice is under genetic control. Effects on body weight and adiposity. J Clin Invest *102*, 412-420.

Guo, C., Chen, W.D., and Wang, Y.D. (2016). TGR5, Not Only a Metabolic Regulator. Front Physiol *7*, 646.

Gupta, S., Stravitz, R.T., Dent, P., and Hylemon, P.B. (2001). Down-regulation of cholesterol 7alpha-hydroxylase (CYP7A1) gene expression by bile acids in primary rat hepatocytes is mediated by the c-Jun N-terminal kinase pathway. The Journal of biological chemistry *276*, 15816-15822.

Guslandi, M. (1990). Treatment of chronic liver disease with ursodeoxycholic acid. J Int Med Res *18*, 497-505.

Hagenbuch, B., and Meier, P.J. (1996). Sinusoidal (basolateral) bile salt uptake systems of hepatocytes. Seminars in liver disease *16*, 129-136.

Hamann, A., Flier, J.S., and Lowell, B.B. (1996). Decreased brown fat markedly enhances susceptibility to diet-induced obesity, diabetes, and hyperlipidemia. Endocrinology *137*, 21-29.

Hamann, A., Flier, J.S., and Lowell, B.B. (1998). Obesity after genetic ablation of brown adipose tissue. Z Ernahrungswiss *37 Suppl 1*, 1-7.

Heaton, J.M. (1972). The distribution of brown adipose tissue in the human. J Anat *112*, 35-39.

Himms-Hagen, J., Melnyk, A., Zingaretti, M.C., Ceresi, E., Barbatelli, G., and Cinti, S. (2000). Multilocular fat cells in WAT of CL-316243-treated rats derive directly from white adipocytes. Am J Physiol Cell Physiol *279*, C670-681.

Hofmann, A.F. (1988). Pathogenesis of cholesterol gallstones. J Clin Gastroenterol *10 Suppl 2*, S1-11.

Hofmann, A.F. (1990). Bile acid secretion, bile flow and biliary lipid secretion in humans. Hepatology *12*, 17S-22S; discussion 22S-25S.

Hofmann, W.E., Liu, X., Bearden, C.M., Harper, M.E., and Kozak, L.P. (2001). Effects of genetic background on thermoregulation and fatty acid-induced uncoupling of mitochondria in UCP1-deficient mice. The Journal of biological chemistry *276*, 12460-12465.

Ikemoto, S., Takahashi, M., Tsunoda, N., Maruyama, K., Itakura, H., Kawanaka, K., Tabata, I., Higuchi, M., Tange, T., Yamamoto, T.T., et al. (1997). Cholate inhibits high-fat diet-induced hyperglycemia and obesity with acyl-CoA synthetase mRNA decrease. Am J Physiol *273*, E37-45.

Inagaki, T., Choi, M., Moschetta, A., Peng, L., Cummins, C.L., McDonald, J.G., Luo, G., Jones, S.A., Goodwin, B., Richardson, J.A., et al. (2005). Fibroblast growth factor 15 functions as an enterohepatic signal to regulate bile acid homeostasis. Cell metabolism *2*, 217-225.

James, W.P., and Trayhurn, P. (1981). Thermogenesis and obesity. Br Med Bull *37*, 43-48.

Jenkins, G., and Hardie, L.J. (2008). Bile acids : toxicology and bioactivity. In Issues in toxicology (Cambridge: Royal Society of Chemistry,), pp. 1 online resource (xi, 163 pages).

Jenkins, G., Hardie, L.J., ebrary Inc., and Royal Society of Chemistry (Great Britain) (2008). Bile acids toxicology and bioactivity. In Issues in toxicology (Cambridge: SC Pub.,), pp. xi, 163 p.

Kalaany, N.Y., and Mangelsdorf, D.J. (2006). LXRS and FXR: the yin and yang of cholesterol and fat metabolism. Annu Rev Physiol *68*, 159-191.

Kashyap, S.R., Bhatt, D.L., Wolski, K., Watanabe, R.M., Abdul-Ghani, M., Abood, B., Pothier, C.E., Brethauer, S., Nissen, S., Gupta, M., et al. (2013). Metabolic effects of bariatric surgery in patients with moderate obesity and type 2 diabetes: analysis of a randomized control trial comparing surgery with intensive medical treatment. Diabetes care *36*, 2175-2182.

Kawamata, Y., Fujii, R., Hosoya, M., Harada, M., Yoshida, H., Miwa, M., Fukusumi, S., Habata, Y., Itoh, T., Shintani, Y., et al. (2003). A G protein-coupled receptor responsive to bile acids. The Journal of biological chemistry *278*, 9435-9440.

Keitel, V., Reinehr, R., Gatsios, P., Rupprecht, C., Gorg, B., Selbach, O., Haussinger, D., and Kubitz, R. (2007). The G-protein coupled bile salt receptor TGR5 is expressed in liver sinusoidal endothelial cells. Hepatology *45*, 695-704.

Klingenspor, M., Fromme, T., Hughes, D.A., Jr., Manzke, L., Polymeropoulos, E., Riemann, T., Trzcionka, M., Hirschberg, V., and Jastroch, M. (2008). An ancient look at UCP1. Biochimica et biophysica acta *1777*, 637-641.

Kohli, R., Bradley, D., Setchell, K.D., Eagon, J.C., Abumrad, N., and Klein, S. (2013). Weight loss induced by Roux-en-Y gastric bypass but not laparoscopic adjustable gastric banding increases circulating bile acids. The Journal of clinical endocrinology and metabolism *98*, E708-712.

Kramer, W., Buscher, H.P., Gerok, W., and Kurz, G. (1979). Bile salt binding to serum components. Taurocholate incorporation into high-density lipoprotein revealed by photoaffinity labelling. Eur J Biochem *102*, 1-9.

Lamri, Y., Erlinger, S., Dumont, M., Roda, A., and Feldmann, G. (1992). Immunoperoxidase localization of ursodeoxycholic acid in rat biliary epithelial cells. Evidence for a cholehepatic circulation. Liver *12*, 351-354.

Lee, Y.H., Petkova, A.P., Mottillo, E.P., and Granneman, J.G. (2012). In vivo identification of bipotential adipocyte progenitors recruited by beta3-adrenoceptor activation and high-fat feeding. Cell metabolism *15*, 480-491.

Leuschner, U., Fischer, H., Kurtz, W., Guldutuna, S., Hubner, K., Hellstern, A., Gatzen, M., and Leuschner, M. (1989). Ursodeoxycholic acid in primary biliary cirrhosis: results of a controlled double-blind trial. Gastroenterology *97*, 1268-1274.

Liaset, B., Hao, Q., Jorgensen, H., Hallenborg, P., Du, Z.Y., Ma, T., Marschall, H.U., Kruhoffer, M., Li, R., Li, Q., et al. (2011). Nutritional regulation of bile acid metabolism is associated with improved pathological characteristics of the metabolic syndrome. The Journal of biological chemistry *286*, 28382-28395.

Lidell, M.E., Betz, M.J., Dahlqvist Leinhard, O., Heglind, M., Elander, L., Slawik, M., Mussack, T., Nilsson, D., Romu, T., Nuutila, P., et al. (2013). Evidence for two types of brown adipose tissue in humans. Nature medicine *19*, 631-634.

Liu, X., Rossmeisl, M., McClaine, J., Riachi, M., Harper, M.E., and Kozak, L.P. (2003). Paradoxical resistance to diet-induced obesity in UCP1-deficient mice. J Clin Invest *111*, 399-407.

Lowell, B.B., V, S.S., Hamann, A., Lawitts, J.A., Himms-Hagen, J., Boyer, B.B., Kozak, L.P., and Flier, J.S. (1993). Development of obesity in transgenic mice after genetic ablation of brown adipose tissue. Nature *366*, 740-742.

Lu, T.T., Makishima, M., Repa, J.J., Schoonjans, K., Kerr, T.A., Auwerx, J., and Mangelsdorf, D.J. (2000). Molecular basis for feedback regulation of bile acid synthesis by nuclear receptors. Mol Cell *6*, 507-515.

Lutz, T.A., and Bueter, M. (2014). Physiological mechanisms behind Roux-en-Y gastric bypass surgery. Dig Surg *31*, 13-24.

Makino, I., Hashimoto, H., Shinozaki, K., Yoshino, K., and Nakagawa, S. (1975). Sulfated and nonsulfated bile acids in urine, serum, and bile of patients with hepatobiliary diseases. Gastroenterology *68*, 545-553.

Makishima, M., Okamoto, A.Y., Repa, J.J., Tu, H., Learned, R.M., Luk, A., Hull, M.V., Lustig, K.D., Mangelsdorf, D.J., and Shan, B. (1999). Identification of a nuclear receptor for bile acids. Science *284*, 1362-1365.

Malhi, H., Guicciardi, M.E., and Gores, G.J. (2010). Hepatocyte death: a clear and present danger. Physiological reviews *90*, 1165-1194.

Maruyama, T., Miyamoto, Y., Nakamura, T., Tamai, Y., Okada, H., Sugiyama, E., Nakamura, T., Itadani, H., and Tanaka, K. (2002). Identification of membrane-type receptor for bile acids (M-BAR). Biochemical and biophysical research communications *298*, 714-719.

Maurer, S.F. (2016). Molecular functions in brown adipose tissue and their physiological significance in the context of systemic glucose homeostasis in mice. In Chair of Molecular Nutritional Medicine (Technical University of Munich).

Mohamed-Ali, V., Pinkney, J.H., and Coppack, S.W. (1998). Adipose tissue as an endocrine and paracrine organ. Int J Obes Relat Metab Disord *22*, 1145-1158.

Nedergaard, J., Bengtsson, T., and Cannon, B. (2007). Unexpected evidence for active brown adipose tissue in adult humans. Am J Physiol Endocrinol Metab *293*, E444-452.

Nedergaard, J., Golozoubova, V., Matthias, A., Asadi, A., Jacobsson, A., and Cannon, B. (2001). UCP1: the only protein able to mediate adaptive non-shivering thermogenesis and metabolic inefficiency. Biochimica et biophysica acta *1504*, 82-106.

Ockenga, J., Valentini, L., Schuetz, T., Wohlgemuth, F., Glaeser, S., Omar, A., Kasim, E., duPlessis, D., Featherstone, K., Davis, J.R., et al. (2012). Plasma bile acids are associated with energy expenditure and thyroid function in humans. J Clin Endocrinol Metab *97*, 535-542.

Parks, D.J., Blanchard, S.G., Bledsoe, R.K., Chandra, G., Consler, T.G., Kliewer, S.A., Stimmel, J.B., Willson, T.M., Zavacki, A.M., Moore, D.D., et al. (1999). Bile acids: natural ligands for an orphan nuclear receptor. Science *284*, 1365-1368.

Patti, M.E., Houten, S.M., Bianco, A.C., Bernier, R., Larsen, P.R., Holst, J.J., Badman, M.K., Maratos-Flier, E., Mun, E.C., Pihlajamaki, J., et al. (2009). Serum bile acids are higher in humans with prior gastric bypass: potential contribution to improved glucose and lipid metabolism. Obesity (Silver Spring) *17*, 1671-1677.

Paumgartner, G., and Reichen, J. (1976). Kinetics of hepatic uptake of unconjugated bilirubin. Clin Sci Mol Med *51*, 169-176.

Pennington, C.R., Ross, P.E., Bateson, M.C., and Bouchier, I.A. (1978). Serum bile acids in patients with hyperlipidaemia. J Clin Pathol *31*, 58-62.

Perez, M.J., and Briz, O. (2009). Bile-acid-induced cell injury and protection. World J Gastroenterol *15*, 1677-1689.

Pournaras, D.J., Glicksman, C., Vincent, R.P., Kuganolipava, S., Alaghband-Zadeh, J., Mahon, D., Bekker, J.H., Ghatei, M.A., Bloom, S.R., Walters, J.R., et al. (2012). The role of bile after Roux-en-Y gastric bypass in promoting weight loss and improving glycaemic control. Endocrinology *153*, 3613-3619.

Qiao, L., Han, S.I., Fang, Y., Park, J.S., Gupta, S., Gilfor, D., Amorino, G., Valerie, K., Sealy, L., Engelhardt, J.F., et al. (2003). Bile acid regulation of C/EBPbeta, CREB, and c-Jun function, via the extracellular signal-regulated kinase and c-Jun NH2-terminal kinase pathways, modulates the apoptotic response of hepatocytes. Molecular and cellular biology *23*, 3052-3066.

Raedsch, R., Lauterburg, B.H., and Hofmann, A.F. (1981). Altered bile acid metabolism in primary biliary cirrhosis. Dig Dis Sci *26*, 394-401.

Rao, A., Haywood, J., Craddock, A.L., Belinsky, M.G., Kruh, G.D., and Dawson, P.A. (2008). The organic solute transporter alpha-beta, Ostalpha-Ostbeta, is essential for intestinal bile acid transport and homeostasis. Proceedings of the National Academy of Sciences of the United States of America *105*, 3891-3896.

Ravussin, Y., Gutman, R., LeDuc, C.A., and Leibel, R.L. (2013). Estimating energy expenditure in mice using an energy balance technique. International journal of obesity *37*, 399-403.

Reuben, A. (1984). Bile formation: sites and mechanisms. Hepatology *4*, 15S-24S.

Rippe, C., Berger, K., Boiers, C., Ricquier, D., and Erlanson-Albertsson, C. (2000). Effect of high-fat diet, surrounding temperature, and enterostatin on uncoupling protein gene expression. Am J Physiol Endocrinol Metab *279*, E293-300.

Rizzo, G., Disante, M., Mencarelli, A., Renga, B., Gioiello, A., Pellicciari, R., and Fiorucci, S. (2006). The farnesoid X receptor promotes adipocyte differentiation and regulates adipose cell function in vivo. Molecular pharmacology *70*, 1164-1173.

Rosenwald, M., Perdikari, A., Rulicke, T., and Wolfrum, C. (2013). Bi-directional interconversion of brite and white adipocytes. Nat Cell Biol *15*, 659-667.

Rowland, L.A., Maurya, S.K., Bal, N.C., Kozak, L., and Periasamy, M. (2016). Sarcolipin and uncoupling protein 1 play distinct roles in diet-induced thermogenesis and do not compensate for one another. Obesity (Silver Spring, Md.) *24*, 1430-1433.

Rudman, D., and Kendall, F.E. (1957). Bile acid content of human serum. I. Serum bile acids in patients with hepatic disease. The Journal of clinical investigation *36*, 530-537.

Sanchez-Gurmaches, J., Hung, C.M., Sparks, C.A., Tang, Y., Li, H., and Guertin, D.A. (2012). PTEN loss in the Myf5 lineage redistributes body fat and reveals subsets of white adipocytes that arise from Myf5 precursors. Cell metabolism *16*, 348-362.

Schauer, P.R., Kashyap, S.R., Wolski, K., Brethauer, S.A., Kirwan, J.P., Pothier, C.E., Thomas, S., Abood, B., Nissen, S.E., and Bhatt, D.L. (2012). Bariatric surgery versus intensive medical therapy in obese patients with diabetes. N Engl J Med *366*, 1567-1576.

Schulz, T.J., Huang, P., Huang, T.L., Xue, R., McDougall, L.E., Townsend, K.L., Cypess, A.M., Mishina, Y., Gussoni, E., and Tseng, Y.H. (2013). Brown-fat paucity due to impaired BMP signalling induces compensatory browning of white fat. Nature *495*, 379-383.

Seale, P., Bjork, B., Yang, W., Kajimura, S., Chin, S., Kuang, S., Scime, A., Devarakonda, S., Conroe, H.M., Erdjument-Bromage, H., et al. (2008). PRDM16 controls a brown fat/skeletal muscle switch. Nature *454*, 961-967.

Seward, D.J., Koh, A.S., Boyer, J.L., and Ballatori, N. (2003). Functional complementation between a novel mammalian polygenic transport complex and an evolutionarily ancient organic solute transporter, OSTalpha-OSTbeta. The Journal of biological chemistry *278*, 27473-27482.

Sheikh Abdul Kadir, S.H., Miragoli, M., Abu-Hayyeh, S., Moshkov, A.V., Xie, Q., Keitel, V., Nikolaev, V.O., Williamson, C., and Gorelik, J. (2010). Bile acid-induced arrhythmia is mediated by muscarinic M2 receptors in neonatal rat cardiomyocytes. PLoS One *5*, e9689.

Shneider, B.L. (2001). Intestinal bile acid transport: biology, physiology, and pathophysiology. J Pediatr Gastroenterol Nutr *32*, 407-417.

Sinal, C.J., Tohkin, M., Miyata, M., Ward, J.M., Lambert, G., and Gonzalez, F.J. (2000). Targeted disruption of the nuclear receptor FXR/BAR impairs bile acid and lipid homeostasis. Cell *102*, 731-744.

Solimando, R., Bazzoli, F., and Ricciardiello, L. (2011). Chemoprevention of colorectal cancer: a role for ursodeoxycholic acid, folate and hormone replacement treatment? Best Pract Res Clin Gastroenterol *25*, 555-568.

Stanford, K.I., Middelbeek, R.J., Townsend, K.L., An, D., Nygaard, E.B., Hitchcox, K.M., Markan, K.R., Nakano, K., Hirshman, M.F., Tseng, Y.H., et al. (2013). Brown adipose tissue regulates glucose homeostasis and insulin sensitivity. J Clin Invest *123*, 215-223.

Stemmer, K., Kotzbeck, P., Zani, F., Bauer, M., Neff, C., Muller, T.D., Pfluger, P.T., Seeley, R.J., and Divanovic, S. (2015). Thermoneutral housing is a critical factor for immune function and diet-induced obesity in C57BL/6 nude mice. International journal of obesity *39*, 791-797.

Stiehl, A. (1974). Bile salt sulphates in cholestasis. Eur J Clin Invest *4*, 59-63.

Stiehl, A., Becker, M., Czygan, P., Frohling, W., Kommerell, B., Rotthauwe, H.W., and Senn, M. (1980). Bile acids and their sulphated and glucuronidated derivatives in bile, plasma, and urine of children with intrahepatic cholestasis: effects of phenobarbital treatment. Eur J Clin Invest *10*, 307-316.

Stiehl, A., Earnest, D.L., and Admirant, W.H. (1975). Sulfation and renal excretion of bile salts in patients with cirrhosis of the liver. Gastroenterology *68*, 534-544.

Stroeve, J.H., Brufau, G., Stellaard, F., Gonzalez, F.J., Staels, B., and Kuipers, F. (2010). Intestinal FXR-mediated FGF15 production contributes to diurnal control of hepatic bile acid synthesis in mice. Lab Invest *90*, 1457-1467.

Suzuki, T., Aoyama, J., Hashimoto, M., Ohara, M., Futami-Suda, S., Suzuki, K., Ouchi, M., Igari, Y., Watanabe, K., and Nakano, H. (2014). Correlation between postprandial bile acids and body fat mass in healthy normal-weight subjects. Clinical biochemistry *47*, 1128-1131.

Tavoloni, N., Reed, J.S., and Boyer, J.L. (1978). Hemodynamic effects on determinants of bile secretion in isolated rat liver. The American journal of physiology *234*, E584-592.

Teng, S., and Piquette-Miller, M. (2007). Hepatoprotective role of PXR activation and MRP3 in cholic acid-induced cholestasis. British journal of pharmacology *151*, 367-376.

Teodoro, J.S., Zouhar, P., Flachs, P., Bardova, K., Janovska, P., Gomes, A.P., Duarte, F.V., Varela, A.T., Rolo, A.P., Palmeira, C.M., et al. (2014). Enhancement of brown fat thermogenesis using chenodeoxycholic acid in mice. Int J Obes (Lond) *38*, 1027-1034.

Thomas, C., Gioiello, A., Noriega, L., Strehle, A., Oury, J., Rizzo, G., Macchiarulo, A., Yamamoto, H., Mataki, C., Pruzanski, M., et al. (2009). TGR5-mediated bile acid sensing controls glucose homeostasis. Cell Metab *10*, 167-177.

Timmons, J.A., Wennmalm, K., Larsson, O., Walden, T.B., Lassmann, T., Petrovic, N., Hamilton, D.L., Gimeno, R.E., Wahlestedt, C., Baar, K., et al. (2007). Myogenic gene expression signature establishes that brown and white adipocytes originate from distinct cell lineages. Proceedings of the National Academy of Sciences of the United States of America *104*, 4401-4406.

Tiwari, A., and Maiti, P. (2009). TGR5: an emerging bile acid G-protein-coupled receptor target for the potential treatment of metabolic disorders. Drug Discov Today *14*, 523-530.

Townsend, K., and Tseng, Y.H. (2012). Brown adipose tissue: Recent insights into development, metabolic function and therapeutic potential. Adipocyte *1*, 13-24.

Trayhurn, P., and Beattie, J.H. (2001). Physiological role of adipose tissue: white adipose tissue as an endocrine and secretory organ. Proc Nutr Soc *60*, 329-339.

Tschop, M.H., Speakman, J.R., Arch, J.R., Auwerx, J., Bruning, J.C., Chan, L., Eckel, R.H., Farese, R.V., Jr., Galgani, J.E., Hambly, C., et al. (2011). A guide to analysis of mouse energy metabolism. Nature methods *9*, 57-63.

van Marken Lichtenbelt, W.D., Vanhommerig, J.W., Smulders, N.M., Drossaerts, J.M., Kemerink, G.J., Bouvy, N.D., Schrauwen, P., and Teule, G.J. (2009). Cold-activated brown adipose tissue in healthy men. N Engl J Med *360*, 1500-1508.

Velazquez-Villegas, L.A., Perino, A., Lemos, V., Zietak, M., Nomura, M., Pols, T.W.H., and Schoonjans, K. (2018). TGR5 signalling promotes mitochondrial fission and beige remodelling of white adipose tissue. Nature communications *9*, 245.

Villarroya, J., Cereijo, R., and Villarroya, F. (2013). An endocrine role for brown adipose tissue? Am J Physiol Endocrinol Metab *305*, E567-572.

Virtanen, K.A., Lidell, M.E., Orava, J., Heglind, M., Westergren, R., Niemi, T., Taittonen, M., Laine, J., Savisto, N.J., Enerback, S., et al. (2009). Functional brown adipose tissue in healthy adults. N Engl J Med *360*, 1518-1525.

Vodenlich, A.D., Jr., Gong, Y.Z., Geoghegan, K.F., Lin, M.C., Lanzetti, A.J., and Wilson, F.A. (1991). Identification of the 14 kDa bile acid transport protein of rat ileal cytosol as gastrotropin. Biochemical and biophysical research communications *177*, 1147-1154.

Von Essen, G. (2017). Energy flow and metabolic efficiency attributed to brown adipose tissue. In Faculty of Science, Department of Molecular Biosciences, The Wenner-Gren Institute (Stockholm University).

von Essen, G., Lindsund, E., Cannon, B., and Nedergaard, J. (2017). Adaptive facultative diet-induced thermogenesis in wild-type but not in UCP1-ablated mice. Am J Physiol Endocrinol Metab *313*, E515-E527.

Wang, H., Chen, J., Hollister, K., Sowers, L.C., and Forman, B.M. (1999). Endogenous bile acids are ligands for the nuclear receptor FXR/BAR. Molecular cell *3*, 543-553.

Watanabe, M., Horai, Y., Houten, S.M., Morimoto, K., Sugizaki, T., Arita, E., Mataki, C., Sato, H., Tanigawara, Y., Schoonjans, K., et al. (2011). Lowering bile acid pool size with a synthetic farnesoid X receptor (FXR) agonist induces obesity and diabetes through reduced energy expenditure. J Biol Chem *286*, 26913-26920.

Watanabe, M., Houten, S.M., Mataki, C., Christoffolete, M.A., Kim, B.W., Sato, H., Messaddeq, N., Harney, J.W., Ezaki, O., Kodama, T., et al. (2006). Bile acids induce energy expenditure by promoting intracellular thyroid hormone activation. Nature *439*, 484-489.

Watanabe, M., Houten, S.M., Wang, L., Moschetta, A., Mangelsdorf, D.J., Heyman, R.A., Moore, D.D., and Auwerx, J. (2004). Bile acids lower triglyceride levels via a pathway involving FXR, SHP, and SREBP-1c. J Clin Invest *113*, 1408-1418.

Watanabe, M., Morimoto, K., Houten, S.M., Kaneko-Iwasaki, N., Sugizaki, T., Horai, Y., Mataki, C., Sato, H., Murahashi, K., Arita, E., et al. (2012). Bile Acid Binding Resin Improves Metabolic Control through the Induction of Energy Expenditure. PLoS One *7*, e38286.

Weiner, I.M., Glasser, J.E., and Lack, L. (1964). Renal Excretion of Bile Acids: Taurocholic, Glycocholic, and Colic Acids. The American journal of physiology *207*, 964-970.

Weitzel, J.M., Iwen, K.A., and Seitz, H.J. (2003). Regulation of mitochondrial biogenesis by thyroid hormone. Exp Physiol *88*, 121-128.

Wilson, F.A., Burckhardt, G., Murer, H., Rumrich, G., and Ullrich, K.J. (1981). Sodium-coupled taurocholate transport in the proximal convolution of the rat kidney in vivo and in vitro. The Journal of clinical investigation *67*, 1141-1150.

Winn, N.C., Vieira-Potter, V.J., Gastecki, M.L., Welly, R.J., Scroggins, R.J., Zidon, T.M., Gaines, T.L., Woodford, M.L., Karasseva, N.G., Kanaley, J.A., et al. (2017). Loss of UCP1 exacerbates Western diet-induced glycemic dysregulation independent of changes in body weight in female mice. Am J Physiol Regul Integr Comp Physiol *312*, R74-R84.

Woolbright, B.L., Dorko, K., Antoine, D.J., Clarke, J.I., Gholami, P., Li, F., Kumer, S.C., Schmitt, T.M., Forster, J., Fan, F., et al. (2015). Bile acid-induced necrosis in primary human hepatocytes and in patients with obstructive cholestasis. Toxicol Appl Pharmacol *283*, 168-177.

Woolbright, B.L., Li, F., Xie, Y., Farhood, A., Fickert, P., Trauner, M., and Jaeschke, H. (2014). Lithocholic acid feeding results in direct hepato-toxicity independent of neutrophil function in mice. Toxicology letters *228*, 56-66.

Worobetz, L.J., Inglis, F.G., and Shaffer, E.A. (1993). The effect of ursodeoxycholic acid therapy on gallstone formation in the morbidly obese during rapid weight loss. Am J Gastroenterol *88*, 1705-1710.

Xue, B., Rim, J.S., Hogan, J.C., Coulter, A.A., Koza, R.A., and Kozak, L.P. (2007). Genetic variability affects the development of brown adipocytes in white fat but not in interscapular brown fat. Journal of lipid research *48*, 41-51.

Zhang, X., Kuo, C., Moore, A., and Ran, C. (2013). In Vivo Optical Imaging of Interscapular Brown Adipose Tissue with (18)F-FDG via Cerenkov Luminescence Imaging. PLoS One *8*, e62007.

Zietak, M., and Kozak, L.P. (2016). Bile acids induce uncoupling protein 1-dependent thermogenesis and stimulate energy expenditure at thermoneutrality in mice. Am J Physiol Endocrinol Metab *310*, E346-354.

APPENDIX

Table 10: External and internal standards used for bile acid quantification by means of UPLC/TOF-MS.

	Abbreviation	Molecular mass [M-H]-	Company	Order number
Chenodeoxycholic acid	CDCA	391.285383	Sigma	C9377
Cholic acid	CA	407.280298	Sigma	C1129
Deoxycholic acid	DCA	391.285383	Sigma	D2510
Glycochenodeoxycholate, sodium	GCDCA	448.306847	Sigma	G0759
Glycocholic acid, hydrate	GCA	464.301762	Sigma	G2878
Glycodeoxycholic acid, sodium	GDCA	448.306847	Calbiochem	361311
Glycoursodeoxycholic acid	GUDCA	448.306847	Sigma	06863
Dehydrocholic acid	Dehydro-CA	391.285383	Sigma	30830
Lithocholic acid	LCA	375.290469	Sigma	L6250
Taurochenodeoxycholate, sodium	TCDCA	498.289483	Sigma	T6260
Taurocholic acid, sodium hydrate	TCA	514.284397	Sigma	T4009
Taurodeoxycholate, sodium hydrate	TDCA	498.289483	Sigma	T0875
Taurolithocholate, sodium	TLCA	482.294568	Sigma	T7515
Tauroursodeoxycholic acid, sodium	TUDCA	498.289483	Calbiochem	580549
Ursodeoxycholic acid	UDCA	391.285383	Sigma	U5127
α-Muricholic acid	αMCA	407.280298	Steraloids	C1890-000
α-Tauromuricholic acid	αTMCA	514.284397	Steraloids	C1893-000
β-Muricholic acid	βMCA	407.280298	Steraloids	C1898-000
β-Tauromuricholic acid	βTMCA	514.284397	Steraloids	C1899-000
ω-Muricholic acid	ωMCA	407.280298	Steraloids	C1888-000
d4-Cholic acid	d4-DCA	411.304308	Sigma	D-2452
d4-Deoxycholic acid	d4-DCA	395.309393	CDN Isotopes	D-2941
d5-Taurocholic acid	d5-TCA	519.314684	Toronto research chemicals	NC0341860

LIST OF FIGURES

LIST OF TABLES

ACKNOWLEDGEMENTS

An dieser Stelle möchte ich mich bei allen bedanken, die auf wissenschaftlicher und persönlicher Ebene zum Gelingen dieser Arbeit beigetragen haben.

An erster Stelle bedanke ich mich bei Prof. Martin Klingenspor für die Bereitstellung des Themas und die Ermöglichung dieser Arbeit im Rahmen des DFG Graduiertenkollegs 1482. Herzlichen Dank für den wissenschaftlichen Input sowie die hilfreichen Diskussionen.

Ich danke Prof. Hannelore Daniel und Prof. Michael Schemann für die Bereitschaft Zweitprüferin und Prüfungsvorsitzender zu sein sowie für die erfolgreiche Zusammenarbeit. Ein herzlicher Dank an Dorothea für die Koordination des GRK und deine Unterstützung.

Ein großes Dankeschön geht an Tobias für die Betreuung und das Korrekturlesen dieser Arbeit. Deine unermüdliche Geduld und Unterstützung, dein stets offenes Ohr und deine Weisheiten in allen Belangen der Wissenschaft und des Lebens haben mir geholfen, den roten Faden nicht zu verlieren und diese Arbeit erfolgreich abzuschließen.

Ich möchte mich bei allen Kollegen, mit denen ich im Laufe der Jahre zusammenarbeiten durfte, für die wunderbare Arbeitsatmosphäre und die große Hilfsbereitschaft bedanken. Zusätzlich danke ich allen GRK-Mitstreitern für die erheiternden Events sowie Steffi und Nadine für die amüsanten Running-Sushi-Abende. Einen lieben Dank auch an Moni, Kathi und Gloria für die freundliche Aufnahme im Büro, die mir den Abschluss meiner Arbeit versüßt hat. Ein herzlicher Dank an Sabine und Anika für eure hervorragende Unterstützung im Labor. Vielen Dank auch an die Tierpflegerinnen für die stets zuverlässige Arbeit.

Sama, Caro, Bienchen- es war mir eine unglaubliche Freude mit euch zusammenzuarbeiten! Ich danke euch für die grandiosen Kaffeepausen, alle unvergesslichen Anekdoten über die vermeintlich unwichtigen Dinge des Lebens sowie die bis heute andauernde Freundschaft!

Ein besonderer Dank gilt meiner gesamten Familie, die immer für mich da ist und immer an mich glaubt. Ihr alle habt diesen Erfolg erst möglich gemacht. Ich danke meinen Eltern für die jahrzehntelange Unterstützung und den besten Bruder den es gibt! Mein größter Dank gilt den beiden wichtigsten Menschen in meinem Leben, meinem Mann Jörg und unserer Tochter Marie. Ohne euch, euren Rückhalt und eure bedingungslose Liebe wäre alles nichts.

EIDESSTATTLICHE ERKLÄRUNG

Ich erkläre an Eides statt, dass ich die bei der Fakultät Wissenschaftszentrum Weihenstephan für Ernährung, Landnutzung und Umwelt der TUM zur Promotionsprüfung vorgelegte Arbeit mit dem Titel:

Prevention of diet-induced obesity conferred by dietary bile acid supplementation in mice is strain specific and not dependent on uncoupling protein 1

am Lehrstuhl für Molekulare Ernährungsmedizin unter der Anleitung und Betreuung durch Univ.-Prof. Dr. Martin Klingenspor ohne sonstige Hilfe erstellt und bei der Abfassung nur die gemäß § 6 Ab. 6 und 7 Satz 2 angebotenen Hilfsmittel benutzt habe.

Ich habe keine Organisation eingeschaltet, die gegen Entgelt Betreuerinnen und Betreuer für die Anfertigung von Dissertationen sucht, oder die mir obliegenden Pflichten hinsichtlich der Prüfungsleistungen für mich ganz oder teilweise erledigt.

Ich habe die Dissertation in dieser oder ähnlicher Form in keinem anderen Prüfungsverfahren als Prüfungsleistung vorgelegt.

Ich habe den angestrebten Doktorgrad noch nicht erworben und bin nicht in einem früheren Promotionsverfahren für den angestrebten Doktorgrad endgültig gescheitert.

Die öffentlich zugängliche Promotionsordnung der TUM ist mir bekannt, insbesondere habe ich die Bedeutung von § 28 (Nichtigkeit der Promotion) und § 29 (Entzug des Doktorgrades) zur Kenntnis genommen. Ich bin mir der Konsequenzen einer falschen Eidesstattlichen Erklärung bewusst.

Mit der Aufnahme meiner personenbezogenen Daten in die Alumni-Datei bei der TUM bin ich einverstanden.

München, den _____ _____

Kristina Hüttinger